School of Mining Engineering

UNIVERSITY OF THE
WITWATERSRAND,
JOHANNESBURG

CRITICAL ANALYSIS OF A KIMBERLITE OPEN–PIT SLOPE DESIGN PRODUCED BY LIMITED GEOTECHNICAL DATA AND SLOPE DESIGN CHARTS

Ian Mason Snyders

A research report submitted to the Faculty of Engineering and the Built Environment, University of the Witwatersrand, Johannesburg, in partial fulfilment of the requirements for the degree of Master of Science in Engineering.

Johannesburg, 2020

DECLARATION

I declare that this report is my own, unaided work. I have read the University Policy on Plagiarism and hereby confirm that no plagiarism exists in this report. I also confirm that there is no copying nor is there any copyright infringement. I willingly submit to any investigation in this regard by the School of Mining Engineering and I undertake to abide by the decision of any such investigation.

24th May 2021

Signature of Candidate Date

ABSTRACT

The purpose of the study was to determine a geotechnical model that could be used in the slope design process at Mine A diamond open pit mine. Geotechnical data was collected from the current pit slopes for the purposes of the fourth mining cut-back and deepening of the pit. Model creation required the constructive grouping of data into the four pillars of the geotechnical model designed by Read and Stacey (2009). Circular failure charts (Hoek and Bray, 1981) were used to determine relevant slopes in the soils. Laubscher’s (1990) Modified Rock Mass Rating classification system was used for individual kimberlite domains, and competent granitic gneiss, respectively. It was possible to analyse the slope in the kimberlite separately to the country rocks, due to the vertical nature of the orebody. This separate analysis allowed for a deeper pit to be created. The results were checked by using numerical modelling software. Furthermore, the probability of reducing bench face angles in the granitic gneiss by analysis of stereonets was investigated to reduce risk of wedge failure. Implementation was, however, not found to be practicle and daily inspections, instrumentation and installation of geotechnical safety berms were suggested as alternative mitigation methods. An additional geotechnical safety berm is to be implemented immediately below the major shear zone in the south east (geotechnical domain 9). Haulage roads planned to be developed below the shear zone must be located below the safety berm. It is also important that haulage roads are not developed in this shear zone.

A geotechnical model was established with geotechnical data collected from the existing pit. Unfortunately, the confidence of the hydrological data is low, meaning that proper monitoring and pumping of water is essential throughout the project life. In particular, circular failure is possible in the upper 20 m to 40 m of the main pit in high rainfall periods. It is therefore very important to setup and maintain a proper monitoring system, that will give an early warning of a pending slope failure. All data collected during the life of the pit should be evaluated against the recommended slope angles. Changes should be made if unstable conditions are determined from the updated analysis.

ACKNOWLEDGMENTS

I would like to acknowledge first the guiding role that Messers Peter Terbrugge and Kuziva Chisi have had in directing my geotechnical career, including motivating me to complete my Masters degree. Without them, I would probably not have even attempted it and I am in great debt to them for this. To my supervisor, Prof Bryan Watson, thank you for your hard work in making this report Masters worthy. To my family and friends who helped me through the late nights and early mornings, you are appreciated! Finally, to the One who made me with the capacity to think, work and live, You are my source and motivation for everything I do.

TABLE OF CONTENTS

LIST OF TABLES

LIST OF FIGURES

LIST OF SYMBOLS

CR	Country Rock
FF	Fracture Frequency
IRS	Intact Rock Strength
Jcon	Joint Condition
MSR	Monitoring Survey Radar
NE-SW	North East – South West
PLT	Point Load Tester
TCS	Triaxial Compressive Strength
UCS	Uniaxial Compressive Strength
QAQC	Quality Assurance Quality Control

1 INTRODUCTION

The purpose of this study was to determine stable slopes for implementation at Mine A diamond open pit mine. The mine has planned a fourth cutback and required a proper slope design. This design is based on an analysis of geotechnical data collected from the existing pit. Previously pit analysis was done on a poor understanding of the geotechnical setting and was also poorly implemented due to poor drilling and blasting practice. The new strategy will consider the current slope condition and provide sound recommendations based on a proper geotechnical review.

1.1 Research Context Backround

Mine A is situated in the Lunda Norté province in the North-East of Angola as indicated in Figure 1.1. The operation is an open-pit kimberlite project which was started in 2007 as an exploration project with three kimberlite pipes targeted for future production. Since then, the operation has undergone an interesting organic growth with exploration and full-scale mining running concurrently.

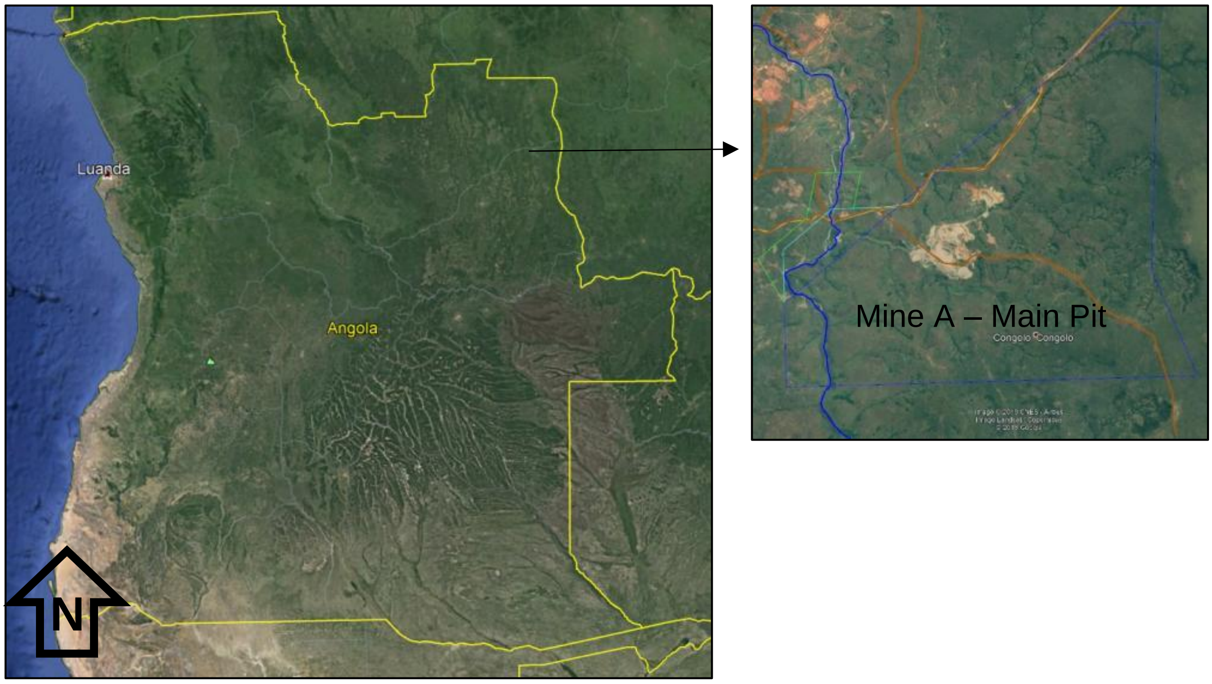

Figure 1-1 Location plan of study area

By November 2015, the main kimberlite intrusion, (Figure 1.2), had been excavated to a depth of 120 m. Up to this point, the pit was designed according to the best-fit economic situation, without any regard to geotechnical conditions. As mining advanced, the services of SRK Consulting were employed to evaluate conditions and make recommendations on slope angles. Due to a lack of a geotechnical database, their design input parameters were limited and much of the design was based on previously encountered similar conditions elsewhere. The design was incorporated into the mine plan for the second mining cut-back, but implementation was poor due to poor drilling, blasting practice and final wall controls. Added to this was a poor understanding of the geotechnical rock mass character of the kimberlites to be intersected in mining advance, which led to a design recommendation based on incorrect rock mass conditions.

Figure 1-2 Areal Photograph of the main pit

This geotechnical data gap led directly to instability and subsequent failure of the Eastern and Southern kimberlite walls at the onset of the rainy season of 2018. A slope monitoring radar was immediately purchased and was received in January 2019 to improve the monitoring of unstable conditions being experienced. However, the data gap required for feasibility level slope-design recommendations needed to be closed. Approval was gained for the construction of a robust geotechnical model by in-pit face mapping (geotechnical rock mass line and window mapping as well as structural mapping); further geotechnical drilling (including laboratory rock testing and point-load testing of rock samples); and hydrogeological characterisation through piezometer construction used in holes drilled for a geotechnical core drilling programme.

Due to the poor implementation of the mine design by poor blasting and final wall limit controls, possible instability in borderline areas was increased. The pit limit final wall programme was instituted through the aid of blast engineering consultants. This served to better train and educate the drilling and blasting team on correct smooth-wall blasting techniques. This programme included a concentrated effort by the geotechnical personnel to design blasts according to geotechnical domains, i.e. rock mass conditions, rather than blanket burden and spacing designs throughout the pit. A focus on timing and spacing proved to be paramount to the success of this high wall programme. The blast movement and hence blast energy force was directed near perpendicular to existing major joint orientations. This prevented the weakening of joint conditions through joint aperture opening by energy propagation. A concerted focus was also made to ensure free-face conditions on all blasts, to limit the effect confinement would have on the direction of energy, and hence prevent the possibility of "back-break" (excessive breakage behind the pre-split blast line as described by Sayadi et al (2013)). Where major discontinuities or geological structures played a role in energy propagation, the sizes of blasts were reduced so as to lessen potential damaging energy. This was done through keeping the burden and spacing required for adequate fragmentation, but decreasing the number of holes that were charged and blasted together and thus decreasing the energy around such structures.

With the pit third and final cutback expected to commence in January 2020, the slope design was required to be completed to the level of a feasibility study by November 2019 so that any changes could be incorporated into the pit design. The produced slope design through geotechnical model creation and subsequent design chart modelling is the focus of this research project. Numerical analysis of the resultant slope design was done using limit equilibrium SLIDE 2D (2018) and boundary element Examine 2D (2006) software. The numerical modelling analyses, did not consider the individual strength of unfavourable discontinuities, but rather the down-rating effects of the discontinuities on rock mass strength.

1.2 Research Motivation

The slope failures (Section 1.1) have been the main motivation for this research. Due to insufficient geotechnical model information on the variable kimberlite domains, individual slope design per domain was not completed. In this study, a separate design was created for each individual rock mass encountered in the study area. The new overall design was based on a better understanding of the geotechnical conditions of the rock mass and thus enabled the design of optimum slopes at angles that comply with the required Factor of Safety (FOS) of 1.5. The proposed design will greatly reduce the risk of pit failures in the future. As increased geotechnical knowledge, specifically regarding hydrogeological conditions, is gained, the risk will decrease, if appropriate measures are put in place.

1.3 Terminology for Slope Design

The terminology used in this report related to pit slopes is provided in Figure 1.3. The diagram explains the different parts of an open pit slope, and shows the difference between overall and inter-ramp slope angles.

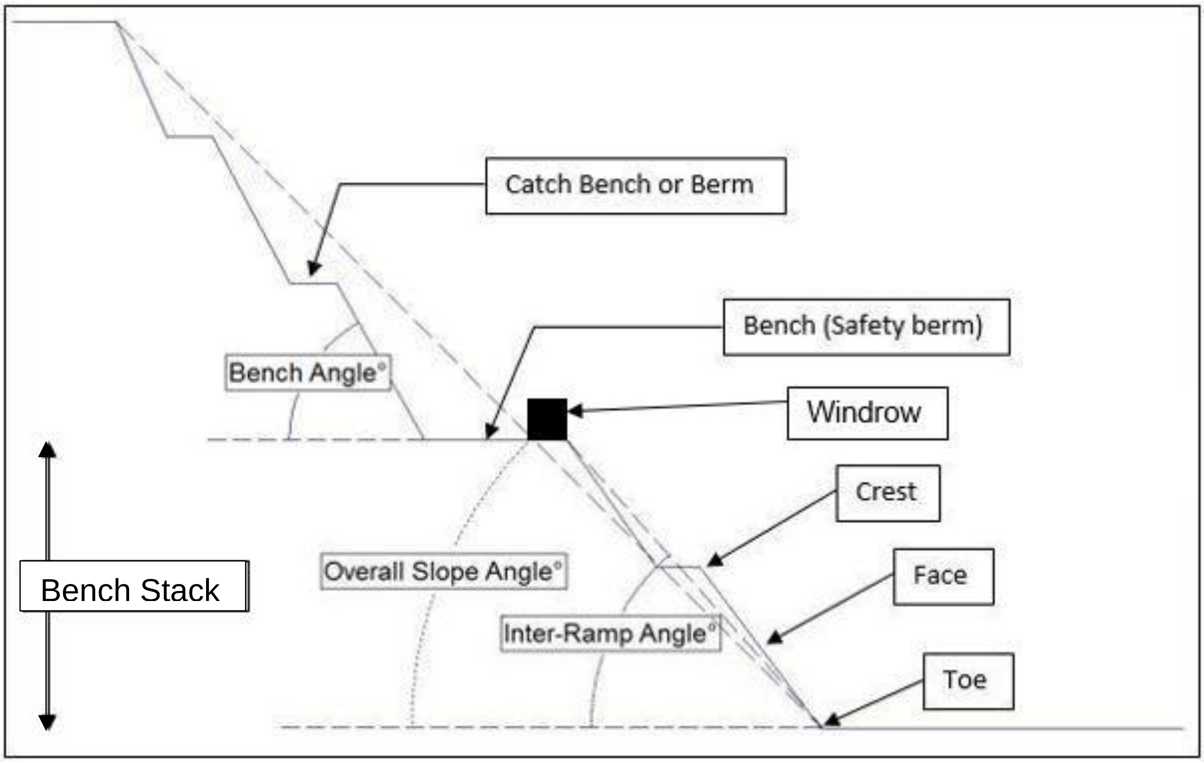

Figure 1-3 Section showing bench configuration terminology for open pit slope design

1.4 Problem Statement

A low level of confidence is attributed to the previous slope design, considering low-level geotechnical model confidence, with regards to overall slope angles, inter-ramp/stack angles, and bench angles and heights. The risk of inadequate design was also exacerbated by poor blasting practice.

1.5 Assumptions

The ground-water will not affect stability in the rockmass if proper pumping arrangements are made, i.e. water pressure will not build up in discontinuities if sufficient pumping facilities are available to keep the bottom of the pit dry. However, it is strongly recommended that piezometers be installed strategically to minimize the risk. Instrumentation used to monitor pit slope movements will be able to give sufficient warning of a pending failure, so that danger to workers is kept to international accepted levels..

2 LITERATURE REVIEW

The process of slope design in open pit slopes is one that has been evolving since the initial research by Talobre (1967). The process has been changed and enhanced by many well-respected authors throughout the years but the framework as well as the philosophy behind slope design, as described by Bieniawski (1992), has endured. A ten-step design process and the philosophy of six design principles was proposed by Bieniawski (1991). The ten-step process below is adapted from Bieniawski's (1991) work:

- **Step 1** : **Statement of the problem** – Performance Objectives (Design Objectives)
- **Step 2** : **Functional Requirements and Constraints** – Design Variables and Design Issues
- **Step 3** : **Collection of Information** – Geological Site Characterization, Rock Properties, In-Situ Stress Field, Groundwater, Applied Pressures
- **Step 4** : **Concept Formulation**
- **Step 5** : **Analysis of Solution Components** – Analytical Methods, Monitoring Methods, Empirical Methods
- **Step 6** : **Synthesis and Specifications for Alternative Solutions** – Shapes and sizes of excavations and associated stability factors
- **Step 7** : **Evaluation** – Performance Assessment including consideration of design concerning non-rock engineering aspects: power supply etc.
- **Step 8** : **Optimization** - Performance Assessment including consideration of design concerning non-rock engineering aspects: power supply etc.

- **Step 9** : **Recommendation** – Feasibility design; Preliminary design; Final design
- **Step 10** : **Implementation** – Efficient construction and monitoring

Steps one to four are generally where most of the main design inputs are gathered and formulated. Of possibly the most importance in this approach is the concept formulation stage (Step four), as this is the step that will have the greatest effect on direct value-added. The impact is clearly illustrated in Figure 2.1. During the pre-feasibility stage, if the conceptualisation of the problem is good, the value-added, in the long run, is high (as seen by the blue line curve). Conversely, if the conceptualisation of the site conditions is poor (orange curve), there will be very little value-added and the operation could end up with an incorrect design, which no matter how well implemented will never achieve the level of value as that of a well-conceptualized site (van der Wijde, 2008).

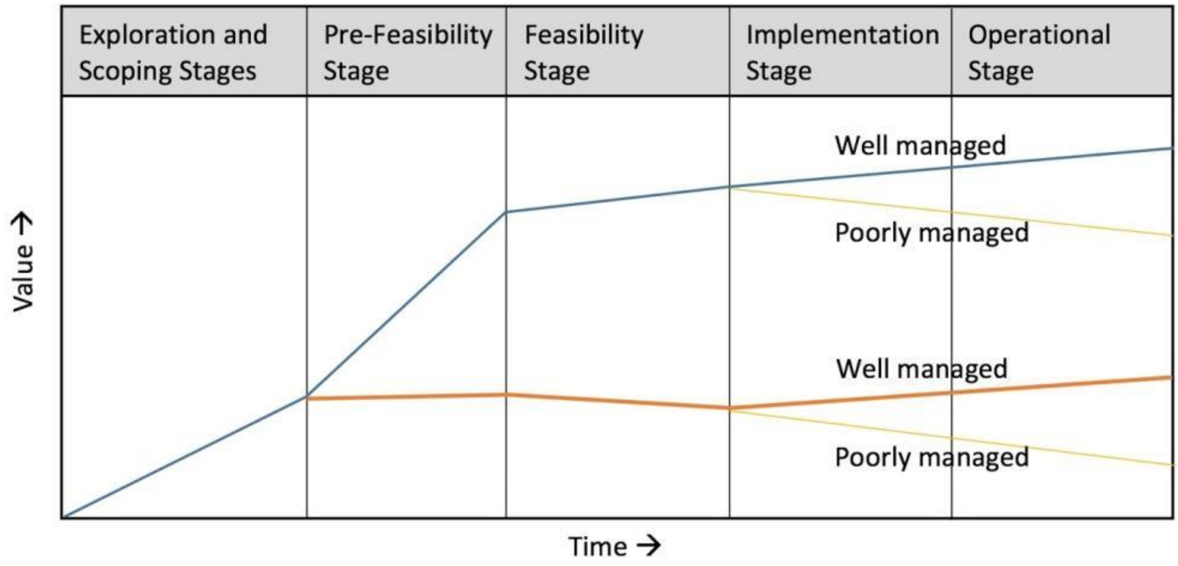

Figure 2-1 Project flow and performance after van der Wijde (2008)

In addition to the ten-step design methodology, an additional 6 principles of design were proposed to act as a guiding philosophy to engineers during the design process (Bieniawski, 1992). The six design principles are shown below:

- **Design Principle 1** : Design Objective Principle – Clear design objectives and the independent functional requirement completely characterised problem definition for a specific need
- **Design Principle 2** : Minimum Uncertainty Principle – The best design is one that poses the least uncertainties. The geotechnical data must be sufficient and traceable to the design objectives as well as to the design solution
- **Design Principle 3** : Simplicity Principle – The complexity of any design solution can be minimized by subdividing the system into components and creating the fewest number of these components forming a part of the overall design solution

- **Design Principle 4** : State-of-the-art Principle – The best design maximizes technology transfer of state-of-the-art research and best industrial practice
- **Design Principle 5** : Optimization Principle – The best design is the optimal design which is evolved from the quantitative evaluation of alternative designs, including cost considerations
- **Design Principle 6** : Constructability Principle – The best design facilitates the most efficient construction of the rock engineering structure by selecting the most appropriate construction method and sequence

Using this baseline as design methodology, the process flow for slope design was introduced in the Guidelines for Open Pit Slope Design (Read and Stacey, 2009). Here, the ten-step process was condensed into the following seven-step approach and a slope design flow chart was added (Figure 2.2) for guiding data collection, analysis and implementation (Read & Stacey, 2009).

- **Step 1** : Formulation of a geotechnical model for the pit area
- **Step 2** : The population of the model with relevant data
- **Step 3** : Division of the model into geotechnical domains
- **Step 4** : Subdivision of the domains into design sectors
- **Step 5** : Design of the slope elements in the respective sectors of the domains
- **Step 6** : Assessment of the stability of the resulting slopes in terms of the project acceptance criteria
- **Step 7** : Definition of implementation and monitoring requirements for the designs

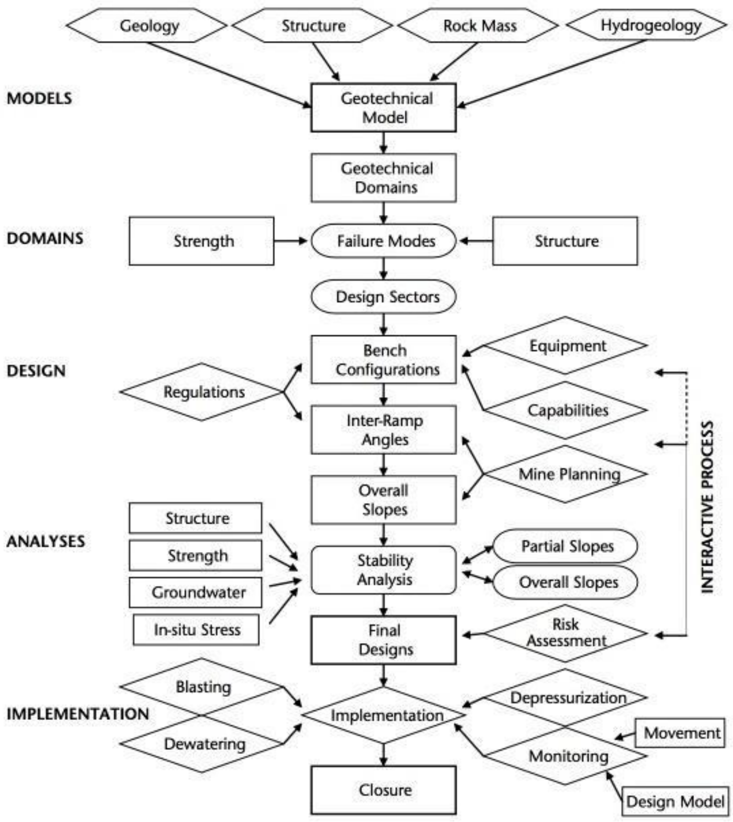

Figure 2-2 Slope design process after Read & Stacey (2009)

Read and Stacey (2009) proposed that a geotechnical model should be constructed before any slope design. This allows for a good conceptualisation of rock mass behaviour and thus accurate recommendation of slope angles. For the establishment of such a geotechnical model, four fields of study or pillars of understanding were suggested (Read & Stacey, 2009). These include:

- Geology,
- Structure,
- Rock mass conditions and
- Hydrogeological conditions.

These four pillars ultimately would feed into the slope design process and lead to bench angle, inter-ramp angle and overall slope angle recommendations. Of main importance to this project was the collection and compilation of the data, which have formed the four above mentioned models. Also, Read and Stacey (2009) outline the level of data, which would be expected at the different stages of a project. Although these are not exhaustive, they do serve as a good guideline to direct geotechnical studies on any project into conceptualisation phase.

2.1 Geology Model

The conceptualisation of the geological conditions is critical to success. The process of constructing such models differs across mining operations, but generally includes the initial field studies of regional and local geological settings, followed by further exploration studies using geophysical methods and ultimately a core drilling program (Bye, 2005). These core samples form the basis from which the 3D model for most projects is constructed. Depending on the geological confidence in the initial model created, there will either be a call for more drilling or continuous drilling and exploration (common in narrow reef mining projects). The geological model should include not only orebody models, but also the lithological units encountered during waste stripping. Although the understanding of the geological conditions is fundamental to the slope design process, it is not traditionally considered the responsibility of the slope design engineer to construct such models. What is of importance to engineering geologists, are the understanding of these models and how the formation of the orebodies and their geological changes, due to environmental and human influences, can affect slope stability (Read & Stacey, 2009).

Considering the regional geology, the three main stages of Angolan geological formation can be summarised as follows:

- Archaean orogeny, comprising the Central Shield, Cuango Shield and Lunda Shield. These Shields are mainly comprised of gabbro, norite and charnockitic complexes, constituting the Angolan basement (De Carvalho et al, 2000).
- Following basal granitic-gneiss formation is that of three Proterozoic cycles, namely the Eburnean-Paleoproterozoic, Kibaran-Mesoproterozoic, and Pan-African-Neoproterozoic cycles. The Eburnean is the most relevant of these for the Lunda Norte region as it would have been through this cycle which complex volcanosedimentary groups would have formed. Concurrently, gneisses, migmatites, granites and syenites would also have intruded through the basal granites as dykes, batoliths, lopoliths and sills. Post Eburnean cycle would have been the Kibaran cycle characterised by major extensional events specifically near the border of the Congo Craton. These events were followed by clastic-carbonatic sequences and local basic magmatism. The final cycle or Pan-African orogeny cycle has been postulated to have developed concurrent with the development of Gondwana and has produced some spectacular fold belts and granitic intrusions (Cruz, 2012).
- The final stage in Angolan geological formational events is the deposition of Phanerozoic sedimentary sequences. These have been found to rest unconformably on the basal granitic-gneiss and intrusion surfaces of stage 2. Groups common to this formational stage are the Colonda Formation and Kalahari Sediments (Pereira et al, 2003).

The break-up of Gondwana during the Jurassic to Cretaceous age have been identified as one of the main reasons for kimberlite intrusion through the basal granite. These deep-seeded fault systems would have facilitated the flow of kimberlitic magmas, as well as other magmatic sources, to surface. A general strike trend of NE-SW persists throughout the entire region of Angola for the fault systems. As such, all kimberlitic intrusions have been found only along this strike, with diamondiferous potential increasing from the SW corner of the country and reaching its maximum in the NE regions (Reis, 1972).

The local geology is comprised of the base rock mass of the study area of basal granitic gneiss, which formed in the Archaean Orogeny. This is unconformably overlain by between two and three layers of sedimentary deposition characterised by a pebble bed base (thickness ranging between 5 cm and 1 m) and Kalahari sands above this layer. The pebbles are postulated to have originated from outcropping bedrock and Eburnian-Paleoproterozoic intrusions. The matrix of these beds occasionally can contain some reworked kimberlitic material and have proven diamond content in some formations e.g. Calonda Formation. The basal granitic-gneiss bedrock is further divided into a competent mass, a highly fractured portion above this and finally highly weathered saprolite. Adjacent to the kimberlite pipe intrusion is pre-kimberlite intrusions of dolerite dykes as well as amphibolitic dykes into the basal rock mass.

2.2 Structural Model

The structural model contains both 2D and 3D structural interpretations of the mining site. Typical geological structures forming part of this database would include discontinuities such as major and minor faults, dykes and other intrusions, joint systems and shear zones. Traditionally, data is obtained by field investigations such as outcrop mapping or face mapping, but with the advent of methods such as photogrammetry, more and more mapping is being done in offices rather than on the rock face (Russell & Stacey, 2019).

2.3 Hydrogeological Model

Hydrogeological models entail all groundwater and surface water inflows into the project area. Data is typically gained from the drilling of monitoring wells or piezometers, from which water levels are measured, flow directions are interpreted, and yield or inflow strength is measured. The recharge characteristics and hence yield or inflow strength is usually gained through step-drawdown tests or pump tests on monitoring wells, where the borehole is pumped dry and the recharge to static water level is measured on a log time interval. Knowledge of the groundwater conditions allows for a better understanding of the level of saturation of slopes and hence stability. With this knowledge, a decision can be made to either incorporate a dewatering programme or to design slopes at shallower angles to prevent groundwater-induced failure. The hydrogeological model is traditionally constructed and maintained by a team of hydrogeologists who advise on water conditions through the project area as the slope designer requires.

2.4 Rock Mass Model

To define the geotechnical character of a project site, a knowledge of the geotechnical properties of the different rock types encountered, is necessary. To be able to accurately predict the behaviour of the rock, the base characteristics of the rock or the intact rock mass character must be known. Laboratory testing needs to be conducted to determine such properties as elastic modulus (E), Poison’s ratio (ν), uniaxial compressive strength (UCS), tensile strength (UTB), shear strength of discontinuities, Hoek-Brown constants and more. Common laboratory tests include uniaxial compressive strength test (UCS), triaxial compressive strength (TCS), Brazilian tensile strength tests (UTB), and point load tests (PLT). Advances in the analysis of laboratory test results have come through the introduction of the RocLab program suites by Rocscience (Marinos & Hoek, 2001). This allows the geotechnical personnel to gain valuable rock mass characteristics for slope design.

In addition to rock laboratory testing, it is common for most projects to have field rock mass classification continually running. These geotechnical mappings serve to verify or adjust the original geotechnical domains, usually through rock mass classification systems. Common classification systems include those of Bieniawski’s RMR (1973), Barton et al (1974), Marinos’ and Hoek’s (2005) Geological Strength Index (GSI) and Laubscher’s RMi system (1977). Each system has its merit and shortcomings, but when used together in the hands of a competent geotechnical engineer, the systems can produce good results (Marinos & Hoek, 2001). It is also important to remember that each system was designed for a different application, e.g. the Q-system was created to analyse rock masses in tunnels and provide support recommendations in the form of rock-bolts, wire-meshing or shotcrete. Rock mass classification systems put empirical numbers to variables (Bieniawski, 1991). Considering that engineering involves design and design ultimately requires the input of numbers, these classification systems allow for quantitative data output.

2.5 Geotechnical Model

Terbrugge et al (2009) stated that geotechnical databases can be separated into three different levels of study. With each increased level of study, the information about the project in the form of data confidence would increase as well (Terbrugge et al, 2009). They proposed that study levels progress from conceptual study level to pre-feasibility, and finally into feasibility level studies. Although the level of confidence in the geotechnical database could be at a minimum in the conceptual stage, enough information should be available to establish initial estimates of slope angles. For pre-feasibility stage studies, a much higher level of data confidence is required, which usually will require additional data to firm up the understanding of the rock mass conditions to be encountered (Terbrugge et al, 2009). Within this level, it is appropriate, according to Terbrugge et al (2009), to advise the relevant stakeholders in the project on risks associated with the development of the project and present alternative mine plans (Stacey, 2017). The final stage of the study, the feasibility stage, involves the final slope design recommendations based on robust geotechnical knowledge and hence a very high level of data confidence. This stage of the study will typically marry the slope angles into the resource classification. The resulting ore/waste stripping ratio should endeavour to remain within a margin of +15% to -10% financial impact on the life of mine plan, as compared to the pit shell being created based only on economic considerations. The final design should therefore aim at providing an economically feasible yet acceptably safe design (Terbrugge et al, 2009).

To illustrate better the safety implications of an increased level of geotechnical database confidence and hence a correlation between FOS and study levels stated above, Terbrugge et al (2009) presented the following two graphs.

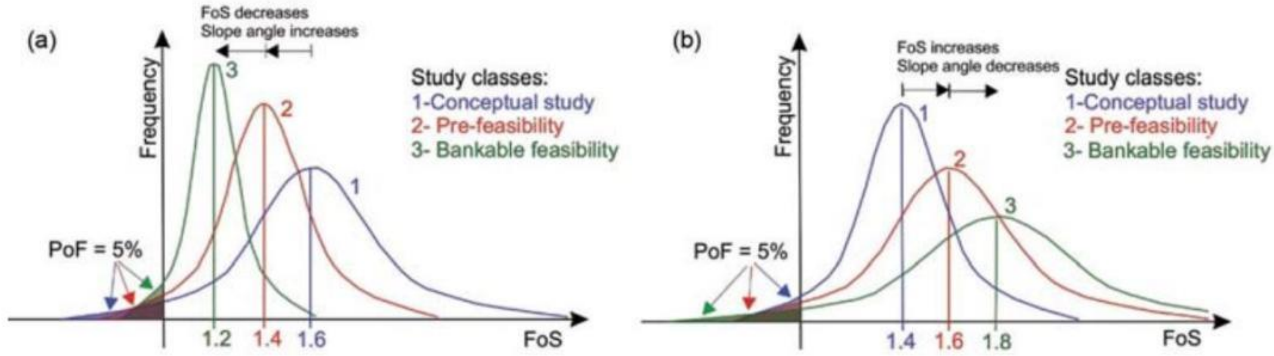

Figure 2-3 The link between FOS and increased confidence (Frequency) in the geotechnical model (Terbrugge, et al., 2009) POF = Probability of Failure

Figure 2.3 (a) shows a conservative or gentler slope angle recommendation at the beginning of the project, i.e. at the conceptual study stage. This conservative approach has a resultant FOS of 1.6. As the study level increases to pre-feasibility and finally feasibility level, the FOS decreases incrementally by 0.2. The opposite is true in Figure 2.3 (b) where a less conservative or steeper slope angle has been suggested initially. The initial approach in Figure 2.3 (b) has been a liberal one, due to low data confidence in conceptual study level. As this level of confidence in the geotechnical database increases, the FOS increases incrementally by a factor of 0.2 per stage change. The slope angle also increases in unison with an increase in FOS. It can thus be deduced from this study that FOS should be directly linked to data confidence. The higher the data confidence, the higher the confidence in the FOS, and inversely, the lower the data confidence, the lower the confidence in FOS obtained through design. If for instance, a geotechnical database has data confidence of 50% as per Read and Stacey's (2009), the FOS obtained through modelling and design will have a 50% confidence (Table 2.1), and should be conveyed to the management of operations as a level of risk.

Table 2.1 Project stage geotechnical confidence as per Read & Stacey (2009)

Project Stage					
Project Level Status	**Conceptual**	**Pre-feasibility**	**Feasibility**	**Design and Construction**	**Operations**
Geotechnical level status	**Level 1**	**Level 2**	**Level 3**	**Level 4**	**Level 5**
Target Levels of Data Confidence					
Geology	>50%	50-70%	65-85%	80-90%	>90%
Structural	>20%	40-50%	45-70%	60-75%	>75%
Hydrogeological	>20%	30-50%	40-65%	60-75%	>75%
Rock Mass	>30%	40-65%	60-75%	70-80%	>80%
Geotechnical	**>30%**	**40-60%**	**50-75%**	**65-85%**	**>80%**

Little (2006) describes a geotechnical database that was created on Potgietersrus Platinum's open-pit (now Mogalakwena Mine). This database has provided a benchmark for all geotechnical databases. In the study, the focus was to construct an organised, easily accessible and robust system for geotechnical data processing. Various software packages such as SABLE®, MineMapper 3D®, MS Access®, AutoCAD®, and Datamine® were used to process the geotechnical database. One of the greatest accomplishments of Little's (2006) study is the sheer magnitude of data that was collected, processed and output. Over 220 km of core was drilled, logged, and tested in three years; roughly 100 km of pit walls were geotechnically mapped and more than 7 000 rock tests were conducted either in the field or laboratory (Little, 2006). In a later study, Little et al (2007) estimated that the construction and implementation of this geotechnical databasing system led to a $25 million value-add to the project (Little et al, 2007). This was due mainly to the effective design based on robust data, and importantly its effective implementation by mining.

From Little (2006), it can be deduced that effective geotechnical databasing and hence the construction of a robust geotechnical model is an invaluable part of the design process and that both negative (when confidence is poor) and positive (when geotechnical confidence is good) economic effects can be determined on any project.

Successful implementation of a slope design requires an effective blasting program. Bye (2005) published quantifiable data to show the influence of blasting on highwall stability. Laubscher's (1990) modified rock mass rating system, provides a correction factor for blasting where the rock mass value is adjusted by a factor of between 80% and 94% where blasts could be described as poor to good conventional blasting, respectively.

2.6 Drilling and Blasting Practices

One method which has been adapted in the study area has been termed a barrel audit and involves quantifying the amount of pre-split barrels (half of the drilled hole remaining in the highwall) after excavation of that specific blast. In the study area, pre-split holes are spaced 1 m apart and thus over a 100 m final wall, in perfect blasting conditions assuming no highwall disturbance due to blast vibration, 100 pre-split barrels should exist. This can be translated into quantitative data through correlation with Laubscher's (1990) adjustment factor for blasting. The amount of pre-split barrels visible in the highwall over the distance blasted will give a percentage, which can be translated into the adjustment factor through Table 2.2. The barrel audit method was created on-site and has not been sufficiently investigated. However, to-date the method appears to have worked well on this mine.

Table 2.2 Correlation between pre-split barrel audit and Laubscher's (1990) MRMR blasting adjustment factor

Technique	Adjustment %	Pre-split Barrel Audit (Open Pit)
Boring	100	N.A.
Smooth-wall blasting	97	100% - 90%
Good conventional blasting	94	90% - 65%
Poor blasting	80	< 65%

3 SLOPE DESIGN PROCESS MINE A

3.1 Research Question

Considering the economic constraints on the operation due to geopolitical pressures, the capacity for robust geotechnical model creation has never been realised. Although the intention for such further studies is indicated, for the next cut-back design this information will not be fully available. The main question to be answered in this research project, was if the current geotechnical model information would be adequate for slope design. The geotechnical database was compared to Read & Stacey's (2009) project stages. This allowed for a confidence to be developed in the pit design with the available geotechnical information.

A slope design was created using manual input into charts. These slope designs were further analysed using numerical modelling software. The FOS computed through software analysis was compared to those formulated by the use of charts and suggested correction factors proposed.

3.2 Research Objectives

The objective of the research project was to recommend stable slope angles for planning the final push-backs. Design chart slope angles were verified using boundary element Examine 2D (2006) and limit equilibrium SLIDE 2D (2018) numerical modelling analyses.

3.3 Slope design Methodology in soils

The slope angles in the upper soils composed of Kalahari Sands, Saprolite and Weathered Granitic Gneiss lithologies, were created through back analysis of the Hoek and Bray (1981) design charts. The chart has 5 different groundwater saturation scenarios to choose from, each influencing the allowable angle of slope. Three example Charts, with sections showing the appropriate groundwater conditions, are shown in Figure 3.1 (Stacey & Swart, 2001).

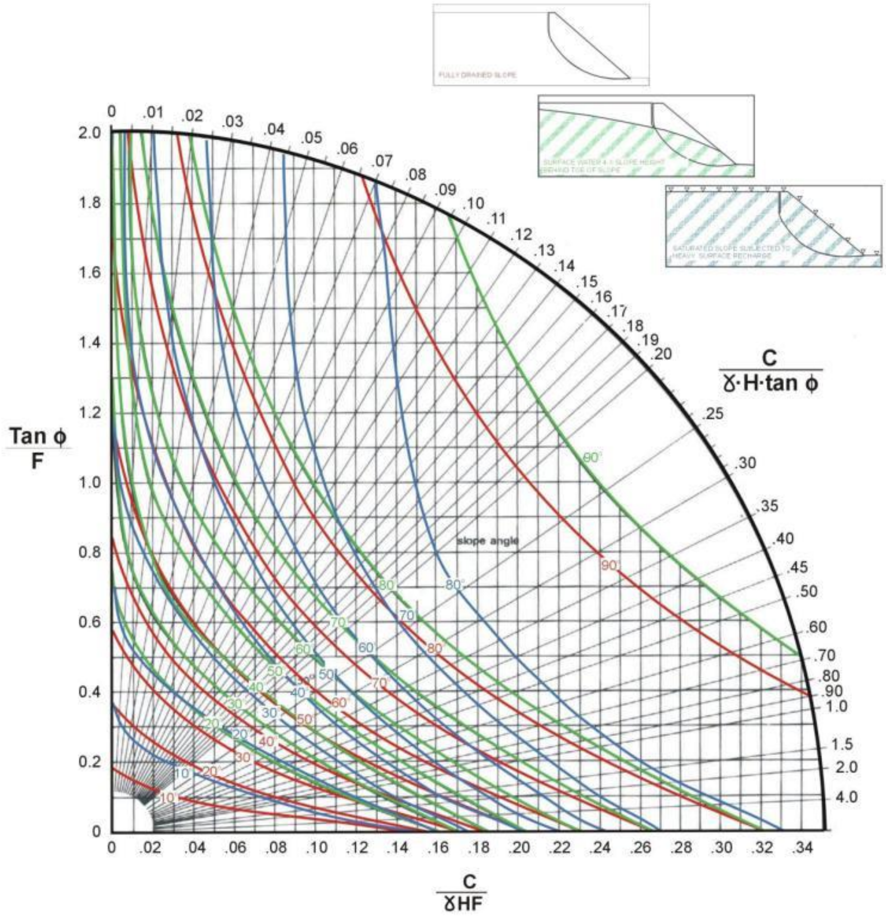

Figure 3-1 Circular failure Chart (Stacey & Swart, 2001) c. Red=dry, green=partially saturated, blue= saturated

The Hoek and Bray (1981) design charts make use of cohesion (C), internal angle of friction (ϕ) and density (γ) of the soil. These parameters are input into Equation 3.1:

$$\frac{\boldsymbol{C}}{\boldsymbol{\gamma} \times \boldsymbol{H} \times \boldsymbol{tan}\, \emptyset}$$

Equation 3.1

Where C=Cohesion; γ=Density; H=Slope Height and $\emptyset$=Internal Angle of Friction

The value obtained is identified on the graph and a straight line is drawn from this number to the graph vertex on the bottom left of the graph. The factor of safety and friction angle soil parameters are then used in Equation 3.2:

$$\frac{\mathbf{tan}\, \emptyset}{\mathbf{FS}}$$

Equation 3.2

Where $\emptyset$=Internal Angle of Friction and FS= Factor of Safety

This value is then identified on the y-axis (Figure 3.1). A horizontal line from this number is then drawn to intersect the previously drawn line (Figure 3.1). Where the two lines intersect, the suggested angle of the slope is determined using the curved lines shown in the figure. This is further demonstrated in Chapter 5.

3.4 Previous experience in the soil slopes

In the first mining cut-back, face angles were cut at 90˚ which proved to be unstable for these units. Minor circular failure occurred in the upper layers and the face angle was then adjusted to 45˚ in the subsequent mining cut-backs. The overall slope angle in the first three mining cut-backs within the upper soil layers was 37˚. Although large rainfall events have gouged the faces of these lithological units, and potholes were created behind some of the faces due to this gouging, the slopes have performed well with no mass failure. In the selection of the correct Hoek and Bray (1981) chart to use for back-analysis, it was considered that groundwater seepage has been mapped at the toe of the lowest weathered granitic gneiss bench. It was thus assumed that a groundwater saturation level similar to that found in Chart 2 (Figure 3.2) is possible.

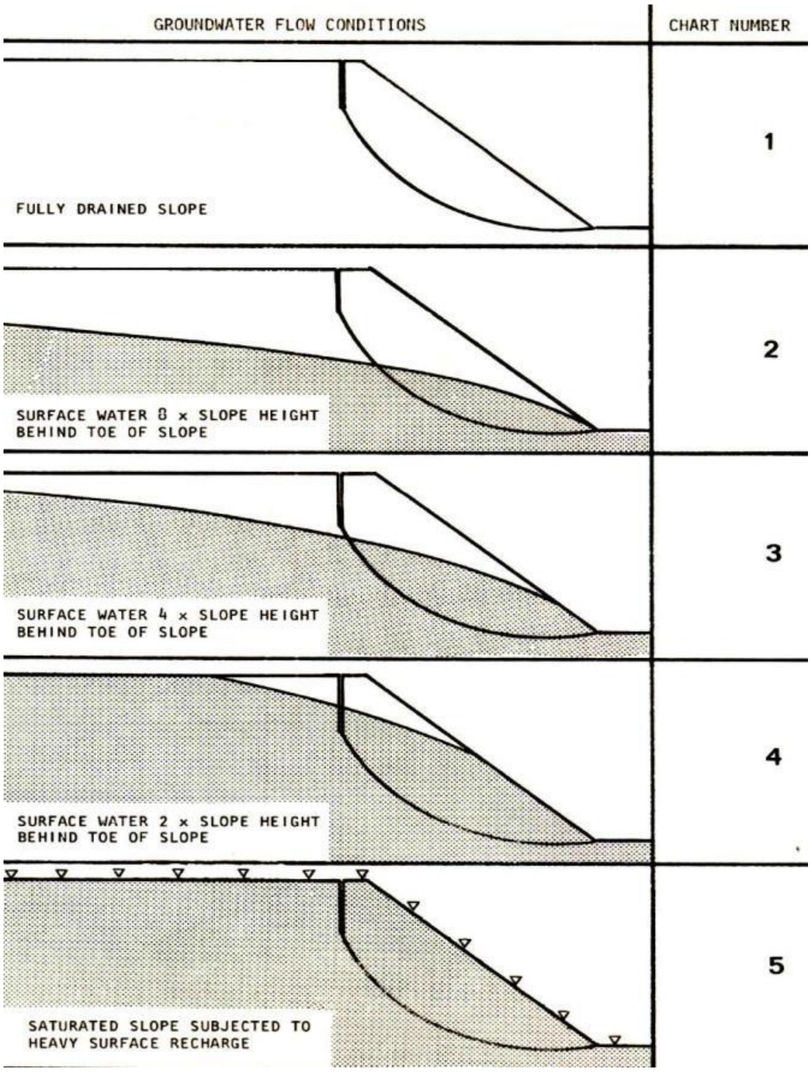

Figure 3-2 Sections showing groundwater saturation scenarios from Hoek and Bray (1981)

3.5 Geotechnical Model Creation Methodology

A robust geotechnical model was described in Read and Stacey (2009), which consists of four pillars. These are the geology model, structural model, rock mass model, and hydrogeological model.

3.5.1 Geology Model

The geological model of the orebody has been constructed during the exploration phase drilling of the operation. During this exploration drilling, no core holes were drilled outside of the kimberlite pipe margin and thus the understanding of the country-rock is of low confidence. For lithological intersections, pit walls have been mapped and through extrapolation of the intersections of the first cut with the second cut's lithological intersections, a 3D waste rock model was created.

3.5.2 Structural Model

Phase one characterisation (pre-feasibility level study) has been completed by line and window mapping of the pit faces of Cut 2 in the main pit. These mappings feed into the 3D structural geological model creation in Micromine (2019) as well as the creation of Geotechnical Domains based on fracture frequency, Intact Rock Strength (IRS) and Joint Condition (Jcon) as per the Laubscher (1990) rock mass classification system. Since face mappings are a limited view of discontinuity intersection due to extrapolation disparities, the extension of such discontinuities into virgin rock is not considered to be as accurate as would be gained from a drilling program. The location and orientation of such discontinuities in the extrapolated virgin rock is thus assumed to be of a much lower accuracy than if the model was developed through a dedicated geotechnical core program.

3.5.3 Rock Mass Model

Unfortunately due to financial and geopolitical circumstances, drilling was not completed as initially anticipated. In an ideal situation, a program of geotechnical core drilling, logging and testing of the waste rock would be used for such characterisation. Drilling would have also firmed up the data gap in the geological model with regards to different lithological intersections. To bolster the lack in drilling information, a greater emphasis on pit face mapping was made. The design approach described in Chapter 2 and shown in Figure 3.3 (b) is the most appropriate to the site.

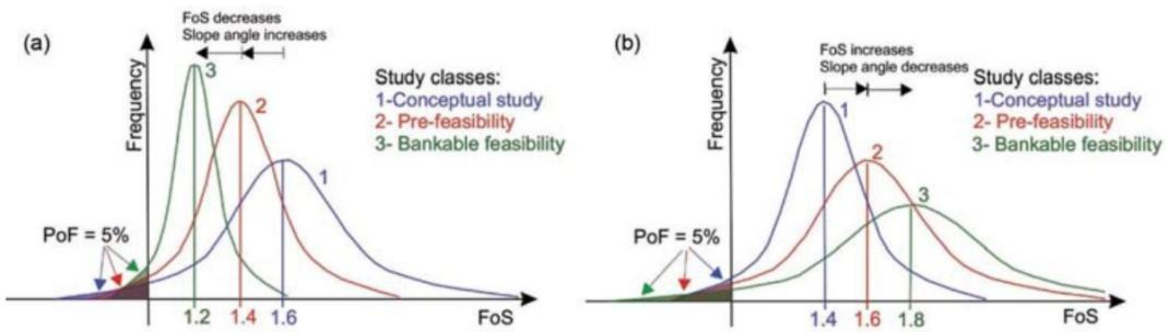

Figure 3-3 The link between FOS and increased confidence (frequency) in the geotechnical model (Terbrugge, et al., 2009) POF = Probability of Failure

The main method of rock mass characterisation of the jointed rock mass (granitic gneiss country rock) was through window mapping of the geotechnical domains. The rock mass classification methods which were used for rock mass characterization in this study, are those of Bieniawski's (1973) RMR and Laubscher's (1990) MRMR system. Laubscher's (1990) MRMR is calculated by input of relevant rock mass parameters into Equation 3.3 and 3.4:

$$\boldsymbol{RMR} = (\boldsymbol{IRS}) + (\boldsymbol{FF}) + (\boldsymbol{Jc}) \quad \textbf{\textit{Equation 3.3}}$$

Where $\boldsymbol{Jc} = (\mathbf{40} \times \boldsymbol{Jma} \times \boldsymbol{Jmi} \times \boldsymbol{Ja} \times \boldsymbol{Jf})$ ***Equation 3.4***

Where: IRS = Intact Rock Strength; FF = Fracture Frequency Jc = Joint Condition; Jma = Large Scale Joint Expression; Jmi = Small scale Joint Expression; Ja = Joint Wall Alteration and Jf = Joint Filling.

The RMR system assigns a rock mass rating based on rock mass joint conditions (joint frequency and joint condition), groundwater conditions and intact rock mass strength. The obtained RMR was then further adjusted according to the Laubscher (1990) MRMR system by multiplying the RMR by correction factors for joint orientation w.r.t. excavation faces, blasting factors and weathering conditions (Equation 3.5).

$$\begin{aligned}\boldsymbol{MRMR} = \boldsymbol{RMR} &\times \boldsymbol{Blasting\ Adjustment} \times \\ &\boldsymbol{Weathering\ Adjustment} \times \\ &\boldsymbol{Joint\ Orientation\ Adjustment}\end{aligned} \quad \textbf{\textit{Equation 3.5}}$$

The product of the adjustments produced an MRMR which can be used for input into the Haines and Terbrugge (1991) design charts.

To increase data confidence in the current geotechnical database of the study area, infill drilling was suggested to improve the 3D understanding of the rock mass model. Infill drilling is the drilling of additional core holes between the already completed patterns. However, due to financial and geopolitical circumstances, no further core drilling was done before the third cut back. The poorly understood rock mass units were therefore sampled using grab samples from the existing pit. These samples were drilled into 50mm diameter cores on a milling machine and subsequently tested with a point-load tester.

3.5.4 Hydro Geological Model

There are currently no piezometer instruments for monitoring groundwater, but there are plans for a drilling program in the future. Ideally, the initial piezometers should be installed in the locations WP01 to WP05, as indicated in Figure 3.4.

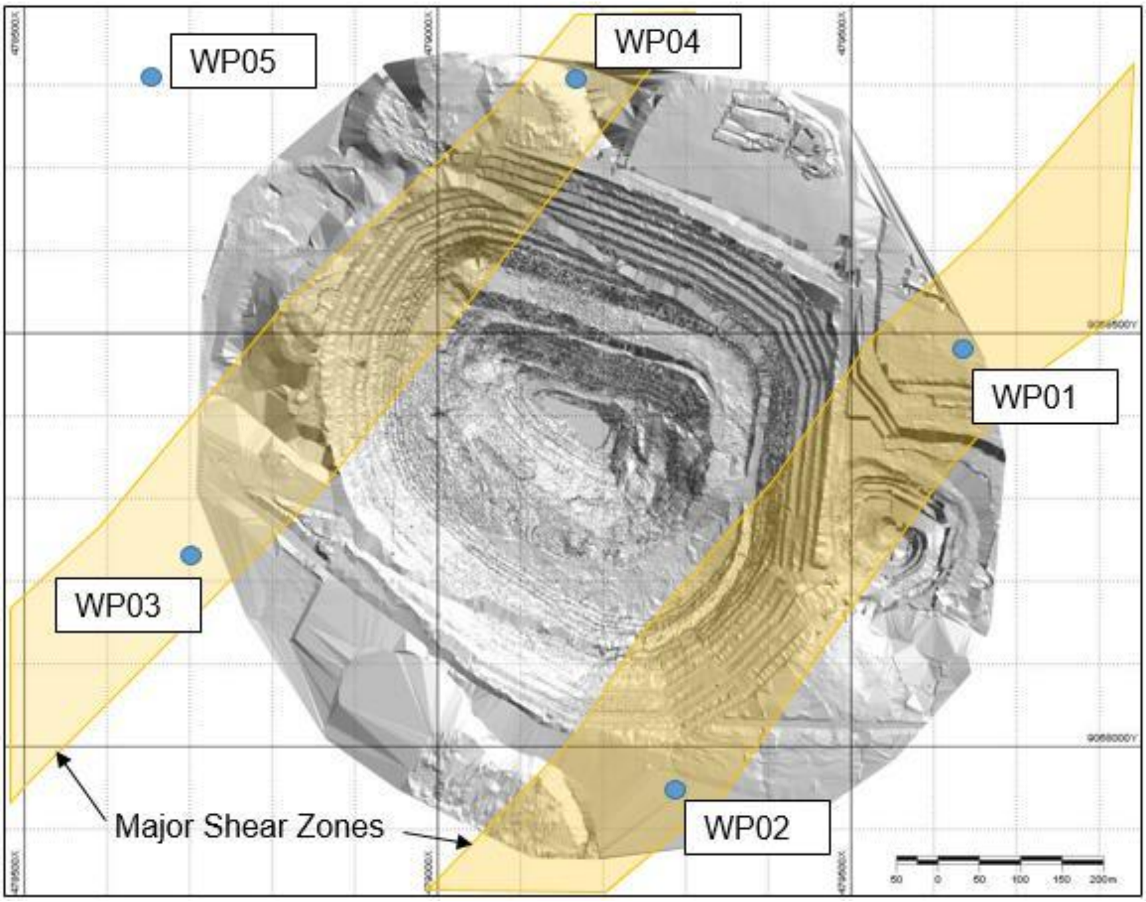

Figure 3-4 Plan of ideal locations for installation of groundwater piezometers

An improved understanding of the hydrogeological character for this study was therefore made by mapping the groundwater seepage into the pit. Inflows at all points were measured and the hydrogeological character was estimated from this data.

3.6 Slope Design Methodology in rock

The bench stack angles for the different rock mass lithological units in the main pit were estimated using the Haines and Terbrugge (1991) Slope Design Chart (Figure 3.5). This was achieved by use of Bieniawski's (1973) RMR classification and further adjusting these ratings to Laubscher's (1990) mining rock mass classification system using Equation 3.3.

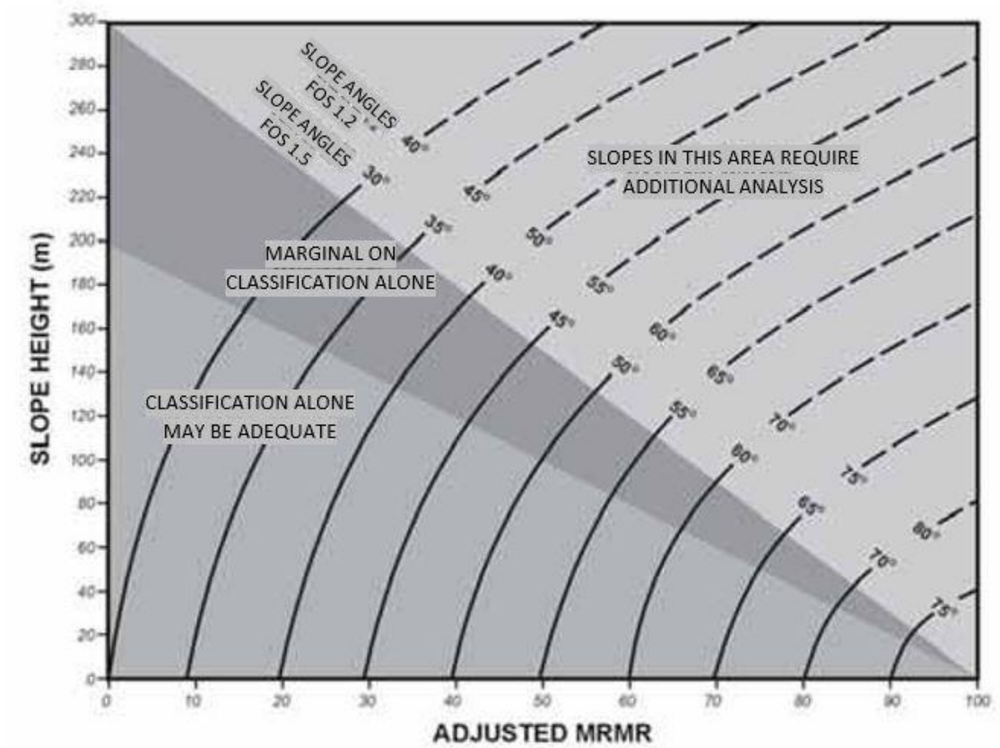

Figure 3-5 Slope Design Chart after Haines and Terbrugge (1991)

The slope angle was determined from Figure 3.5 by drawing a vertical line up from the appropriate adjusted MRMR, and a horizontal line across from the appropriate slope height. The point of intersection of these two lines provided the slope angle by reading off the angle from the curved lines, or the applicable angle between the curves. The angles at the top of the solid curves represents a FOS of 1.5, whereas the values provided at the bottom of the dashed curves show the angles applicable to a FOS of 1.2 (Figure 3.5). The angles are appropriate to both the solid and dashed lines.

Considering the competence of the country-rock and the expected overall height exposed in the next cut, rock mass classification alone was inadequate for overall slope angle determination (Haines and Terbrugge, 1991) and further analysis through numerical modelling techniques was required. A FOS of 1.5 was used to determine stable slope angles specifically considering the geotechnical data confidence level.

Indirect UCS values were obtained for each individual kimberlite domain through point-load testing. Each domain underwent 10 tests to be converted to UCS values using a correlation factor C determined by comparing the average UCS results to the average PLT results, in zones where UCS tests were done. These values were then used in Laubscher's (1990) geomechanics classification, which makes use of the strength of intact rock material, RQD, Spacing of joints, condition of joints, groundwater and strike and dip orientations of joints to gain an RMR value. The RMR was further adjusted into an MRMR through Laubscher's (1990) rock mass classification and finally, input into the Haines and Terbrugge (1991) Chart. Average MRMR values were used in the Haines and Terbrugge (1991) Chart for the country rocks and the kimberlites, to determine two separate slope angles.

These bench stack angles were then input into a cross-section along the North-West to South-East and another along the South-West to North-East. The limit line of economic feasibility was used as a guide for where the pit bottom should end and bench stack angles for each of the two lithological units were then interpolated upward from this lower limit. The cross-sectional design which was created, was input into the numerical modelling analyses SLIDE 2D (2018) and Examine 2D (2006). These analyses were used to validate the design.

3.7 Previous Kimberlite Failure Back-Analysis

As stated in the introduction, failure has occurred in the kimberlite benches of the previous mining cut-back. Of specific note is the failure which occurred on the 31st of October 2018 in the Eastern walls of the pit. The failure occurred in the kimberlite portion classed as Volcanoclastic Kimberlite Breccia (VKB) and consists of interlayered kimberlite Domain 2 and kimberlite Domain 6. Kimberlite Domain 2 here is present as high grade kimberlite lenses, while kimberlite Domain 6 has been identified as the brecciated country rock mass which slumped into the cone during formation. After failure, a consulting firm was contracted to assess the failure as well as recommend remediation strategies for the failure (SRK, 2018). It was found that due to the complex interlayering of weaker kimberlite Domain 2 and stronger Kimberlite 6, in conjunction with a higher rainfall season, squeezing of the weaker kimberlite Domain 2 lenses occurred with ensuing failure. The long term recommendations which were made in this report (SRK, 2018) for remediation of such failure in the future, constituted a re-design of the overall slope angles within the kimberlite portions of the pit. The slope angle within the kimberlite domains at the time of the failure was 52˚ crest-to-toe angle.

4 GEOTECHNICAL MODEL

4.1 Geology Model

4.1.1 Mine A main pit ore model

The geological model for the Mine A main pit kimberlite pipe in previous years was purely focussed on ore characterisation, with little to no regard for the change in lithological units in the country rock surrounding the kimberlite intrusion. For the delineation of the kimberlite domains in this pipe, and to create the three dimensional (3D) ore model, 7 060.5 m of diamond core was drilled and logged (see Appendix B). The core was logged and an ore model was created by an external ore modelling consulting firm. Kimberlite domains which showed the same mineralogical character were grouped. All three types of kimberlites, as designated by formational processes, are found in this pipe, namely Volcanoclastic Kimberlite Breccia (VKB), Pyroclastic Kimberlite (PK) and Reworked Volcanoclastic Kimberlite (RVK). The domains created, however, have not been classed according to these formational origins, but have rather been separated into mineralogically unique domains. Further to the initial characterisation by the ore modelling consulting firm, monthly domain in-pit mapping takes place to serve as quality assurance and quality control (QAQC) and to consolidate expected versus actual domain volumes. A 3D representation of the ore body is presented in Figure 4.1:

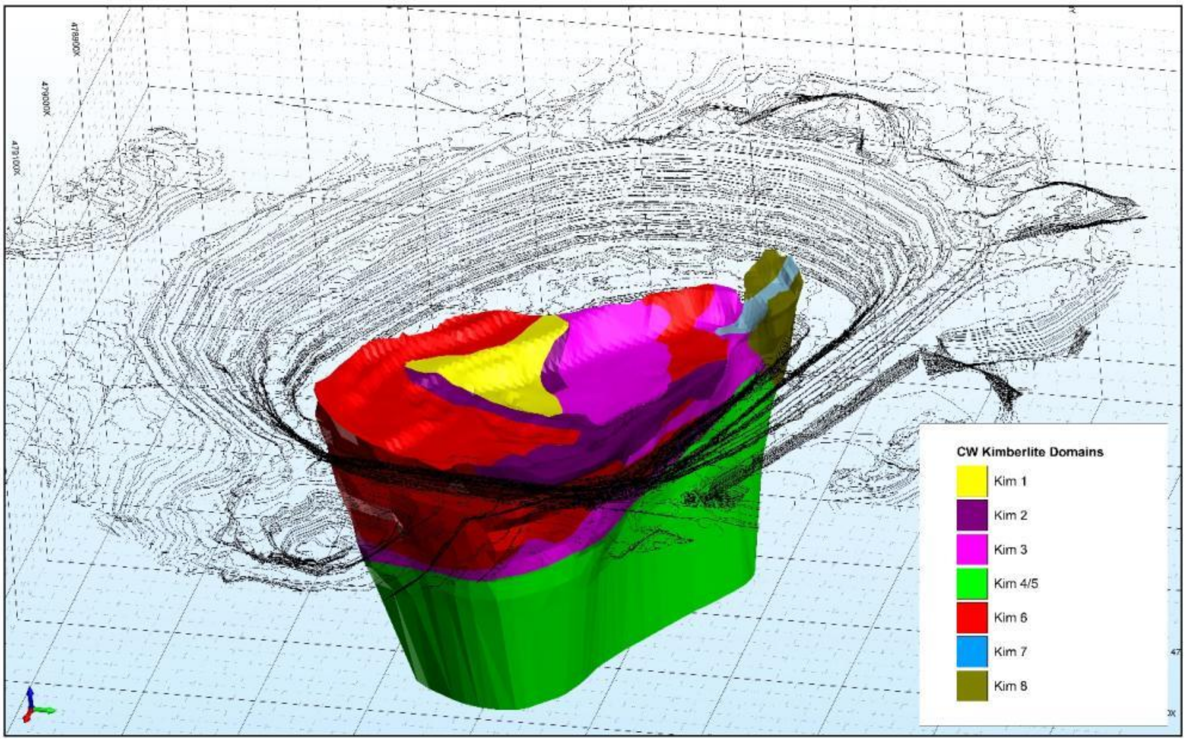

Figure 4-1 Ore Model of the Mine A main pit Kimberlite Pipe Domains in Micromine

4.1.2 Mine A main pit waste model

The ore component of the geological model is thus well understood, but the waste rock component prior to this study was fairly unknown. Considering the lack of core holes outside of the pipe margin, accurate lithological modelling of the country rock has not been possible. To construct a rough model of these different units, face mapping was done on the existing pit surface, and extrapolated. These extrapolations were completed in Micromine and an image of the 3D representation of this is provided in Figure 4.2:

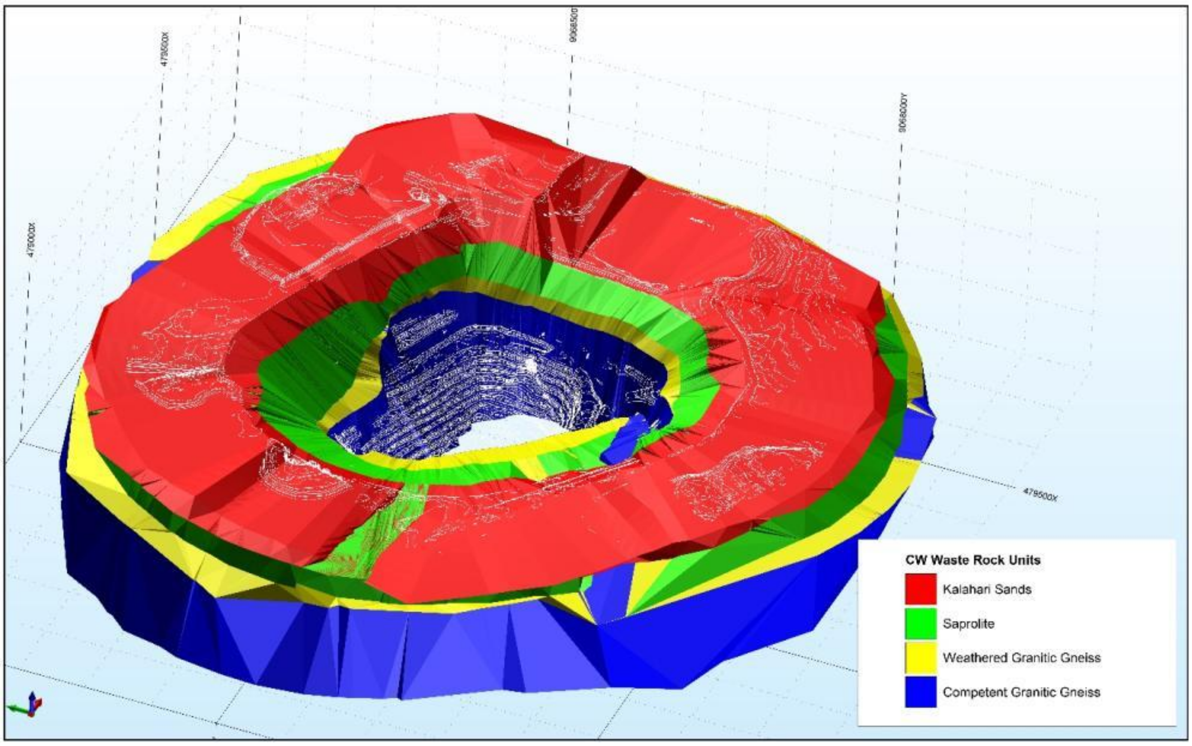

Figure 4-2 3D Waste Rock Model of Mine A Main Pit in Micromine

As indicated in the legend, the basal granite is subdivided into three parts. The upper highly weathered granitic-gneiss remnant (saprolite), the mid-layer of fractured and weathered granitic-gneiss (ranges between 15 m and 30m in thickness) and the competent or fresh granitic-gneiss basal rock mass. Unconformably overlain by the saprolitic material, the Kalahari Sands group consists of a thin pebble bed base layer and upper red sands.

4.2 Structural Model

Due to the absence of geotechnical core, there was no initial structural map created before excavation. For the structural map to be created, mapping was done on the existing pit walls through line mapping. The line of intersection for all structures was captured from the toe of all bench faces. These intersections have been marked, surveyed and input into the 3D software database in Micromine. The character of each feature was determined to corroborate data continuity from consecutive mining cuts and thus create extrapolated planes. Figure 4.3 shows the plan view of the structural map that was created using the structure intersection of the second mining cut-back. The 3rd cutback structural intersections can only be tied into Cut 2 once all faces in Cut 3 are exposed.

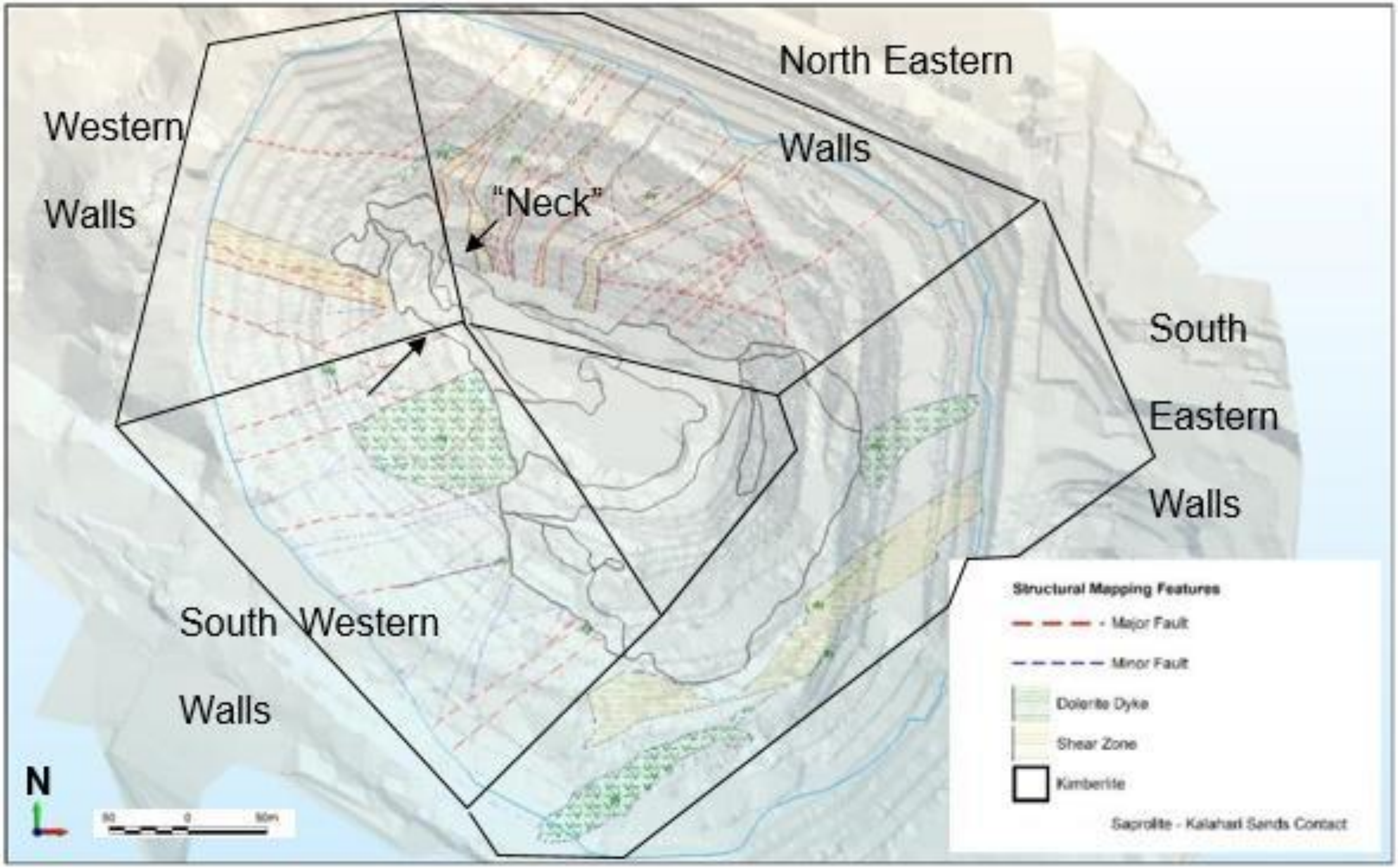

Figure 4-3 Initial Structural Map of Mine A main pit (2nd Cut back)

From Figure 4.3 it can be seen that structures were only extrapolated to the blue line, representing the Saprolite and Kalahari Sands contact. Figure 4.3, therefore, only showed the known extent of the exposed structural rock mass at the time of mapping. In addition to the four macro-scale discontinuity zones presented in Figure 4.3, ten isolated geotechnical domains indicating different kinematic failure situations will be discussed in section 4.2.5.7.South Western walls.

4.2.1 South Western walls

The South Western walls of the pit are dominated by high angle faults and dyke structures striking near parallel to the regional discontinuities. These discontinuities are in alignment with the pervasive deep-seeded fracture systems described in the regional geology (Section 4.1.1), striking generally NE-SW. Where the major dolerite dyke is found adjacent to the kimberlite intrusion, some sub-horizontal discontinuities are observed with a strike near perpendicular to the regional rock discontinuities. It is postulated that the dyke and fault systems in the country-rock would have occurred prior to kimberlite intrusion since none of the structures enter the kimberlite.

4.2.2 Western Walls

The major structures found in the North Western part of the pit, strike near perpendicular to the regional foliation. This could be an indication that they have been formed as part of the intrusion process through the force exerted on the country rock during volcanoclastic events. Kimberlite 8 (a pyroclastic type kimberlite) forms a neck area to the North-West extremity. The kimberlitic event was dated as post main pipe intrusion (Pereira et al, 2003), and would have provided the gas releasing force required to create the shear zone and subsequent faults encountered here.

4.2.3 North Eastern walls

The general strike of the major structures present is aligned with the regional NE-SW foliation. All structures are postulated to have formed prior to kimberlite intrusion, syn-orogeny of the granitic-gneiss basal rock mass. Towards the further eastern side, some sub-horizontal structures started surfacing in the second cut-back indicating the presence of possible intrusion magmas, prior to kimberlite emplacement. On the third cut-back, a dolerite dyke was intersected in the highwalls in the same place, substantiating the predictions made in the second cut-back.

4.2.4 South Eastern walls

To the South Eastern part of the pit, another dyke is found running parallel with the shear zone that strikes WSW-ENE. This dyke is postulated to have occurred around the same time as the first dolerite dyke and concurrent with the shear zone. Auxiliary dyke stringers are found through the rock discontinuity towards the upper part of the South Eastern zone. These are postulated to link in with the major dyke running congruent with the shear zone and may converge with depth to the same source. The main shear zone which is identified as the yellow shaded area in Figure 4.3 is striking roughly at 225˚ and dips between 70˚ and 90˚ away from the pit centre. Intersections of excavation benches create conditions conducive for toppling failure and will be further discussed in Section 4.2.5.7.

4.2.5 Rock joint discontinuity analysis

All joint systems were recorded and measured through window mapping of the different geotechnical zones. These systems were plotted on stereonets through the geotechnical analysis software, DIPS (2013) and an average plane was constructed using great circles. In the same program, these joint systems were analysed for failure probability. Using the excavation face dip and dip direction and well as the internal angle of friction, the program was used to predict the probability of certain types of failure mechanisms. These include wedge failure, planar failure and toppling failure. These results are discussed further in Appendix D as part of the Slope Stability Monitoring Strategy. The stereonet in Figure 4.4 is a summary of the individual geotechnical domain stereonet analyses and represents all the joint sets present in the main pit. Each joint set is discussed further in the following section.

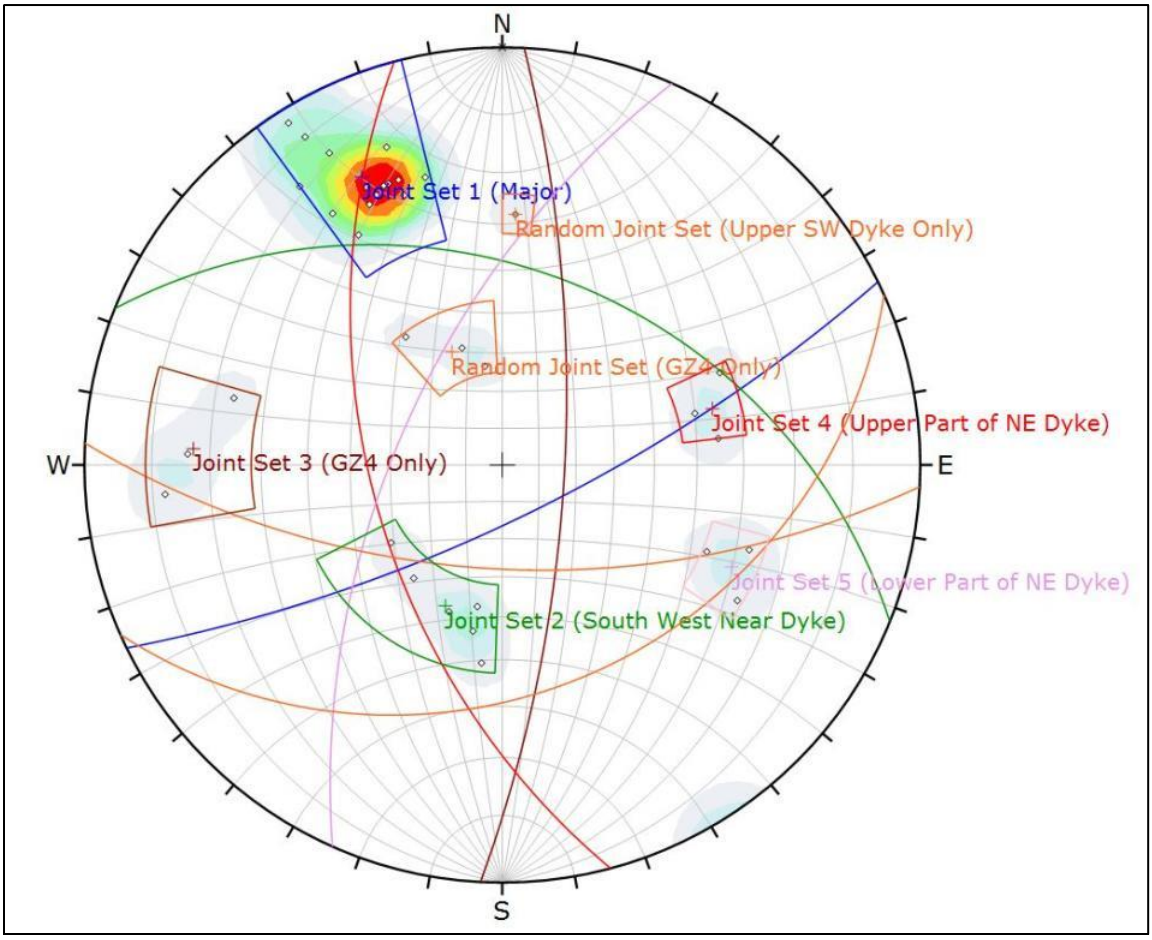

Figure 4-4 Stereonet of joint set poles encountered in the main pit

4.2.5.1 Joint Set 1 (J1) – 66-88˚ Dip / 144-165˚ Dip Direction (Major)

This joint system is pervasive throughout all geotechnical domains in the pit and is in concurrent strike with the regional NE-SW striking rock discontinuities. The system maintains a high dip angle throughout the study area, in places reaching near vertical. The joint condition of this system is characterised by joints with a large scale expression of curved to slightly undulating display. Small scale joint expressions are commonly rough undulating to smooth undulating. The joint wall alteration is weaker than the wall rock, but not weaker than the filling, with fillings of finely sheared country-rock in certain areas, but overwhelmingly characterised by only surface staining. This joint system is considered the major system in the direct mining environment.

4.2.5.2 Joint Set 2 (J2) – 36-44˚ Dip / 010-050˚ Dip Direction (Localised Minor)

Joint system 2 is localised around the dolerite dyke found on the SW side of the main pit, as indicated in the structural map (Fig.4.3). The joints are shallow-dipping around this dyke, possibly a product of the dolerite dyke intrusion. On a macro scale, the system shows curved to slightly undulating strikes. Micro expressions of the joints show slickensided undulating to rough planar. No alteration, apart from staining on the joint walls, or infill were observed.

4.2.5.3 Joint Set 3 (J3) – 67-78˚ Dip / 085-104˚ Dip Direction (Localised Minor)

J3 was only found on the western extremity of the excavated study area and thus has been classed as a localised minor joint system. This system is postulated to have formed through the intrusion of Kim 8 (see Figure 4.1), a pyroclastic type kimberlite which intruded post main pipe formation and is found in the “neck” area on the western pit limit. This random joint set combines with J1 and J6 to form wedge and block conditions in the western pit limit. The joint system surface conditions display curved to slight undulation on large-scale expression, with rough or irregular to smooth stepped on small scale expression. No alteration is visible on joint walls and no joint filling is present.

4.2.5.4 Joint Set 4 (J4) – 51-59˚ Dip / 247-263˚ Dip Direction (Localised Minor)

Joint systems 4 and 5 are linked in that they are both localised in the region of the NE major dolerite dyke (see the Dyke in the South Eastern Walls in Figure 4.3). J4 is found predominantly in the upper part of the dyke intrusion and changes into J5 90 m below the surface of the pit. The low angle joint system is postulated to have formed from the horizontal stresses generated by the dolerite dyke intrusion, in this region. The joint system surface conditions display multi wavy direction large-scale expression, with rough or irregular to smooth stepped small scale expression. No alteration is visible on joint walls and no joint filling is present.

4.2.5.5 Joint Set 5 (J5) – 55-66˚ Dip / 293-300˚ Dip Direction (Localised Minor)

As indicated in the description of J4, J5 has been encountered below the J4 joint system and is postulated to be part of the same family, but having a steeper dip and slightly altered strike. The joint system surface conditions display multi wavy direction large-scale expression, with rough or irregular to smooth stepped small scale expression. No alteration is visible on joint walls and no joint filling is present.

4.2.5.6 Joint Set 6 (Random) – 42-51˚ Dip / 006-143˚ Dip Direction (Localised Minor)

This random joint system is present in very small localised areas. The extent is about 10 m -15 m and is only found near the major dyke in the SW and the NW corner of geotechnical Domain 4. Both are postulated to have formed subject to intrusive events of the major dolerite dyke and Kim 8 pyroclastic intrusion in the "neck" area (Figure 4.3). The joint system surface conditions display multi wavy direction large-scale expression, with rough or irregular to smooth stepped small scale expression. No alteration is visible on joint walls and no joint filling is present.

4.2.5.7 Domains based on discontinuity orientation

The pit was divided into ten geotechnical domains according to likelihood of various types of failure. A full analysis of the results is provided in Apendix F, and a summary is shown in Figure 4.5. The analysis was done assuming a bench face angle of 90°. The analysis in Figure 4.5 was also used in determining final bench face slopes and blasting configurations. In each stereonet, there is a yellow shaded semi-circle which represents the critical zone for wedge sliding. The shaded area is encompassed by the great circle of the bench face orientation (in this 90° case - a straight line) and a great circle in the same orientation but at the limit of the friction cone (circle in the centre of the stereonet). The plane friction cone is derived from the joint systems friction angle, usually from laboratory testing of these discontinuities. Since no laboratory tests were done on the friction angle of the joint systems in the study area, an angle of 30˚ was used as per Jager and Ryder's (1999) recommendation. The risk of failure is then calculated through the intersection of planes falling within the yellow shaded area. The number of intersections of great circles which fall within the shaded area are divided by the total number of intersections of great circles in the stereonet to produce a percentage risk of failure.

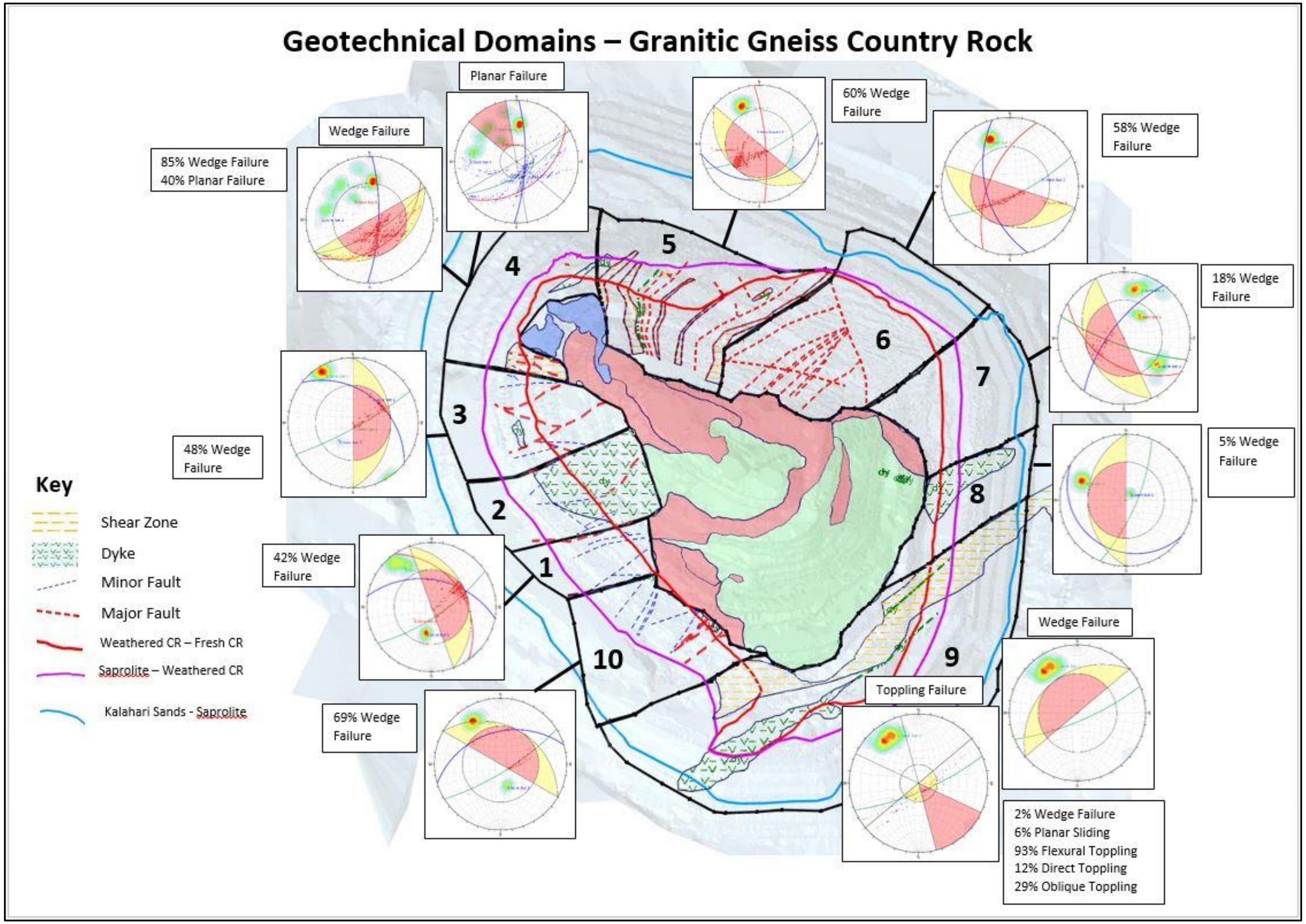

Figure 4-5 Geotechnical Domains showing possible failures due to discontinuity orientations

4.3 Rock Mass Model

4.3.1 Rock mass mapping of country rock

The information collected from the joint mapping exercise was used to determine Bieniawski's (1973) RMR ratings for the jointed country-rock portions of the open pit. Subsequently, Laubscher's (1990) rock mass classification was used to transform the RMR into an MRMR using Laubscher's (1990) adjustments. All the assumptions and classification methodology is described in Chapter 3.3, Equations 3.1 to 3.3.

4.3.2 Laboratory testing

A very small suite of core samples from a couple of lithologies was sent for laboratory testing. The rock tests included Uniaxial Compressive Strength (UCS), Triaxial Compressive Strength (TCS) and Base Friction Angle tests, through Direct Shear tests. Although not all lithologies were sampled, some good results were obtained for isolated rock mass parameters such as kimberlite domains 2 and 3. Where large data gaps were present, such as in individual kimberlite domains, PLT were done. The results for the aforementioned laboratory tests are included in Appendix C and summarised in Table 4.1. Due to the kimberlite rock mass not being structurally controlled but rather a massive intrusion, base friction angle through simple tilt testing was not applicable.

Table 4.1 Rock Laboratory Testing Results Summarised

Rock Type	Test Type		
	Base Friction Angle (˚)	**Triaxial Compressive Strength (MPa)**	**Uniaxial Compressive Strength (MPa)**
Granitic Gneiss **(F) = Fresh** **(W) = Weathered**	32 - 37	σ_3 = 5 => 207 – 267 σ_3 = 10 => 274 – 302 σ_3 = 20 => 227 – 408	Max (F)260.1 (W)72.6 Min (F)124.4 (W)32.5 Ave (F)192.0 (W)54.3
Kim 2	No Data	NO DATA	Max 9.1 Min 3.3 Ave 7.2
Kim 3	No data	NO DATA	Max 12.7 Min 7.0 Ave 7.2

4.3.3 Point-load testing

To obtain UCS values for the relatively uncharacterized kimberlite domains, the indirect method of point-load index conversion into UCS as described by the ISRM standard method of testing (ISRM, 1985) was used. Due to the weathered condition of core samples of the kimberlite, grab samples were taken directly from the pit. These samples were cored by a core bit to the correct diameter size of 53 mm (ISRM, 1985).

Two orientations of point-load testing have been applied to the kimberlite rocks. These include diametric and axial testing. For diametric testing, the sample lengths ranged between 54 mm and 114 mm for all samples, in line with the ISRM (1985) standard of L>0.5D. The summarised results of the tests results are provided in Table 4.2. These were used in Laubscher's (1990) Mining Rock Mass Rating (MRMR) classification as seen in Table 4.3. The raw data for test results are included in Appendix D.

Table 4.2 Summarised results from Point-Load Testing

Rock Domain	**Is(50) range (kN)**	**C-factor (as determined through Laboratory UCS result correlation)**	**UCS range (MPa)**
Kim 2	0.181 – 0.259	24	4.13 – 6.22 AVE 6.00
Kim 3	0.238 – 0.265	24	5.72 – 6.37 AVE 6.00
Kim 4	0.384 – 1.094	24	9.23 – 20.81 AVE 10.50
Competent Granitic Gneiss	3.734 – 11.596	22.4	89.07 – 259.76 AVE 180.00

Table 4.3 Summarised results of the geotechnical analyses (Bieniawski, 1973 and Laubscher, 1990)

Rock Domain	IRS (15)	RQD (20)	Spacing of Discontinuities (20)	Condition of Discontinuities (30)	Ground-water (15)	RMR
Kim 2	2	10	15	25	10	62
Kim 3	2	10	15	25	10	62
Kim 4	2	10	15	25	10	62
Competent Granitic Gneiss	12	13	10	25	15	75

Rock Domain	RMR	Weathering Adjustment	Blasting Adjustment	MRMR
Kim 2	62	0.62	0.90	34
Kim 3	62	0.62	0.90	34
Kim 4	62	0.78	0.90	43
Competent Granitic Gneiss	75	1.00	0.94	70.5

4.4 Hydrogeology Model

The biggest current data gap is in the hydrogeological understanding of the Mine A main pit. To date, no groundwater characterisation has been done, due to a lack of piezometers or boreholes. The only option to understand groundwater movement was to map and measure groundwater flow points into the pit during rainy and dry seasons.

The groundwater seepage flow-path model was estimated through such data collection and is shown in Figure 4.6.

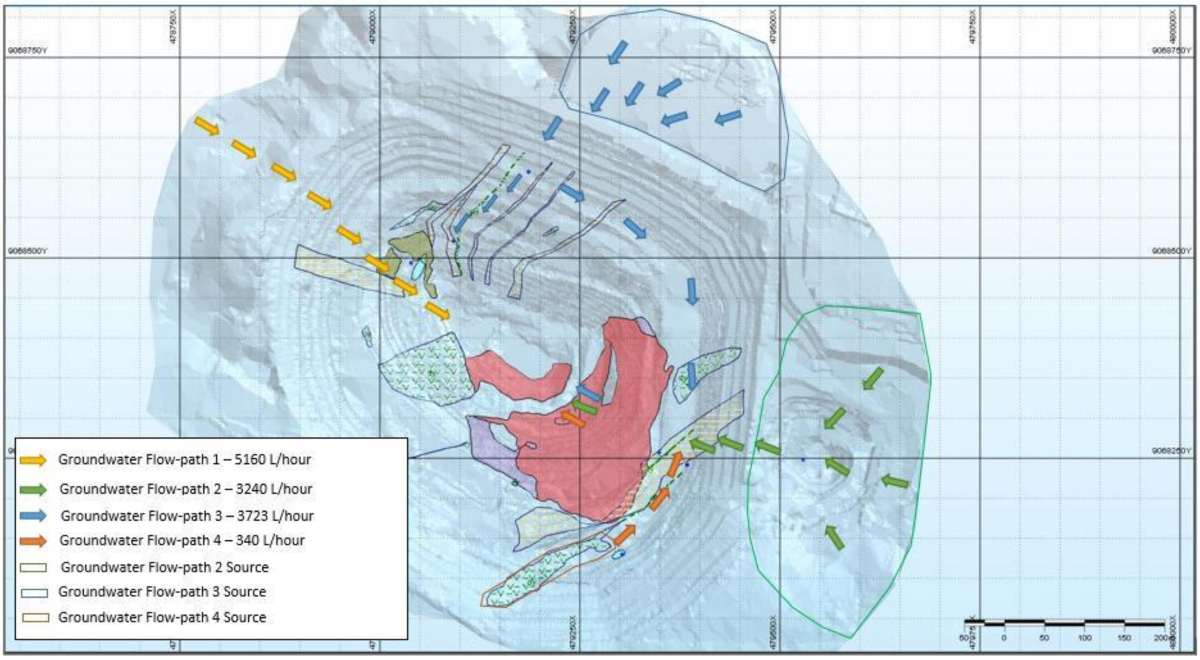

Figure 4-6 Groundwater seepage mapping and flow characterisation

4.4.1.1 Groundwater flow-path 1

Groundwater from this flow-path has been estimated to be sourced from River A to the North-West of Mine A main pit. Outflow points have been mapped and compared to the river's elevation to confirm the probability of flow direction. The rate of inflow has been measured from seepage surfaces to be around 5 to 180 litres/hour at its highest rate during the peak rainy season. Inflow occurs throughout the year.

4.4.1.2 Groundwater flow-path 2

A major component of groundwater inflow into the main pit is sourced from the eastern kimberlite test pit basin. Groundwater flow from the surroundings of this test pit accumulates at the lowest point where the eastern kimberlite pipe has been bulk sampled. Due to the persistence of the shear zone in the South-East of the main pit, entering into the sidewall between main pit and the eastern test pit, groundwater flow finds its path of least resistance along these fault lines. Furthermore, this shear zone is connected to volcanoclastic breccia kimberlite of kimberlite domain six (shaded red area in Figure 4.6). This kimberlite domain is highly porous consisting mainly of brecciated country-rock interlayered with kimberlite domain 2 lenses. The lithological unit allows for continuous and uninterrupted flow to the pit bottom. Outflows have been measured in the proximity of 3 to 240 litres/hour and persist all year-round.

4.4.1.3 Groundwater flow-path 3

The groundwater inflow from this source has been observed to only appear at the onset of the rainy season and dissipate towards its end. It is postulated that the eastern kimberlite stockpile (shown in Figure 4.6 by a blue line) acts as a sponge for rainfall during this period. The rainwater is channelled by the roads adjacent to the pit limit over the benches in the North of the pit and then flows on to the Northern main ramp down into pit bottom via haulage roads. A small component of the water penetrates the shear zone present in the North of the pit and flows through these planes of weakness to the pit bottom. The mass of water flowing down the Northern ramp was measured to be in the region of 3 to 723 litres/hour, while the component flowing through the shear zone measured to be roughly 720 litres/hour.

4.4.1.4 Groundwater flow-path 4

The source of groundwater from this flow-path is uncertain but is estimated to be from deep-seated water sources upwelling through the major shear zone in the South-East of the pit. The volume of contribution has been measured as minor compared to other existing inflows, with volumes in the region of 340 litres/hour. The water seepage generally flows from the shear zone intersection with the Southern ramp, down the ramp to the pit bottom.

4.4.2 Conclusion

Although hydrogeological inflow rates have been mapped by seepage and a relatively good qualitative indication of groundwater inflows has been determined, no quantitative data will be available until groundwater piezometers are installed. The current estimated total inflow from all four flowpath sources is 1480 litres/hour during the peak rain season (November). These only represent seepage outlows identified in the highwalls and thus are expected to be much higher when quantitative data has been collected.

5 BENCH STACK DESIGN BY DESIGN CHART

The slope design process requires a thorough knowledge of the rock mass and soil strength parameters. Two different methods of chart stability analysis were employed to determine optimum slope angles in the Mine A main pit. Hoek & Bray (1981) Circular Failure Charts were used to calculate overall slope angles for the Kalahari Sands and Saprolite lithologies. In this analysis, the soil strength parameters were evaluated in terms of a FOS of 1.25 as dictated by management.

The Hoek and Bray (1981) design charts make use of cohesion (C), internal angle of friction (ϕ) and density (γ) of the soil. These parameters (Table 5.1) are used in equation 5.1:

Table 5.1 Soil Strength Parameters for Kalahari Sands and Saprolite (Weathered Granitic Gneiss)*

Soil Type	Cohesion (kPa)	Density (kN/m³)	Angle of Internal Friction (˚)	Height of the slope (m)	Face Angle	Factor of Safety (FS)
Kalahari Sands	1	17.8	30˚	70m	45˚	1.25
Saprolite	22.5	20.3	30˚			

$$\frac{C}{\gamma \times H \times \tan \emptyset}$$ ***Equation 5.1***

Where C=Cohesion; γ=Density; H=Slope Height and $\emptyset$=Internal Angle of Friction

The value (0.03) obtained is identified on the graph and a straight line is drawn from this number to the graph vertex on the bottom left of the graph. The FOS and friction angle soil parameters are then used in equation 5.2:

$$\frac{\tan \emptyset}{\mathrm{FS}}$$ ***Equation 5.2***

Where $\emptyset$=Internal Angle of Friction and FS= Factor of Safety

This value (0.48) is then identified on the y-axis (Figure 5.1). A horizontal line from this number is then drawn to intersect the previously drawn line (Figure 5.1). Where the two lines (red lines in Figure 5.1) intersect, the suggested angle of the slope is determined using the curved lines shown in the figure. For the combined Kalahari Sands and Saprolite overall slope, an inter-ramp angle of 24° was determined (red cross in Figure 5.1). Since the weathered granitic gneiss and saprolite lithological units are soil type lithologies they have been incorporated into the upper sediments lithological unit and will adhere to the inter-ramp angle of the Kalahari Sands (24°). The results of the investigations are shown in Table 5.1. Figure 5.1 indicates the Hoek and Bray (1981) Chart 2 (inflows at the toe of the pit), while Figure 5.2 shows Chart 5 for fully saturated groundwater conditions.

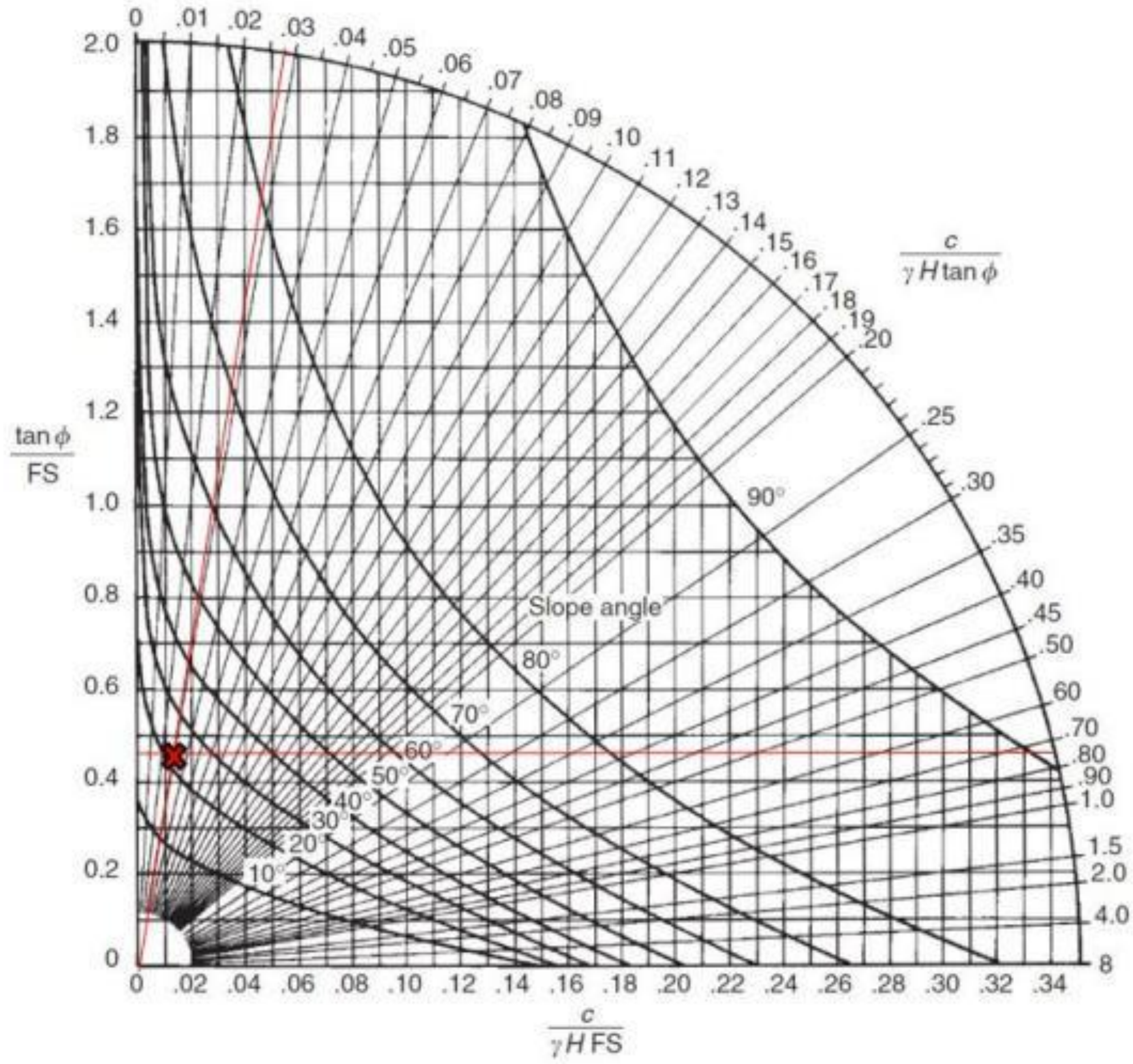

Figure 5-1 Input of soil strength parameters into the Hoek and Bray (1981) circular failure Chart 2

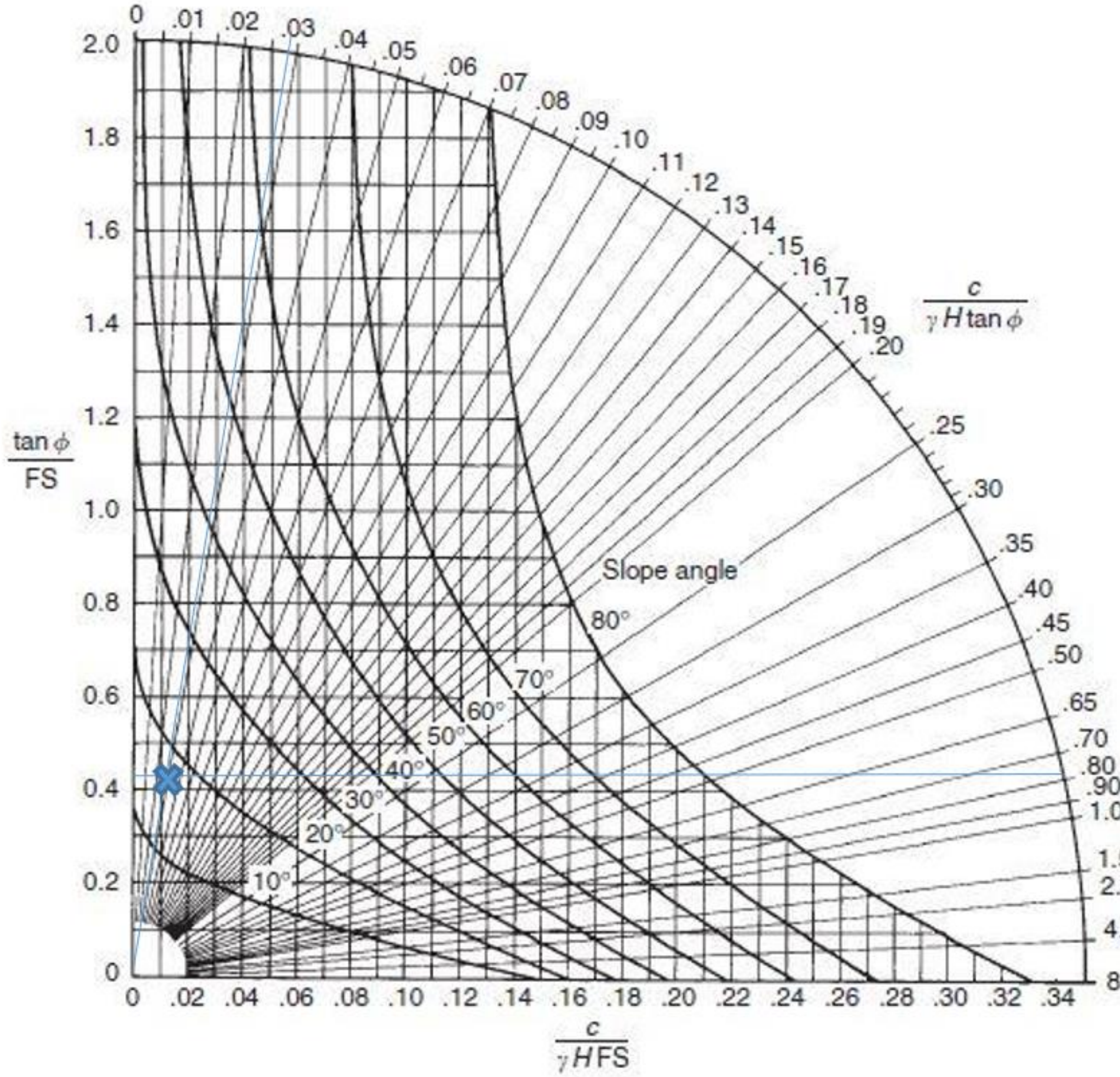

Figure 5-2 Hoek and Bray (1981) Chart 5 indicating saturated groundwater conditions.

Table 5.2 Soil Strength Parameters for Kalahari Sands and Saprolite (Weathered Granitic Gneiss)*

Soil Type	Height of the slope (m)	Factor of Safety (FS)	Face Angle (˚) (Dry)	Slope Angle (˚) (Dry)	Face Angle (Wet)*	Slope Angle (˚) (Wet)*
Kalahari Sands Saprolite	70m	1.25	45˚	24˚	45˚	18˚

*Conditions during the rainy season using design Chart 5, (Hoek & Bray, 1981)

The country rocks and kimberlite domains were characterized through window and scanline mapping. The maximum vertical height of competent granitic gneiss as well as each kimberlite domain was extrapolated from cross-sections of the current geological model. These were then divided into practical bench stack heights per lithological unit mainly through mining equipment constraints and the bench stack heights were used as the heights to be analysed in the Haines and Terbrugge (1991) Design Chart for jointed rock masses. The UCS parameter in the MRMR for the kimberlite domains was determined through UCS laboratory results for kimberlite Domains 2 and 3. Since no UCS results for kimberlite domain 4 was available PLT results for this unit had to be used. This was achieved by obtaining a correlation C-factor by kimberlite Domain 2 and 3 comparison with UCS tests and using this factor in conversion of point-load strength index to UCS. Grab samples were collected from each kimberlite domain, cored to the correct core size, and tested using a point-load tester. Point-load testing was also done on the competent granitic gneiss to compare indirect UCS values with UCS values obtained through laboratory testing. Results from the point-load tests showed excellent correlation to laboratory obtained results, and the same MRMR value was obtained when using ether of the two test results. These correlations can be seen in the results provided in Appendix D. A FOS of 1.5 in the Haines and Terbrugge (1991) Chart was selected due to the level of geotechnical data available as per Read and Stacey's (2009) project level guidelines. This FOS was used to determine the overall slope angles for the jointed country-rock masses and kimberlite domains. The geomechanical parameters obtained for each rock type in the pit are shown in Table 5.3.

Table 5.3 Geotechnical Parameters for Jointed Rock Mass and Kimberlite Domains (lowest values used)

Rock Domain	RMR	MRMR
Competent Granitic Gneiss	75	70
Competent Granitic Gneiss – Shear Zone	75	57
Kim 2/6	62	34
Kim 3	62	34
Kim 4/5	62	43

The MRMR values for the competent grantic gneiss and the kimberlite domains in Table 5.3 is representative of the weakest conditions to be encountered in the main pit. One outlier, where the values are abnormally low, is found in geotechnical domain 9, where the shear zone cuts throught the pit on the Southern and North Eastern part of the pit (Figure 5.3). Here, due to the high density of discontinuities, the MRMR drops to 57. Considering that the shear zone is only 10 m in thickness, this high-risk zone will be considered separately through monitoring and installation of geotechnical safety berms. The shear zone is presented as the orange shaded area in Figure 5.3.

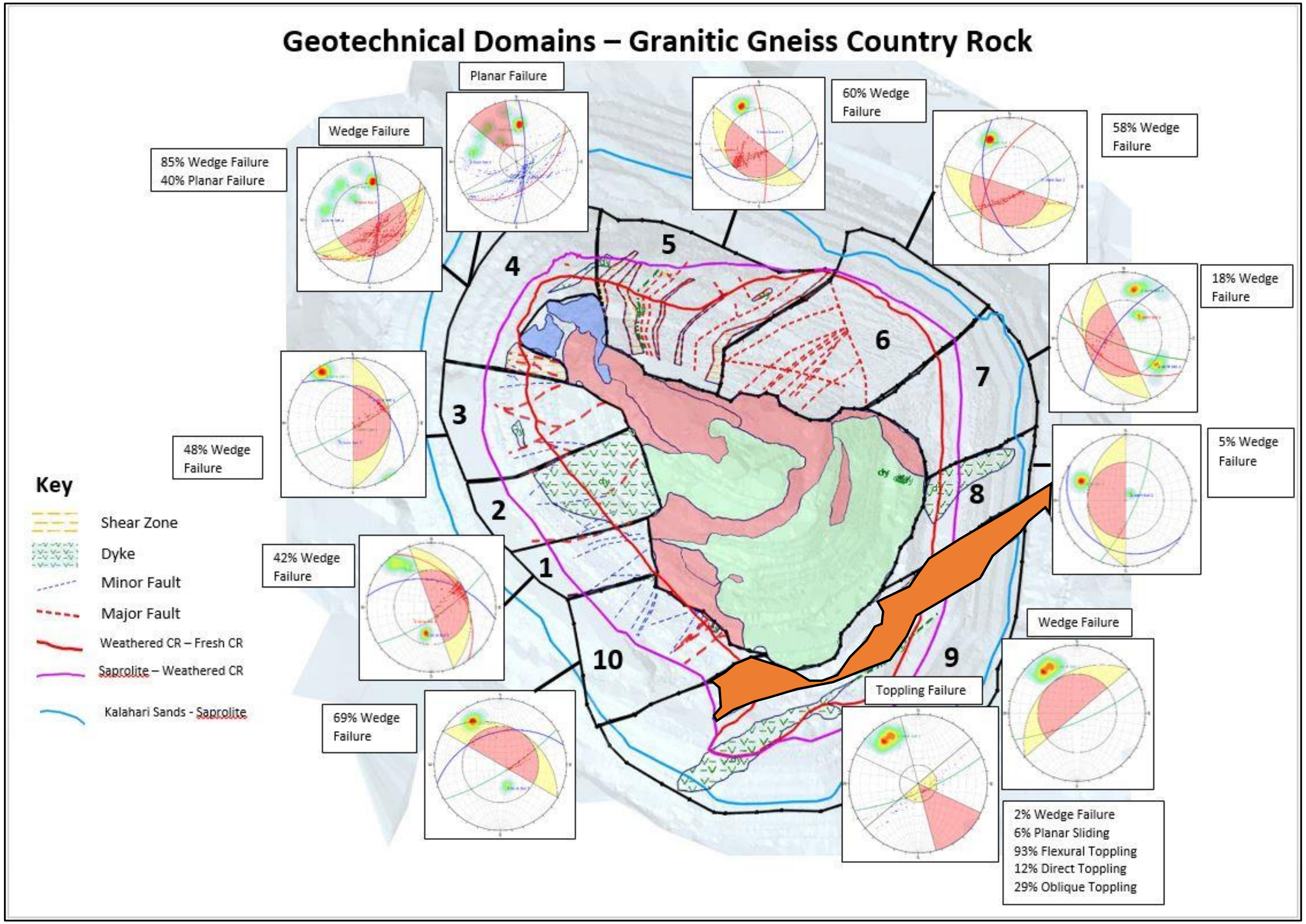

Figure 5-3 Geotechnical domains map with shaded orange area representing 10 m wide shear zone of MRMR 57

It was necessary to consider the strength of the soils and rocks from the bottom of the stack, as these geomechanical units would be loaded to the greatest stress. The geomechanical unit at the bottom of the country rock would therefore need to be considered first as it would have the highest stress acting on it due to the weight of the material above. The slope angle was determined for this geomechanical unit first, using Figure 5.4. No geotechnical units above this could have a steeper slope than the lowest geotechnical unit. The kimberlites were assessed separately, but using a similar approach. The analyses showed that there were only two slope angles in the solid rock masses, i.e. one for the country rocks and one for the kimberlites. The soils were inclined at a more gentle angle, and although the weight was considered in the analysis, their angle of repose was considered separately. A similar approach was used to analyse the soils. The results for each of the two lithological bench stacks in the hard rocks are presented in Figure 5.4. The weaker of the three kimberlite MRMR values from Table 5.3 has been used (39), while 61 was used for the competent granitic gneiss rock mass.

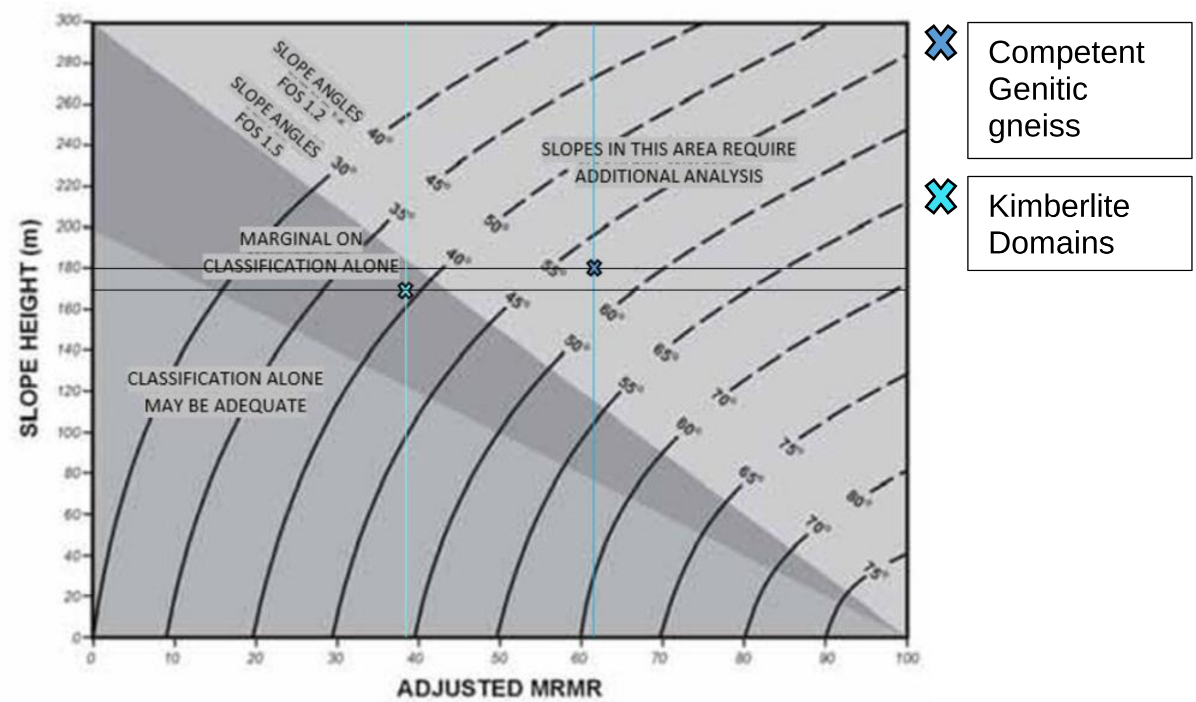

Figure 5-4 Haines and Terbrugge (1991) Design Chart, showing the results of the various geotechnical domains from Table 5.3

The adjusted MRMR was identified on the x-axis of Figure 5.4. A straight line was then projected vertically upwards. A horizontal line was drawn from the slope height shown on the Y-axis, to intersect the appropriate vertical line. The slope angle was determined from the position of the intersection within the chart. Due to the vertical intrusion of the kimberlites, the country rocks and the kimberlites can be considered separately. This separate investigation was made possible because the country rocks are not loading the kimberlites, except by the Poisson effect. Figure 5.4 shows the slope of the country rocks in the upper portion of the pit and the Kimberlites in the lower pit region.

The angles shown at the base of the dotted lines in Figure 5.4 represent slope angles with a FOS of 1.2, while the values above the solid lines represent slope angles with a FOS of 1.5. A FOS line of 1.5 was used for angle prediction. Note that the dotted lines are an extension of the solid lines and can also be used to predict a slope angle with a FOS of 1.5 by using the corresponding slope angle provided for the solid lines, e.g. a slope angle of 55° corresponding to a FOS=1.2, would need to be decreased to 45° to achieve a FOS=1.5.

There is no difference in the MRMR classification when using UCS or PLT results. MRMR takes into consideration IRS, RQD, Spacing of discontinuities and groundwater conditions. Each is weighted to form part of a 100 point system. Of this 100 points, IRS only contributes 15 points. The contributing scale difference is thus minor when considering the cost of laboratory testing. The MRMR range used to determine the granitic gneiss country rock mass slope angles was obtained from the most conservative estimate of the mapping results. The results of the jointed rock mass investigations are summarised in Table 5.4. The data provided in Table 5.4 was used in the numerical model analyses.

Table 5.4 Rock Mass Strength Parameters for Jointed Rock Mass and Kimberlite Domains (bench face angle assumed at 90° in solid rock)

Rock Domain	RMR	MRMR	Height of the bench stack (m)	Overall Slope Angle (crest-to-toe)	Face Angle	Class
Weathered Granitic Gneiss	38	32	20m	24° (Incorporated into Upper Sediments)	45° (Incorported into Upper Sediments)	C
Competent Granitic Gneiss	67	61	180m	47°	90°	AA
Kim 2/6	62	34	80m	39°	90°	M
Kim 3	62	34	30m (small remnant)			M
Kim 4/5	62	43	90m			M

*C = Classification alone may be adequate; M = Marginal on classification alone; AA = Slopes in this area require additional analysis

A cross-section for each of the three lithological unit's bench stack configuration was drawn and is presented with the methodology to obtain these bench stack angles in the following sections. The overall slope angles as per the Haines and Terbrugge (1991) Chart were incorporated into the cross-sections of Chapter 6 where overall slope angle was analysed. Bench angles have not been considered in the influence of results from the numerical analyses, and an angle of 90° was used in the solid rocks. The sections were created in SLIDE 2D (2018) by use of the chart data inputs.

5.1 Kalahari Sands, Saprolite and Weathered Granitic Gneiss

Due to the relatively insignificant lithological height of Kalahari Sands and weathered granitic gneiss remaining in the fourth mining cut-back, this layer was included in the saprolite unit. A slope face angle of 45˚ was suggested by Hoek and Bray (1981), to be the most competent face angle in unconsolidated Kalahari Sands (the weaker of the three lithologies). The Hoek and Bray (1981) Design Chart in Figure 5.1 shows a bench stack angle of 24˚. This angle was then used with a 10 m bench height and a 90 m total slope height to determine bench widths. Inter-bench bench widths of 14 m were selected as being close to the 13.8 m extrapolated width. This gives bench stack angle (crest-to-toe) of 24˚ and a crest-to-crest angle of 23˚. This angle corresponds to the results provided by the Hoek and Bray (1981) analysis when a FOS of 1.25 is used. A cross-section of the bench configuration is provided in Figure 5.5.

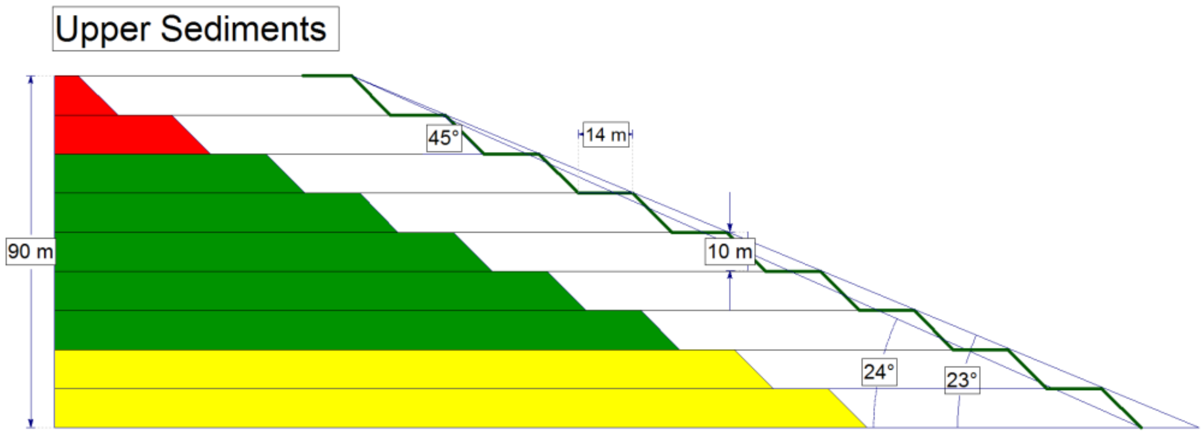

Figure 5-5 Bench configuration as per design chart modelling for Kalahari Sands (red)Saprolite (green) and Weathered Granitic Gneiss (yellow) lithologies

5.2 Granitic-Gneiss Country Rock

The bench configuration for the competent portion of the granitic gneiss country rock required a more complicated approach. According to the geological model, a vertical height of up to 180 m is expected in the fourth mining cut-back. When this height together with the corresponding MRMR of 61 is plotted in the Haines and Terbrugge (1991) Design Chart, the slope angle located in the region where additional analysis is required (Figure 5.4 – dark blue cross). Further analysis was done using numerical modelling analysis, which is discussed in Chapter 6 where an overall slope angle of 47˚ was employed. For these bench configurations, bench faces should be cut at 90˚ with bench heights of 10 m and bench width of 10.5 m. This computes into an overall slope angle (crest-to-toe) of 47˚ and crest-to-crest angle of 44˚. A bench configuration for a 100 m portion of the competent granitic gneiss is provided in Figure 5.6.

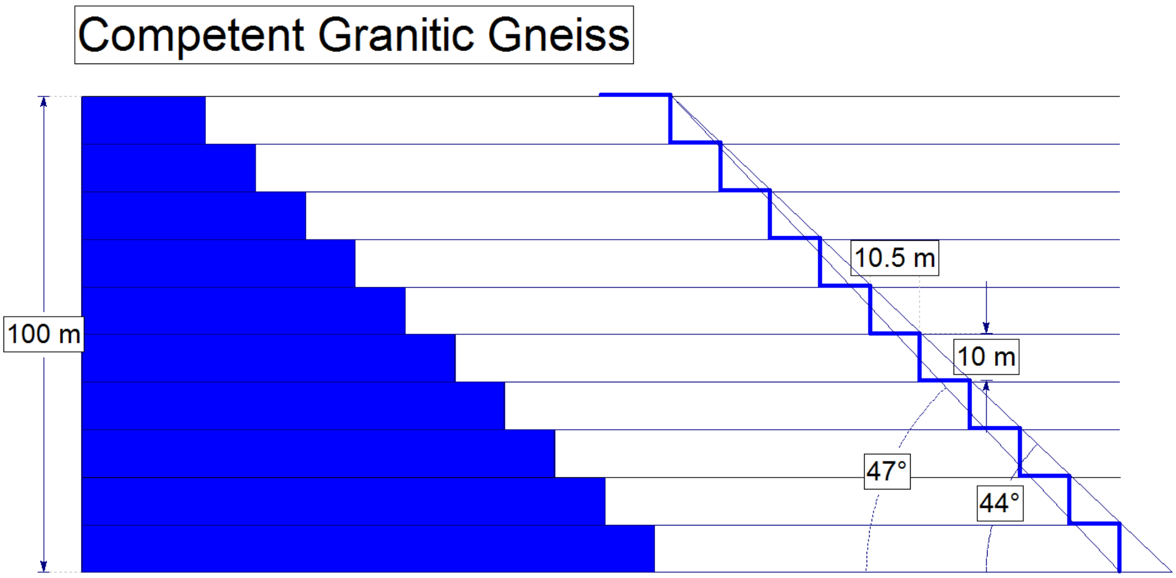

Figure 5-6 Bench configuration for competent granitic gneiss country-rock by use of design chart

5.3 Kimberlite

Considering the complex nature of the kimberlite intrusion and the interlayered character of certain domains, some domains had to be combined for slope design analysis. Specifically, kimberlite domain 2, which is found as lenses in kimberlite Domain 6 (Volcanoclastic Kimberlite Breccia) has been analysed as one. Since kimberlite Domain 2 exhibited weaker rock mass strength than Kimberlite 6, the design has been based on rock mass parameters of Kimberlite 2. An insufficient volume of kimberlite Domain 3 exists in the fourth mining cut-back to be analysed in isolation. Kimberlite Domains 4 and 5 have a similar interlayered character to that of kimberlite Domains 2 and 6. Since expected vertical heights of kimberlite Domain 2 and kimberlite Domain 4 were 80 m and 90 m respectively, the overall slope angle was determined through combining these lithologies into one unit and determining an overall slope angle based on the weakest unit's rock mass properties (MRMR). The MRMR of kimberlite Domain 2 was thus used with the 170 m vertical height to obtain an overall slope angle from the Haines and Terbrugge (1991) Design Chart of 39˚. The expected bench configuration in a 80 m bench stack is presented in Figure 5.7. The final overall slope angles for the three different lithological units are summarised in Table 5.5, and will be checked by the numerical models.

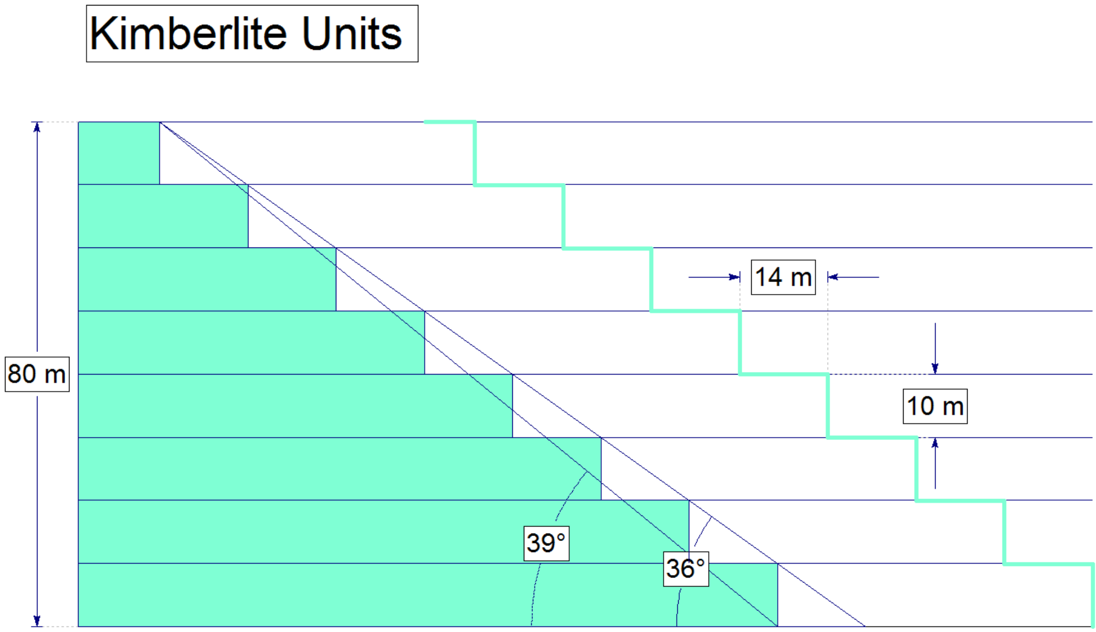

Figure 5-7 Bench stack configuration for kimberlite units as per kimberlite domain 2 rock mass properties and Haines and Terbrugge (1991) Design Chart

Table 5.5 Overall slope angles through design chart (bench face angles of 90° used for the solid rock in the numerical models)

Lithological Unit	**Face Angle**	**Overall Slope Angle (crest-to-toe)**
Kalahari Sands	45˚	24˚
Saprolite		
Weathered Granitic Gneiss		
Competent Granitic Gneiss	90˚	47˚
Kimberlite Domain 2/6	90˚	39˚
Kimberlite Domain 3		
Kimberlite Domain 4/5		

6 SLOPE ANGLE CONFIRMATION THROUGH NUMERICAL MODELLING

The sections which were created in SLIDE 2D (2018) as seen from Figures 6.4 and 6.5 were analysed using this limit equilibrium numerical modelling software. In addition, a boundary element package, Examine 2D (2006), was used to determine the strength to stress ratio of the rock mass geotechnical units in the pit slopes and pit floor at the toe of the slopes. Since design charts were only used to determine bench stack configurations, the resultant overall slope angle from the implementation of these bench configurations would need to be validated. This was done through firstly creating cross-sections from the NW to SE and SW to NE across the long and short axis of the pit. The locations of these cross-sections are presented in Figure 6.1 with actual cross-sections following in Figures 6.2 and 6.3. The lower lines in Figures 6.2 and 6.3 indicate the limit of economic feasibility of the pit and this was used as the boundary for cross-section creation. The bench stack angles per lithological unit were then input into the cross-sections so that the pit bottom as per feasibility line was achieved. The resultant overall slope configuration is presented in Figures 6.4 and 6.5.

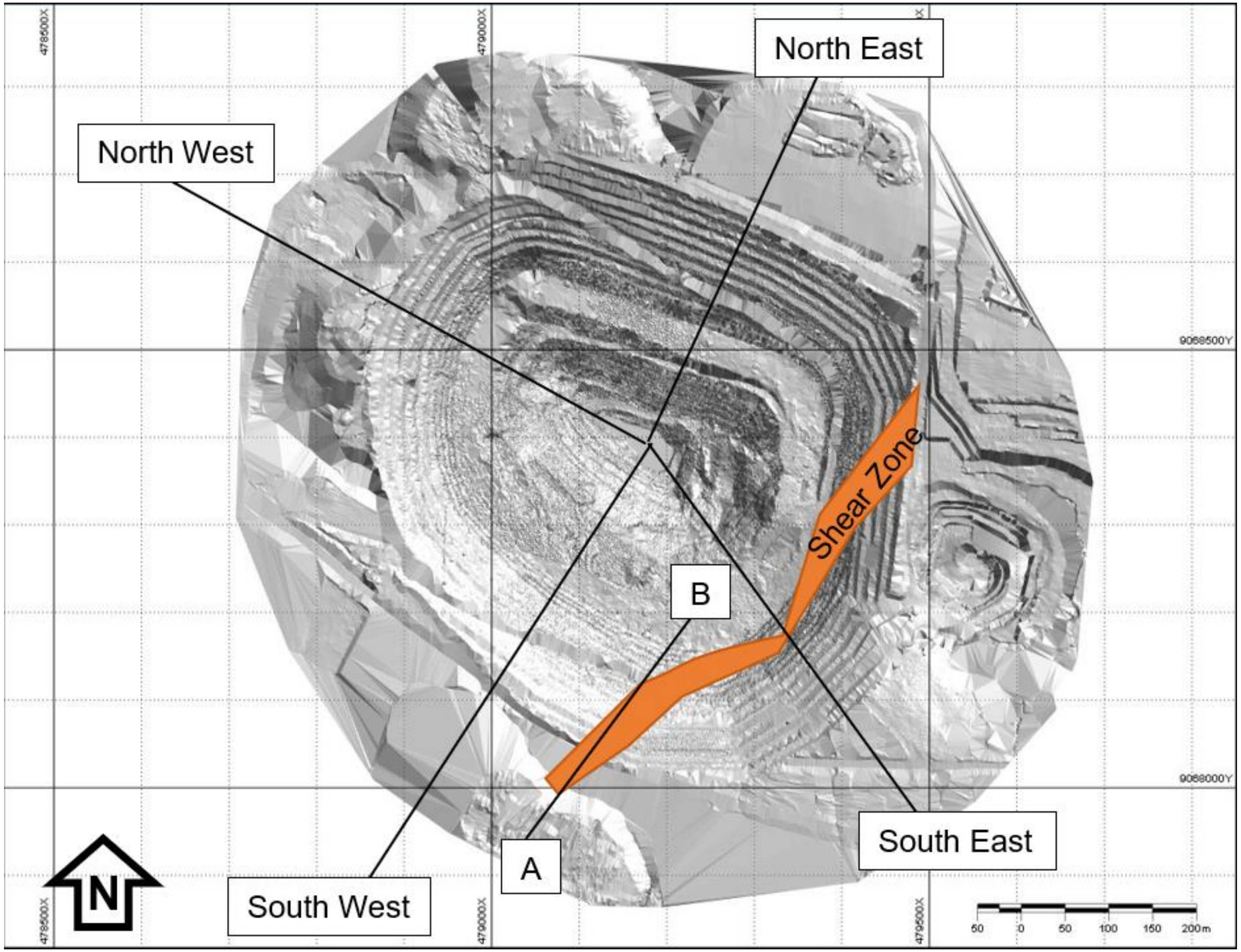

Figure 6-1 Plan view of main pit with sections to be analysed in Examine 2D (2006)

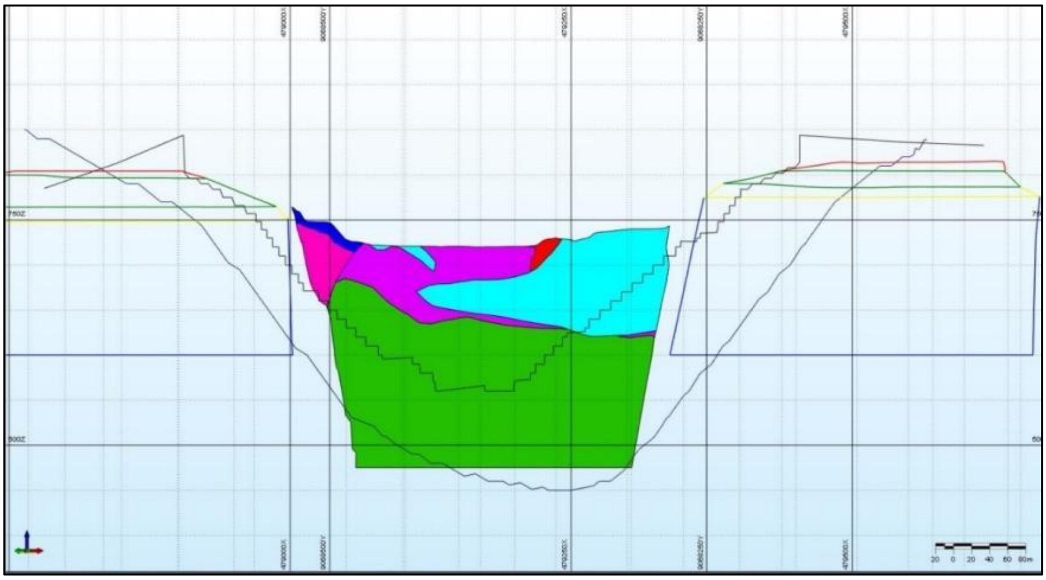

Figure 6-2 North-West (left) to South-East (right) cross section of the main pit

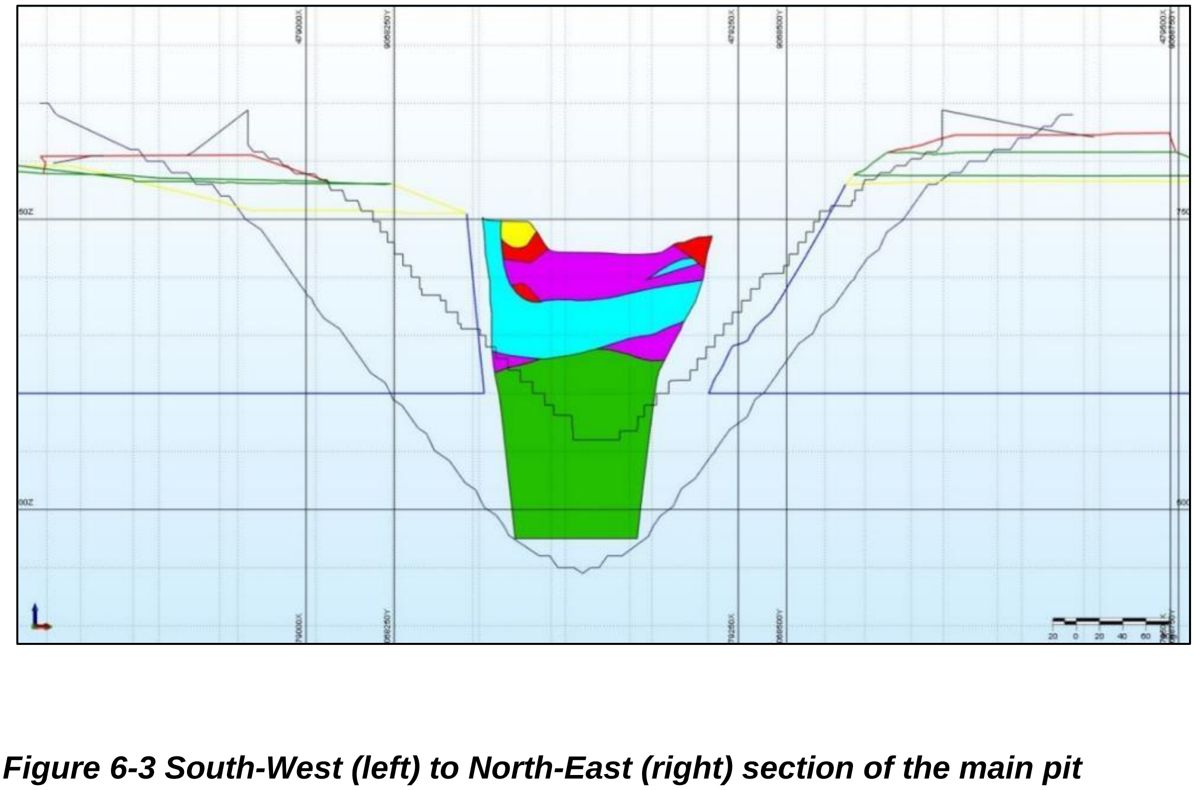

Figure 6-3 South-West (left) to North-East (right) section of the main pit

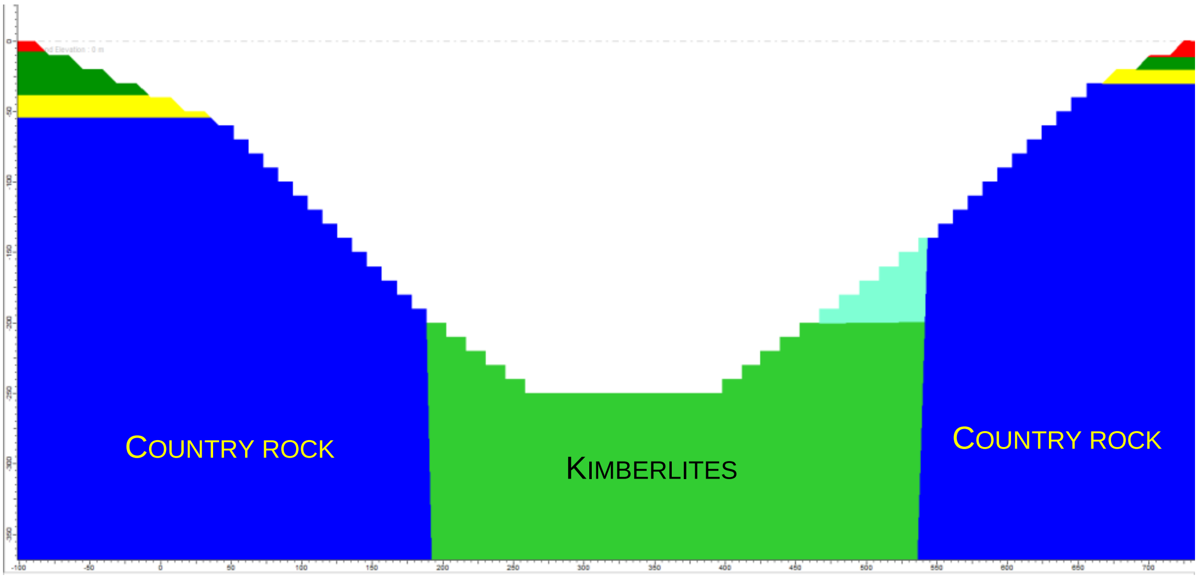

Figure 6-4 North-West to South-East cross-section with bench stack configurations input to produce overall slope angle. Blue=Granite, Green and turquois = Kimberlites

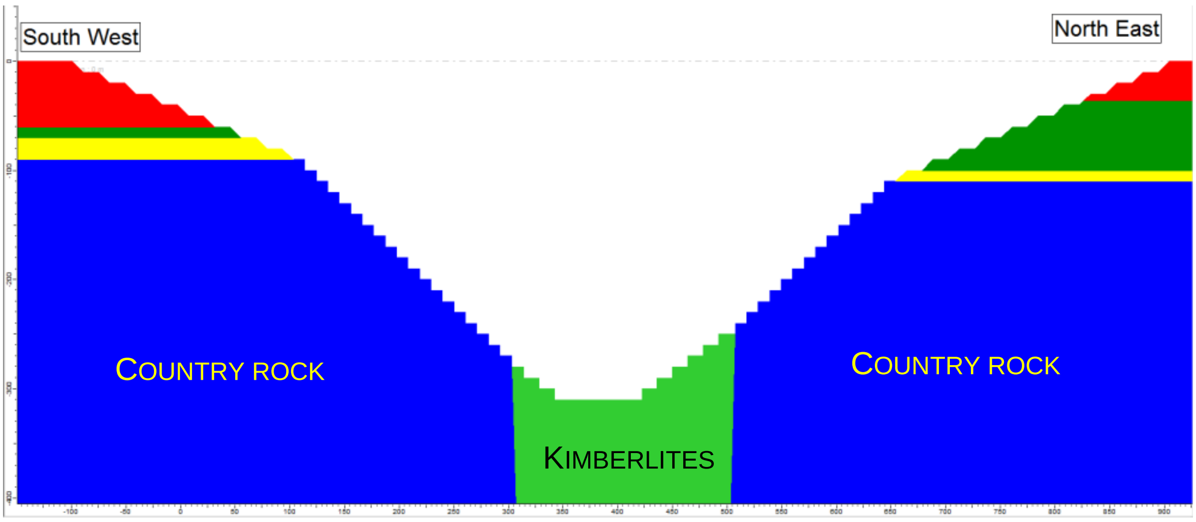

Figure 6-5 South-West to North-East cross-section with bench stack configurations input to produce overall slope angle

6.1 Limit Equilibrium Analysis – SLIDE 2D (2018)

In the soil lithologies (Kalahari Sands and Saprolite), the Mohr-Coulomb failure criterion for shear strength has been used to model the FOS for this unit. The criterion uses cohesion, internal angle of friction and unit weight in its calculation, as well as a Hu factor (groundwater saturation of the lithological unit) which can also be assigned based on the character of the lithological unit.

The jointed rock mass, as well as kimberlite domains, have been modelled using the Hoek-Brown failure criterion. Since no laboratory data were available to determine the required strength parameters apart from UCS, the GSI calculator was used, as well as mi and D calculation from the rock mass parameter calculating tool in the SLIDE 2D (2018) software.

Considering that kimberlite domain 2 and 6 have been classed together, it was decided to analyse the weakest component of the unit. As kimberlite 6 consists of brecciated country rock and is thus a more competent intact rock mass than kimberlite domain 2, the unit was modelled using kimberlite domain 2 strength parameters. The same approach was used for the kimberlite domain 4 and 5 unit which is also complex and interlayered. The results from numerical modelling by SLIDE 2D (2018) have been included in Appendix E.

The parameters chosen for each of the SLIDE 2D (2018) analyses have been summarised in Table 6.1.

Table 6.1 Rock and soil characteristics used for SLIDE 2D (2018) analysis

Lithological Unit	Unit Weight (kN/m³)	Strength Type (Failure Criteria)	Strength Parameters				
			Cohesion		Φ		Hu
Kalahari Sands	18	*Mohr-Coulomb*	*2*		*30˚*		*1*
Saprolite	*23*	*Mohr-Coulomb*	*22.5*		*30˚*		*1*
Lithological Unit	**Unit Weight (kN/m³)**	**Strength Type (Failure Criteria)**	**Strength Parameters**				
			UCS (MPa)	**Ru**	**GSI**	**mi**	**D**
Weathered Granitic Gneiss	*20*	*Generalised Hoek-Brown*	*3.0*	*1*	*30***	*14*	*0.2*
Competent Granitic Gneiss	*28*	*Generalised Hoek-Brown*	*250.0*	*1*	*70***	*22*	*0.2*
Kimberlite 2	*24*	*Generalised Hoek-Brown*	*7.1*	*1*	*57***	*13*	*0.2*
Kimberlite 3	*24*	*Generalised Hoek-Brown*	*7.1*	*1*	*57***	*13*	*0.2*
Kimberlite 4	*24*	*Generalised Hoek-Brown*	*9.2*	*1*	*57***	*13*	*0.2*

**UCS = Unconfined Compressive Strength; mb = Hoek-Brown coefficient; s = Hoek Brown Coefficient; a = Hoek Brown Coefficient; Ru = Groundwater saturation factor; GSI = Geological Strength Index; mi = Intact Rock Constant; D = Disturbance Factor by blasting; φ = Internal Angle of Friction; Hu = Soil Water Conditions **Calculated from Bieniawski's (1976) RMR = GSI + 5*

Four sections were analysed through SLIDE 2D (2018) as per the cross-sections in Figures 6.4 and 6.5. The failure surfaces which were predicted by the software were then analysed and a FOS for each of the three overall slope angles introduced in Chapter 5 were calculated. Figures 6.6 to 6.9 represent the FOS results obtained from these sections.

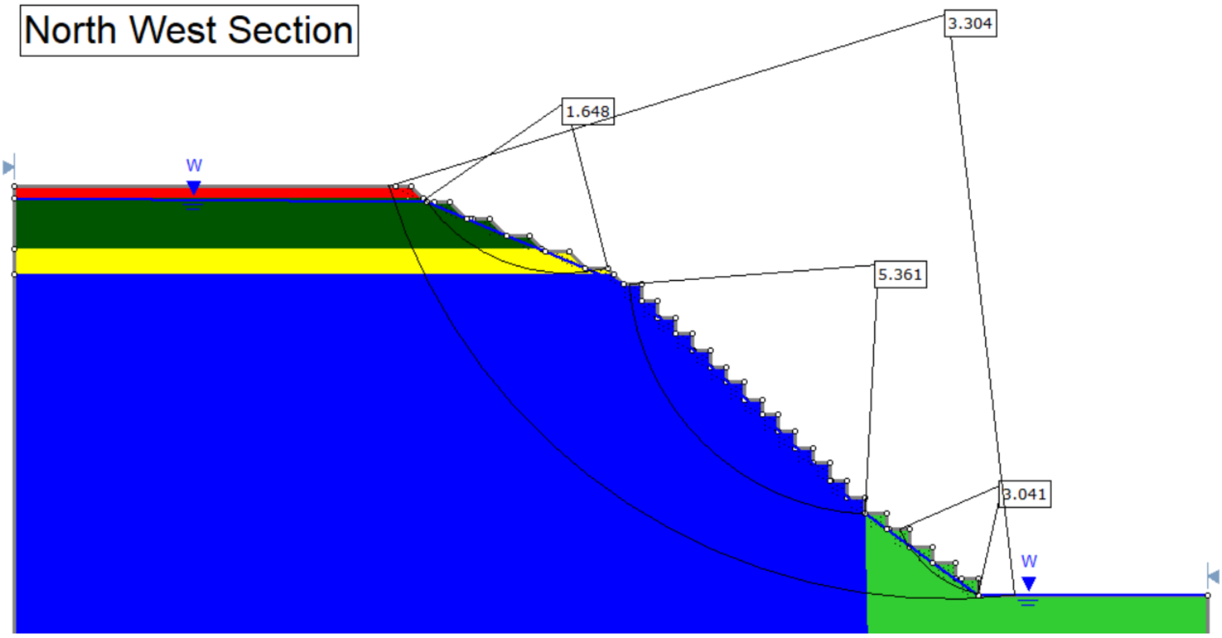

Material Name	Color	Unit Weight (kN/m3)	Strength Type	Cohesion (kPa)	Phi (deg)	UCS (kPa)	GSI	mi	D	Water Surface	Hu Type	Hu
Kalahari Sands		18	Mohr-Coulomb	2	30					Water Surface	Custom	1
Kalahari Sands (SRZ)		18	Mohr-Coulomb	2	30					Water Surface	Custom	1
Saprolite		23	Mohr-Coulomb	22.5	30					Water Surface	Custom	1
Saprolite (SRZ)		23	Mohr-Coulomb	22.5	30					Water Surface	Custom	1
Weathered Granitic Gneiss		20	Generalized Hoek-Brown			3000	30	14	0	Water Surface	Custom	1
Weathered Granitic Gneiss (SRZ)		20	Generalized Hoek-Brown			3000	30	14	0.7	Water Surface	Custom	1
Competent Granitic Gneiss		28	Generalized Hoek-Brown			250000	70	10	0	Water Surface	Custom	1
Competent Granitic Gneiss (SRZ)		28	Generalized Hoek-Brown			250000	70	10	0.7	Water Surface	Custom	1
Kimberlite Domain 4/5		24	Generalized Hoek-Brown			9200	90	13	0	Water Surface	Custom	1
Kimberlite Domain 4/5 (SRZ)		24	Generalized Hoek-Brown			9200	57	13	0.7	Water Surface	Custom	1

Figure 6-6 North Western Section analysed through SLIDE 2D (2018)

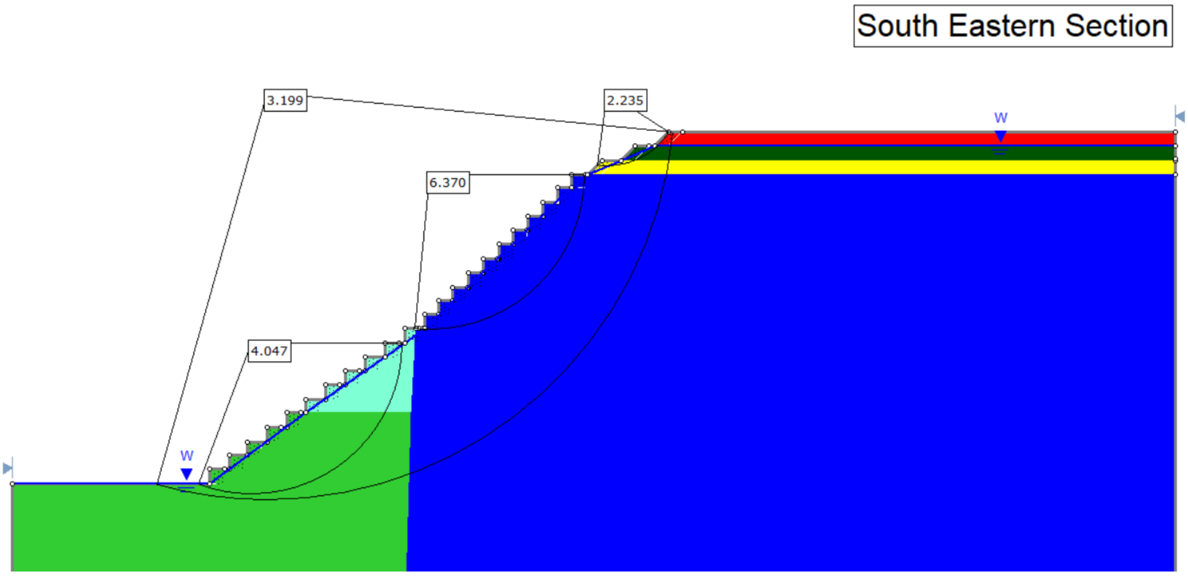

Material Name	Color	Unit Weight (kN/m3)	Strength Type	Cohesion (kPa)	Phi (deg)	UCS (kPa)	GSI	mi	D	Water Surface	Hu Type	Hu
Kalahari Sands		18	Mohr-Coulomb	2	30					Water Surface	Custom	1
Kalahari Sands (SRZ)		18	Mohr-Coulomb	2	30					Water Surface	Custom	1
Saprolite		23	Mohr-Coulomb	22.5	30					Water Surface	Custom	1
Saprolite (SRZ)		23	Mohr-Coulomb	22.5	30					Water Surface	Custom	1
Weathered Granitic Gneiss		20	Generalized Hoek-Brown			3000	30	14	0	Water Surface	Custom	1
Weathered Granitic Gneiss (SRZ)		20	Generalized Hoek-Brown			3000	30	14	0.7	Water Surface	Custom	1
Competent Granitic Gneiss		28	Generalized Hoek-Brown			250000	50	10	0	Water Surface	Custom	1
Competent Granitic Gneiss (SRZ)		28	Generalized Hoek-Brown			250000	50	10	0.7	Water Surface	Custom	1
Kimberlite Domain 4/5		24	Generalized Hoek-Brown			9200	90	13	0	Water Surface	Custom	1
Kimberlite Domain 4/5 (SRZ)		24	Generalized Hoek-Brown			50000	50	10	0	Water Surface	Custom	1
Kimberlite Domain 2/6		24	Generalized Hoek-Brown			7100	45	13	0	Water Surface	Custom	1
Kimberlite Domain 2/6 (SRZ)		24	Generalized Hoek-Brown			7100	45	13	0.7	Water Surface	Custom	1

Figure 6-7 South Eastern Section analysed through SLIDE 2D (2018)

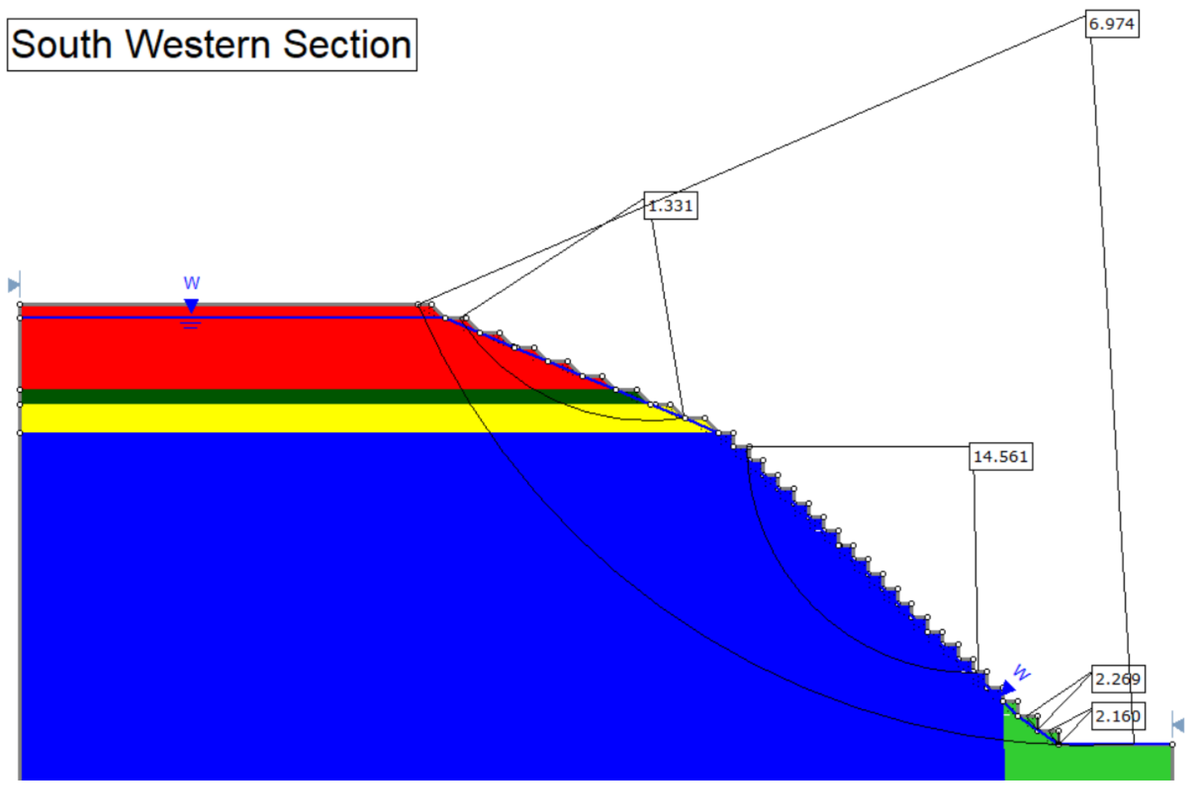

Material Name	Color	Unit Weight (kN/m3)	Strength Type	Cohesion (kPa)	Phi (deg)	UCS (kPa)	GSI	mi	D	Water Surface	Hu Type	Hu
Kalahari Sands		18	Mohr-Coulomb	2	30					Water Surface	Custom	1
Kalahari Sands (SRZ)		18	Mohr-Coulomb	2	30					Water Surface	Custom	1
Saprolite		23	Mohr-Coulomb	22.5	30					Water Surface	Custom	1
Saprolite (SRZ)		23	Mohr-Coulomb	22.5	30					Water Surface	Custom	1
Weathered Granitic Gneiss		20	Generalized Hoek-Brown			3000	30	14	0	Water Surface	Custom	1
Weathered Granitic Gneiss (SRZ)		20	Generalized Hoek-Brown			3000	30	14	0.7	Water Surface	Custom	1
Competent Granitic Gneiss		28	Generalized Hoek-Brown			250000	70	10	0	Water Surface	Custom	1
Competent Granitic Gneiss (SRZ)		28	Generalized Hoek-Brown			250000	70	10	0.7	Water Surface	Custom	1
Kimberlite Domain 4/5		24	Generalized Hoek-Brown			9200	90	13	0	Water Surface	Custom	1
Kimberlite Domain 4/5 (SRZ)		24	Generalized Hoek-Brown			9200	57	13	0.7	Water Surface	Custom	1

Figure 6-8 South Western Section analysed through SLIDE 2D (2018)

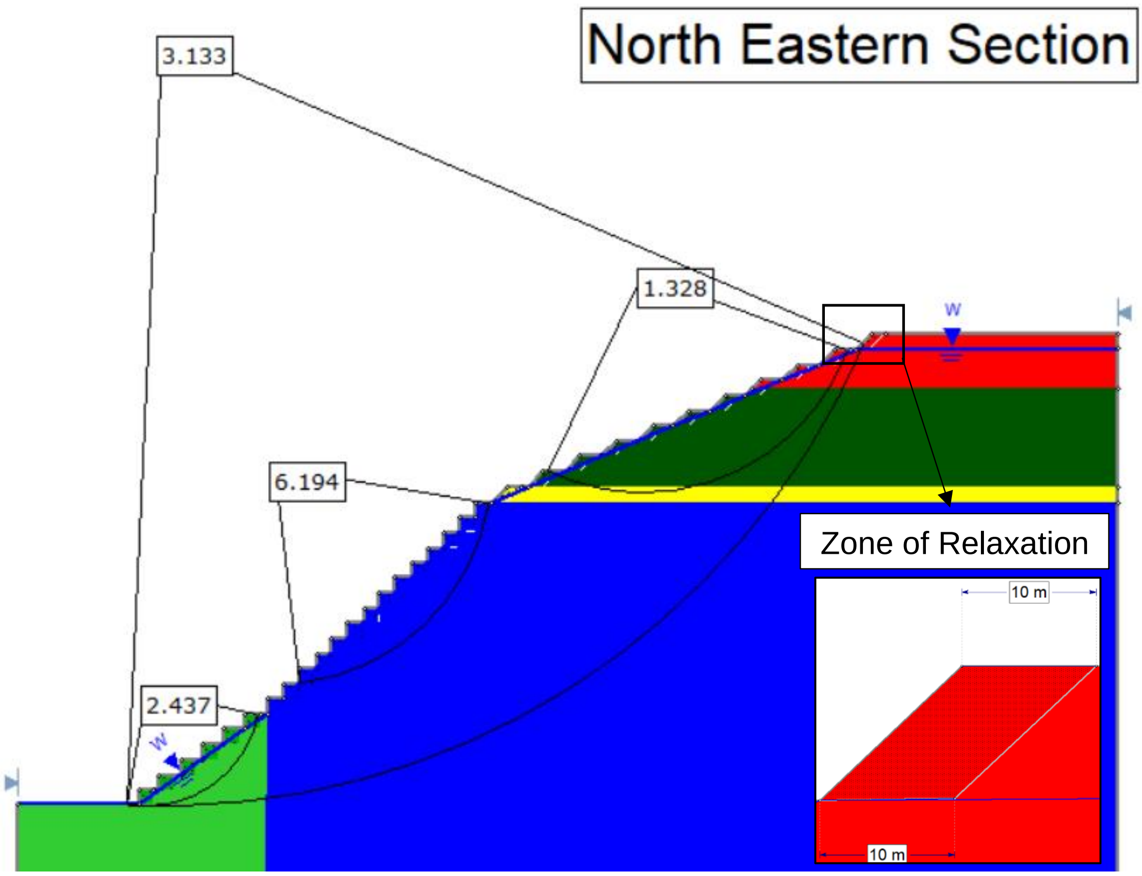

Material Name	Color	Unit Weight (kN/ m3)	Strength Type	Cohesion (kPa)	Phi (deg)	UCS (kPa)	GSI	mi	D	Water Surface	Hu Type	Hu
Kalahari Sands		18	Mohr-Coulomb	2	30					Water Surface	Custom	1
Kalahari Sands (SRZ)		18	Mohr-Coulomb	2	30					Water Surface	Custom	1
Saprolite		23	Mohr-Coulomb	22.5	30					Water Surface	Custom	1
Saprolite (SRZ)		23	Mohr-Coulomb	22.5	30					Water Surface	Custom	1
Weathered Granitic Gneiss		20	Generalized Hoek-Brown			3000	30	14	0	Water Surface	Custom	1
Weathered Granitic Gneiss (SRZ)		20	Generalized Hoek-Brown			3000	30	14	0.7	Water Surface	Custom	1
Competent Granitic Gneiss		28	Generalized Hoek-Brown			250000	70	10	0	Water Surface	Custom	1
Competent Granitic Gneiss (SRZ)		28	Generalized Hoek-Brown			250000	70	10	0.7	Water Surface	Custom	1
Kimberlite Domain 4/5		24	Generalized Hoek-Brown			9200	90	13	0	Water Surface	Custom	1
Kimberlite Domain 4/5 (SRZ)		24	Generalized Hoek-Brown			9200	57	13	0.7	Water Surface	Custom	1

Figure 6-9 North Eastern Section analysed through SLIDE 2D (2018)

A water table was introduced in each section roughly 10 m below surface level and would served to model a FOS at worst case conditions without dewatering. Here the saturation level factor or Hu Factor would be 1 for each lithological unit in the model. Another model was run for each section in dry conditions and the FOS's have been compared with results presented in Table 6.2. Conversely, the saturation level factor or Hu factor would be 0 to represent the dry conditions. The results for each of the section analyses are presented in Appendix E.

Table 6.2 FOS of the different lithological units as predicted through SLIDE 2D (2018) analysis

Wet Conditions				
Section	Kimberlite Domain FOS	Competent Granitic Gneiss FOS	Upper Sediments FOS	Overall Slope FOS
North-East	1.328	6.194	2.437	3.133
North-West	1.648	5.361	3.041	3.304
South-East	2.235	6.370	4.047	3.199
South-West	1.331	14.561	2.160	6.974
Lowest FOS	**1.328**	**5.361**	**2.160**	**3.133**
Dry Conditions				
Section	Kimberlite Domain FOS	Competent Granitic Gneiss FOS	Upper Sediments FOS	Overall Slope FOS
North-East	1.926	7.347	3.337	4.568
North-West	2.318	6.797	4.203	4.849
South-East	2.772	8.030	4.871	4.551
South-West	2.259	15.969	2.160	8.341
Lowest FOS	**1.926**	**6.797**	**2.160**	**4.551**

In addition to hydrogeological impact, the effect of the 10 m wide shear zone striking WSW to ENE was analysed in SLIDE 2D (2018). Hoek & Karzulovic's (2002) zone of stress relaxation (SRZ) for blasts with some control (SRZ = 0.5 to 1H) was incorporated into each SLIDE 2D (2018) model. Since the height of all benches are 10 m, the most damaged parameter of 1H was used, giving a SRZ of 10 m behind the crest and 10 m behind the toe of each bench face. These zones were then modelled in SLIDE 2D (2018) using a blast factor (D) of 0.7. This is considered a standard value for good blasting in smaller open pit excavations (Hoek & Karzulovic (2002)). The zone has been enhanced in Figure 6.9 for illustration purposes.

To quantify the effect that the major sheared zone shown in Figure 6.1 would have on slope stability, a section (A – B) was analysed in SLIDE 2D (2018) (Figure 6.10). The section was taken parallel to the bench faces in the South and was analysed using the anisotropic strength properties gained by direct shear tests on the granitic gneiss (Appendix C). Since the shear zone has been estimated as pre-kimberlite formation by Cruz (2012), it has only been modelled in the granitic gneiss country rock and saprolite lithological units. The SLIDE 2D (2018) model was evaluated with shearing not persisting into the kimberlite units of Figure 6.10.

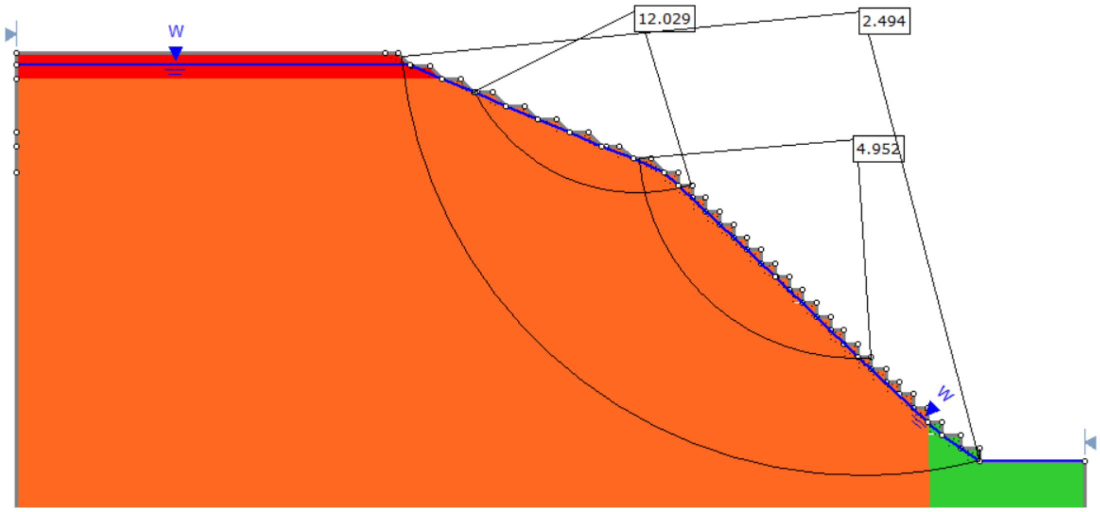

Material Name	Color	Unit Weight (kN/m3)	Strength Type	Cohesion (kPa)	Phi (deg)	Cohesion 2 (kPa)	Phi 2 (deg)	Angle (ccw to 1) (deg)	UCS (kPa)	GSI	mi	D	Water Surface	Hu Type	Hu
Kalahari Sands		18	Mohr-Coulomb	2	30								Water Surface	Custom	1
Kalahari Sands (SRZ)		18	Mohr-Coulomb	2	30								Water Surface	Custom	1
Kimberlite Domain 4/5		24	Generalized Hoek-Brown						9200	90	13	0	Water Surface	Custom	1
Kimberlite Domain 4/5 (SRZ)		24	Generalized Hoek-Brown						9200	57	13	0.7	Water Surface	Custom	1
Shear Zone		20	Anisotropic strength	1690	32	1720	37	-88					Water Surface	Custom	1
Shear Zone (SRZ)		20	Anisotropic strength	1690	32	1720	37	-88					Water Surface	Custom	1

Figure 6-10 SLIDE 2D (2018) model of the shear zone conditions experienced in Section A - B, Figure 6.1

6.2 Boundary Element Analysis – Examine 2D (2006)

To examine the effect of stress on designed total slope faces, a boundary element analysis was done with Examine 2D (2006). Two cross-sections were considered across, and along the expected pit dimensions as shown in Figure 6.1. The sections were aligned to North-West and South-East.

The parameters which were used to analyse the expected conditions are indicated in Table 6.3. It is important to note that this software is an elastic plane strain analysis and thus has certain base assumptions regarding the rock mass. These include that the rock mass is homogeneous, isotropic or transversely isotropic, linearly elastic and infinitely long in the third dimension. These assumptions are approximations and do not represent absolute conditions. In particular, the effects of discontinuities are used to down-rate the rock mass strength, and their orientations are not considered in the analyses. The software assumes a continuum where joints are not explicitly modelled. Another limitation of the software is that the effect of groundwater is not considered. The results from this software were used as a comparison to the charts and the limit equilibrium modelling.

Table 6.3 Summary of Rock Mass Parameters used for Examine 2D (2006) analyses

Lithological Unit	**Rock Mass Properties**					
	Elastic Modulus	**Pois. Ratio**	**Intact Comp. Strength**	**Geolo. Strength Index**	**Hoek-Brown Con (mi)**	**Blast Disturbance Factor D**
Competent Granitic Gneiss	91 GPa	0.25	250 MPa	70	28	0.2
Kimberlite 2 **Kimberlite 3**	0.069 GPa	0.2	7.10 MPa	57	13	0.2
Kimberlite 4	0.87 GPa	0.2	9.23 MPa	57	13	0.2

Separate models were run on the same pit sections, using Hoek and Brown (1980) failure criteria determined for each lithological unit. The results of each model were considered applicable only to the appropriate areas of exposure in the pit sidewalls and floor. The analysis was used to determine whether shear failure would occur due to the strength/stress relationship.

Down-rating of the granitic gneiss rock mass, as previously mentioned, involved the use of the Hoek-Brown rock mass strength parameters and estimating a GSI for each of the lithological units in conjunction with isotropic elastic rock mass properties. The GSI down-rates the rock according to the inferred effect of discontinuities on the rock mass. Since this is only practicable for the country rock mass, the GSI had little effect on the kimberlite models due to its massive nature. For the horizontal and out of plane stress ratios, a k-ratio of 2 was assumed to be sufficient for the anticipated conditions in shallow level excavations above 500 m vertical depth. The Hoek-Brown constant (mi) was selected from the software's list of mi values. For the granitic gneiss rock, mi values of gneiss were selected from the table. For the kimberlite domains 2 and 4, mi values were estimated to be similar to those of tuff and thus a value of 13 from the table was selected. The blast disturbance factor (D) was estimated from expected blasting effect on these lithological units with the current blasting limit wall program achievements.

To analyse the ratio of material strength against the expected induced stress, the Strength Factor function was used in the software. Where results display a value of 1, equilibrium is assumed and thus failure is not anticipated. Contour values below 1 would therefore represent conditions in which failure is anticipated. Since the weathered granitic gneiss unit is not an elastic model material, this unit could not be analysed using the boundary element numerical modelling software.

In total, three models were run for the North-West to South-East Section and two for the South-West to North-East Section, using the input parameters shown Table 6.2. The results from the modelling are presented in Appendix G.

6.2.1 Competent Granitic Gneiss Country Rock

From the results presented in Figures 6.11 and 6.12, and also in Appendix G, it can be observed that when granitic gneiss country rock conditions are input, no failure in the lithological unit is expected. The lowest FOS expected is 1.2 in the North-West side benches in Figure 6.11 and FOS of 1.3 being the lowest in the South Western benches of Figure 6.12. The positions of the granitic gneiss rock in the pit sidewalls is shown in Figures 6.11 and 6.12 by the blue outlines.

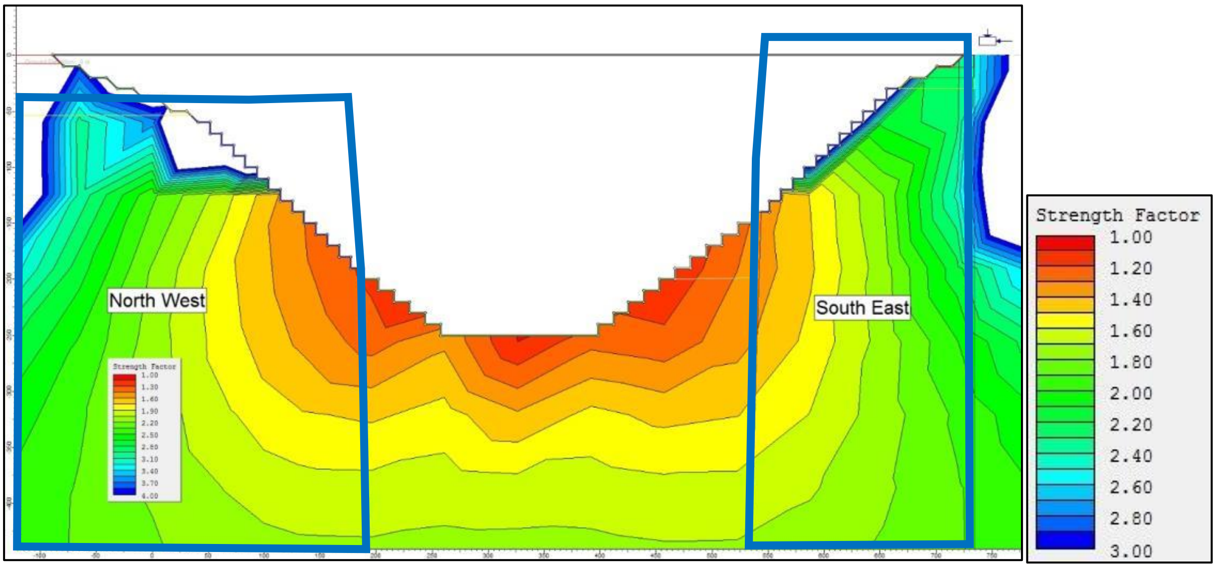

Figure 6-11 Strength Factor analysis of the granitic gneiss rock in the North-West to South-East section through Examine 2D (2006) as indicated by the blue outlined areas

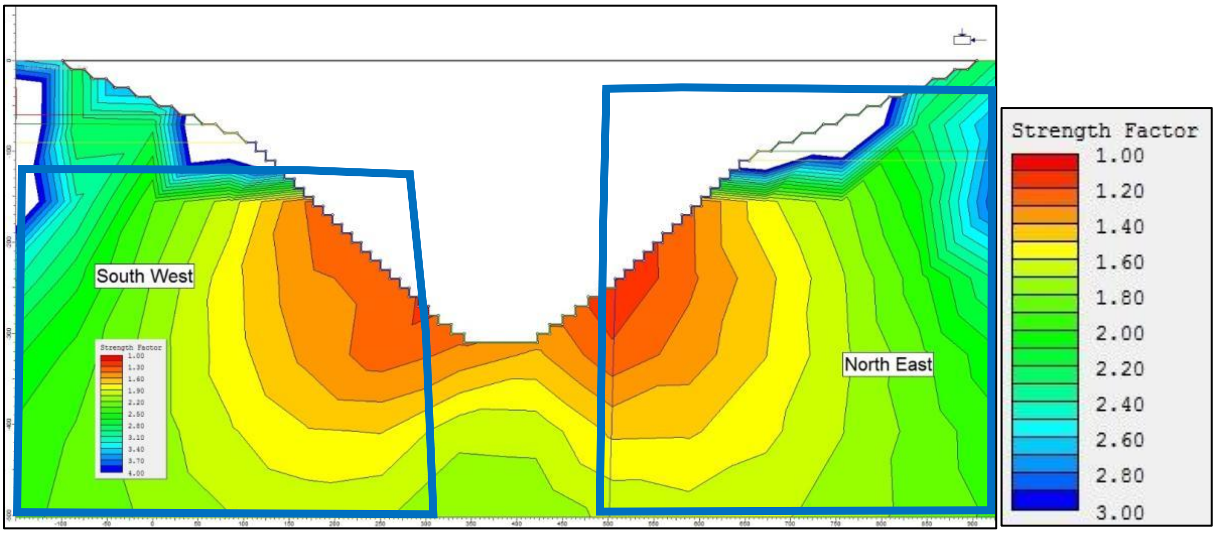

Figure 6-12 Strength Factor analysis of the granitic gneiss rock in the South-West to North-East section through Examine 2D (2006) as indicated by the blue outlined areas

6.2.2 Weathered Granitic Gneiss Rock

Considering that Examine 2D (2006) is an elastic model analysis, the modelling of soil type lithologies such as the weathered granitic gneiss is not applicable. For this lithological unit, boundary element analysis was therefore not done.

6.2.3 Kimberlite Domain 2

When the rock mass strength parameters for kimberlite domains 2 are input into the model, no failure is expected. The geological contacts are indicated through a turquoise outline of the kimberlite domain in Figure 6.13. Since kimberlite domain 2 is only found in minor portions in the North-West to South-East Section and is not present in the South-West to North-East Section, only one model was analysed.

The complete results of the cross-sections have been attached in Appendix G. In this isolated kimberlite unit, the FOS is analysed to be in the range of 1.5 to 2 as indicated by the contour gradients in the turquoise area.

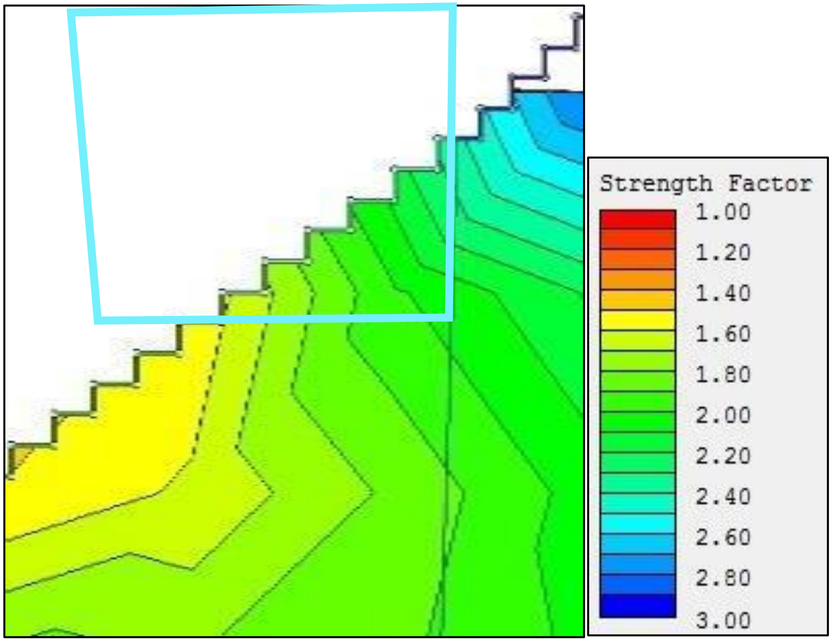

Figure 6-13 North-West to South-East section of strength factor analysis of kimberlite domain 2 using Examine 2D (2006) as indicated by the light blue outlined area

6.2.4 Kimberlite Domains 4

From Figure 6.14 and Figures 6.15, it can be seen that the Examine 2D (2006) FOS for both North-West to South-East as well as South-West to North-East Sections, show stable conditions. For the North-West to South-East Section as presented in Figure 6.14, the lowest FOS is 1.5 with most of the lower slopes and pit bottom in the region of 1.6 to 2. The green outline indicates the extent of kimberlite domain 4 in Figure 6.14.

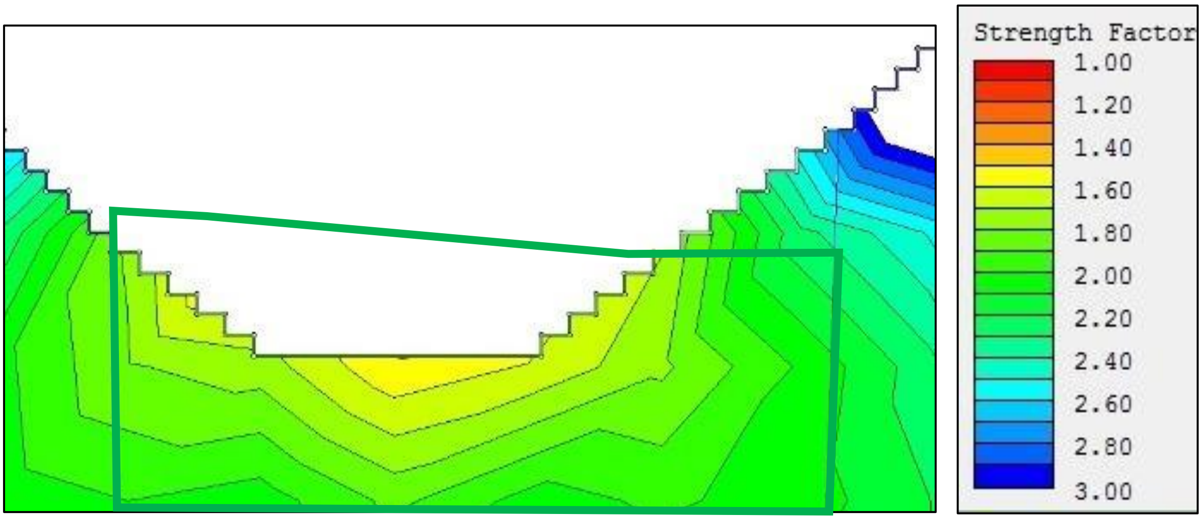

Figure 6-14 North-West to South-East Section strength factor analysis of kimberlite domain 4 using Examine 2D (2006) as indicated by the green outlined area

The South-West to North-East Section (Figure 6.15), predicts a slightly higher FOS than in the North-West to South-East Section. In this section, the FOS ranges between 1.6 to 2. The extent of the kimberlite 4 domain is shown by the green outline. Since the pit is oval in shape, the results provided in Figure 6.15 are closer to reality.

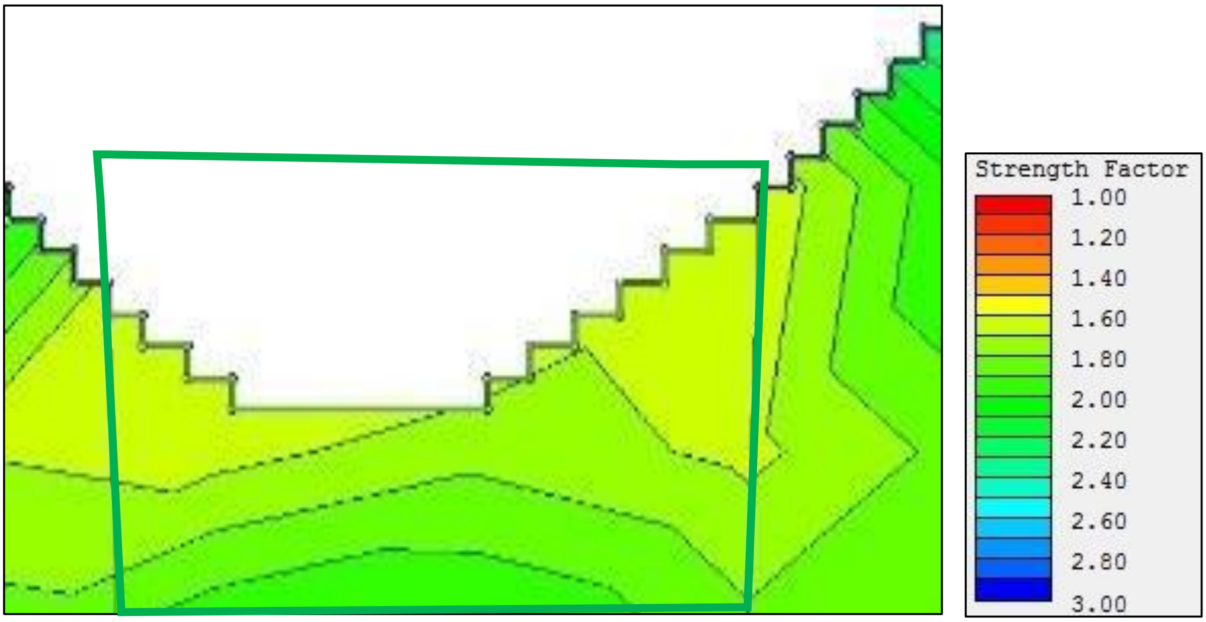

Figure 6-15 North-West to South-East Section strength factor analysis of kimberlite domain 4 using Examine 2D (2006) as indicated by the green outlined area

The resultant FOS per lithological units as inferred by Examine 2D (2006) analysis are presented in Table 6.4.

Table 6.4 FOS results per lithological unit from Examine 2D (2006) analysis

Lithological Unit	Factor of Safety through Examine 2D (2006)
Kalahari Sands	N.A.
Saprolite	N.A.
Weathered Granitic Gneiss	N.A.
Competent Granitic Gneiss	1.2 – 1.4
Kimberlite 2	1.5 – 2
Kimberlite 4	1.6 - 2

7 IMPLEMENTATION

7.1 Pit Limit Blasting Program

Considering the effect which blasting has on highwall stability as explained by Bye (2005) and summarised in Chapter 2, a final pit wall limit program was implemented at Mine A main pit to increase highwall stability and therefore allow for steeper design angles. The program comprised of a three-pronged approach which included focussing on blast timing, size and configuration. The quality of the blasts have been evaluated through the use of pre-split barrel audits in conjunction with Laubscher's (1990) MRMR adjustment factor for blasting (as described in Chapter 2).

The adjustment factor, as well as that for weathering and joint orientation, are multiplied by the RMR to obtain an MRMR. The influence of blasting can be as much as 14 % when applying the barrel audits. This method does not take into consideration blast vibration into the country-rock. However, it is a qualitative way of assigning a value to the adjustment factor suggested by Laubscher (1990).

7.1.1 Blast Timing

The historical blast timing at the site was changed only after the structural conceptualization of the rock mass discontinuities was completed. This project involved window mapping of the structurally controlled rock masses (which is only the granitic gneiss country rock). The burden, spacing, timing requirements as well as optimum directions for blast movement for each specific area is dictated by the geotechnical domains (Section 4.5). An example of movement through timing on a specific blast is shown in Figure 7.1. The arrows indicate movement direction as simulated by the Sasol Surface Blasting Program. The firing sequence of the blast was timed to ensure that the direction of movement was perpendicular to the major structures as well as major joint systems in the region.

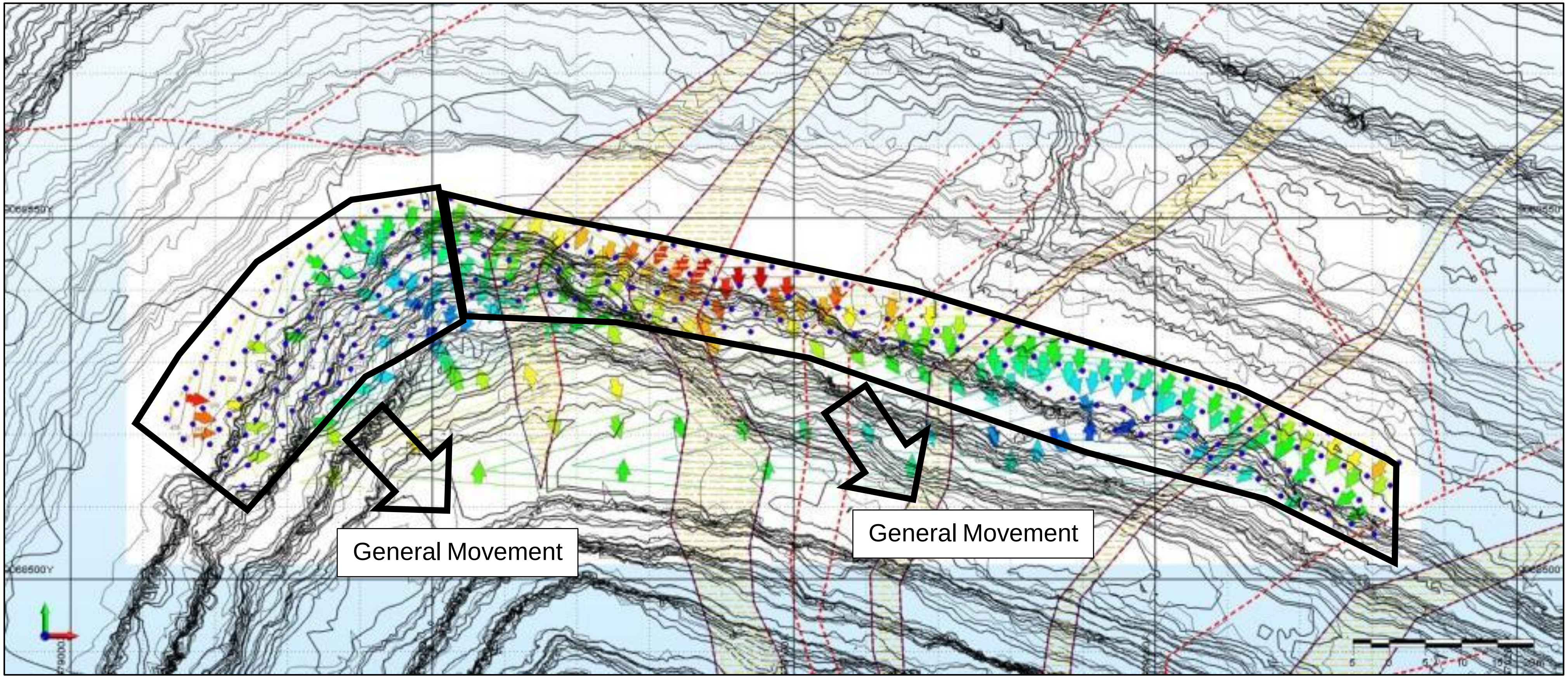

Figure 7-1 Movement of a blast in the 730 m level in the NW of the main pit

The geotechnical blasting domains shown in Figure 7.2 (with suggested direction of movement indicated by arrows) have been turned into isolated blast patterns and timing was done initially purely by the geotechnical department to direct the movement of wave energy created through blasting perpendicular to the orientation of the major jointing systems and thus prevent energy propagation into the discontinuities. Damage due to blast energy penetration into other discontinuities is thus minimised. An added benefit of this approach was the blast fragmentation size decrease. This was attributed to the energy being directed perpendicular to planes as opposed to oblique or along strike. The smaller fragmentation size allowed for faster loading and hauling and thus improved productivity.

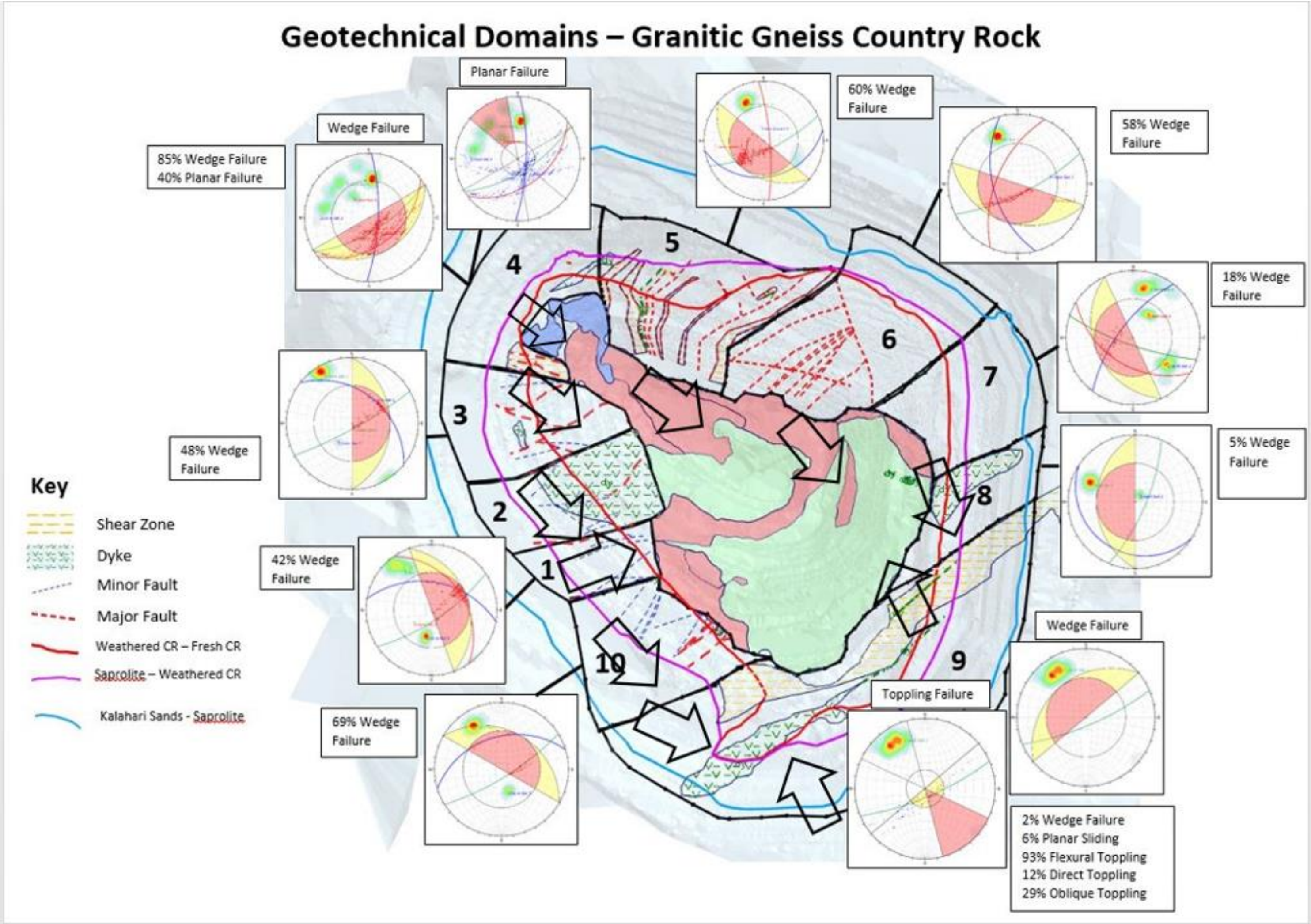

Figure 7-2 Geotechnical Blast Domains with suggested blast movement indicated through arrows

7.1.2 Blasthole spacing

To ensure energy propagation into highwalls was kept within acceptable limits, the numbers of holes to be detonated in a single blast, were reduced. Originally patterns in the region of 500 holes were being charged and blasted as one blast, but with separation of blasts into the geotechnical zones, no more than 200 holes were exceeded in blasts. The 102 mm drill holes were spaced in the competent granitic gneiss initially at a burden and spacing of 2.5 m, but with smaller blasts and better movement, this could be increased to 3.5 m. The increase not only saved on drilling time, but also on explosives usage.

7.1.3 Perimeter blasting

Prior to the final wall blast program implementation, no pre-split or highwall control blasting existed. Since such highwall controls have been implemented, visible barrels in final highwalls have increased from 30-40% on the granitic gneiss to 80-100%. A clear highwall stability improvement has thus been achieved using the following process flow:

- Pre-split detonation
- Production blast detonation; and
- trim and buffer line blasts.

Special attention was also paid to ensuring that the free face was clear of all material and that no toes were present on the initiation face, prior to highwall control blasting (trim and buffer blasts). This allowed for movement of energy to be directed away from the highwalls and thus decrease the negative effect of energy propagation into the rock mass discontinuities behind the final wall limit. The policy of isolated blasting in the sequence pre-split, production, buffer and trim blasts will need to be strictly followed in the new pit design during the mining cut-backs.

Regarding pre-split spacings, the industry standard 10 times the hole diameter should remain as practice. This will equate to 1 m spacing for the 102 mm drill holes as currently employed. In the competent granitic gneiss, a burden and spacing of 3.5 m x 3.5 m which has been proven to produce best fragmentation results should continue. In the softer kimberlite domains the burden and spacing of 4 m x 4 m current standard should continue.

7.2 Slope Stability Monitoring Strategy

7.2.1 Introduction

Considering the lack of geotechnical data available and the probability of minor and major sidewall failure due to unexpected intersection of discontinuities, a robust monitoring strategy is required. The three-phase monitoring strategy which has been selected and implemented at the main pit involves hazard identification, strategic monitoring as well as safety-critical monitoring. Numerous safety protocols have also been introduced and will be discussed in the following sections.

First pass hazard identification is a monitoring strategy which relies on:

- visual observations;
- photogrammetry through input of final wall pictures into the 3D model in Micromine;
- crack measurements through tensiometers and extensometers;

- seepage water mapping;
- joint discontinuities mapping and stereonet analysis.

Considering financial constraints on the geotechnical program, techniques which have been employed at Mine A remain elementary by nature, but highly effective when implemented consistently.

Strategic monitoring entails quantified results of slope movement. Such true observations in x-, y- and z-axis can be obtained through prism monitoring. The strategic monitoring program started with infrastructure establishment in November 2019 but awaits prisms for full-scale implementation.

Critical monitoring is a real-time monitoring strategy which employs either radar systems or laser scanning systems. The purpose of such monitoring systems is to monitor critically identified areas through prism monitoring and hazard identification. The Reutech MSR trailer-mounted radar was purchased post-September 2018's mass failures and has been in operation ever since. The system provides qualitative data only, as measurements are of the relative range changes from the radar to the slope face and thus not movement in x-, y- and z- directions as is the case with prism monitoring.

7.2.2 Range of Possible Mechanisms of Failure expected

Before deciding on the type of system to be implemented on any site, the expected failure systems and rock mass behaviour need first to be understood. Once this is known, it is possible to determine the most efficient, fit-for-purpose, resilient and defensible system. The different types of failure expected, have been summarised in the subsections below. Modelling has been done using the DIPS (2013) by Rocscience software and stereonet analysis. Figure 7.3 shows the probability of failure per geotechnical zone as predicted by DIPS (2013) through analysis of major joint set orientations in relation to the excavated face. In addition, four greater zones have been identified with similar failure mechanism conditions and have been discussed further in the following sections. Note that a bench slope angle of 90° was used in the analysis shown in Figure 7.3.

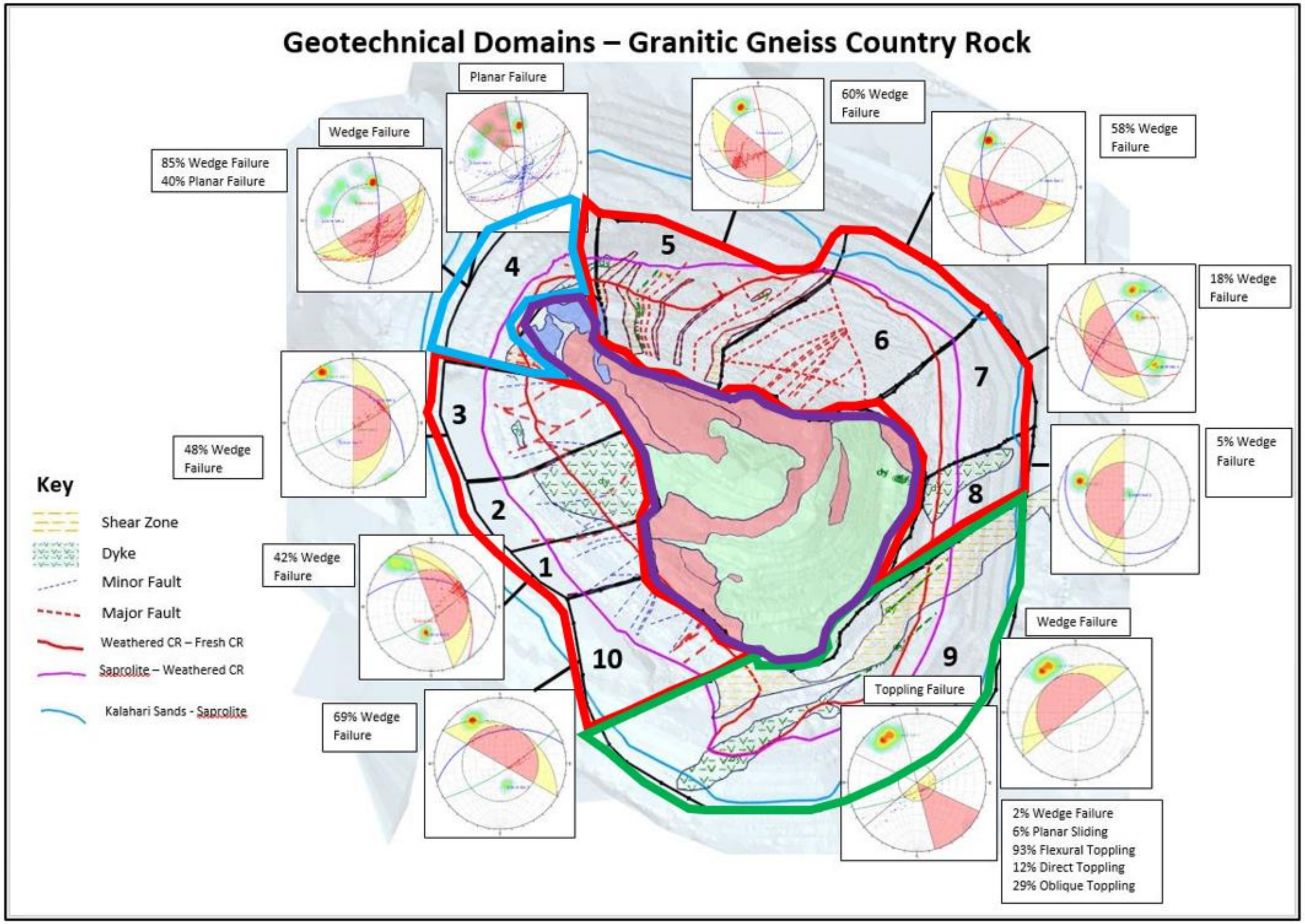

Figure 7-3 Probability of failure per geotechnical zone as predicted by DIPS (2013)

The yellow shaded semi-circle in the stereonets represents the critical zone of intersection of planes. If any great circle intersections fall within this shaded area, the probability is that they will fail. The smaller circle in the centre of the stereonet indicates the friction angle of the joint systems (30˚ as per Ryder and Jager (1999)). The function predicts the failure probability in the rock mass due to the intersection and orientation of discontinuity planes and excavation faces. These have been presented with each stereonet and are individually presented in Appendix F.

*7.2.2.1 Wedge Failure in the North-East and South-West Country Rock Domains (**Red** Fig. 7.3)*

Due to intersecting jointing systems in the North and South of the main pit, small scale wedge failure has a high probability to occur according to DIPS (2013) failure probability analysis. Although this failure is expected, mitigation measures can be implemented to prevent failure having any effect on the safety of personnel or equipment. The risk of wedge failure in these areas is relatively high, with the DIPS (2013) kinematic failure analysis tool predicting between 42% to 60% of great circle intersections falling within the shaded critical failure zone (yellow shading). The failure probability takes into consideration the orientation of the major joint systems involved with regards to the excavation face. The friction angle of the critical joint set in the rock mass, is incorporated into analysis of the specific block. This angle should be obtained through laboratory shear testing of granitic country rock core, but since this was not done, a standard 30˚ as suggested by Jager and Ryder (1999) was used. With these parameters, a probability of failure can be calculated through simplistic stereographic analysis, which has been incorporated into the DIPS (2013) software.

*7.2.2.2 Planar Failure in the Western Country Rock Domain (**Blue** Fig. 7.3)*

Due to slope geometry intersecting the major jointing systems on the Western limb of the main pit, the probability of failure of planes here had been calculated as 40% through probability analysis in DIPS (2013). A risk of wedge failure is also present with 85% of intersections of great circles falling within the shaded critical failure zone.

*7.2.2.3 Toppling in the Eastern Country Rock Domain (**Green** Fig. 7.3)*

To the eastern limit of the main pit, the major joint systems are conducive to toppling failure, due to planes dipping away from the excavation. The probability of toppling failure in this area has been calculated through intersection of great circle intersections within the critical failure zone (yellow shaded area) to be at 93% by the DIPS (2013) kinematic failure analysis tool.

*7.2.2.4 Curvilinear Failure in the Kimberlite Domains (**Purple** Fig. 7.3)*

The kimberlite intrusion into country rock is void of internal jointing systems or major structures. The rock is thus considered massive and rock mass behaviour is conducive to circular or curvilinear failure. Due to the initial design not conforming to the rock mass strength of the different kimberlite types, failure has occurred in areas where the mass was incapable of maintaining the stress conditions created due to the excavation depth. The demand thus exceeded capacity and failure ensued. With the new proposed design, however, failure is not predicted in the lower kimberlite portions due to a proper design and consequent shallowing of the slope angle.

7.2.2.5 Mitigation Measures

Mitigation of all the brittle rock failure types would involve primarily identifying areas that would require mitigation. Since mining is active in most of the pit, no permanent means would be economically feasible. For semi-permanent areas such as haul roads, mitigation is required. This would involve the implementation of a wire meshing program to catch any loose rock from wedge, toppling and planar failure. In addition to these measures, small scale (less than 2 m^2) wedge blocks identified during the excavation and prior to final wall sign off, must be brought down with excavators to prevent future failure.

7.2.3 Recommended Hazard Identification Systems

7.2.3.1 Visual Inspections

For greater coverage of hazardous areas, all personnel are to be trained and briefed in the identification of different types of failure behaviours, alarm levels and hazard reporting. As such, all personnel working in the pit environment become field observers and allow for early identification of slope failure. Figure 7.4 is recommended to be used in the training of field observers. It has been adapted from a presentation by Mossop and Terbrugge (2019) at the University of the Witwatersrand slope stability monitoring course.

<table>
<tr><td rowspan="3">1. Spot the Hazard</td><td>Bench crest and berm</td><td colspan="2">• Has the bench been scaled?
• Are there overhanging or unstable blocks on the crest/is the crest undermined?
• Are cracks visibly worse than in the previous inspection?
• Is there dust coming from any cracks?
• Are there loose rocks on the crest?</td></tr>
<tr><td>Highwall</td><td colspan="2">• Has the highwall been scaled?
• Is the highwall undermined anywhere?
• Are there unstable blocks against the highwall?
• Are there open cracks in the highwall?
• Are cracks visibly worse than in the previous inspection?
• Is there dust coming from any cracks?
• Are there small stones and boulders ravelling off the wall?
• Is there water seeping from the highwall?
• Is there water standing on the bench above?
• How far are you from the highwall?</td></tr>
<tr><td>General</td><td colspan="2">• Has there been recent rainfall (heavy or prolonged)?
• Has there been recent blasting or excavation nearby?</td></tr>
<tr><td>2. Do a RISK ASSESSMENT</td><td colspan="2">✓ Do the Hazards affect necessary access?
✓ How can the hazards affect the job to be done?</td><td>✓ How can the hazards affect people doing the job?
✓ Can the work continue without direct supervision?</td></tr>
<tr><td>3. Do an act of safety</td><td colspan="3">➢ Demarcate the hazardous area
➢ Make people aware of the hazards and make sure they understand instructions
➢ Can the hazards be avoided?
➢ If YES – Proceed with care
➢ If NO – Report hazards to the Pit Superintendent
➢ Don’t park or stand within 45˚ of a highwall
➢ Don’t remove material from the wall or crest yourself
➢ Redo risk assessment each time you access an area below the highwall
➢ Contact Geotechnical Engineer if in doubt</td></tr>
<tr><td>Things to look out for:</td><td>Uncleaned Highwalls</td><td>❖ Open Fractures on the berm
❖ Loose blocks against the face
❖</td><td>❖ Loose material at the toe
❖ Has the situation been reported and demarcated</td></tr>
<tr><td></td><td>Clean Highwalls</td><td>▪ Properly scaled and cleaned crest
▪ No loose material against the face</td><td>▪ Cleaned and graded at the toe
▪ Visible pre-split barrels</td></tr>
</table>

Figure 7-4 Visual Inspection Check List after Mossop and Terbrugge (2019)

In addition to training of all personnel to be vigilant with regards to geotechnical hazards in the pit, the geotechnical engineer will be responsible to keep a record of his visual inspections. These should be conveyed to the mining manager daily to be briefed to shift supervisors and ultimately personnel working in the pit. Four different colours are used to depict four levels of danger and thus alarm level. These are in order of lowest to greatest danger, green; yellow; orange; and red. An example of a visual observation report can be seen in Figure 7.5.

GEOTECHNICAL INSPECTION LOG SHEET FOR PROJECTO CAMUTUE

Date	Person	Pit	Quadrant	Section	Comments
24-Oct-19	Ian Mason Snyders	CW	Q3	C3	VKB upper portion. Where minor curvilinear collapse has occurred on this portion at ramp level, some minor cracks showing. Due to caving of kimberlite below more competent country rock breccia lense. Has a catch bench two benches down. Level **YELLOW**.
			Q2	B3/B4	Where major collapse has occurred, upper benches appear to be without cracks. A triple bench stack is present though with seepage water being channelled over this failed portion. Due to the 660m catch bench and currently ramp being cleaned, no danger is present. Level **YELLOW**. Once ramp has been cleaned and the 660m catch bench for this area will need to be cleaned and re-established.
		RADAR			All walls on the South and Eastern side of the pit are stable, with normal elastic rebound/slope relaxation curves. Current Status of scanning area level **GREEN**.
Mining Manager					

Figure 7-5 Geotechnical Inspection Log Sheet example

For practicality, a quadrant and section system was introduced, to identify hazardous regions and relay this information to the mining department. The quadrant map in Figure 7.6 allows for easy identification of areas within the pit.

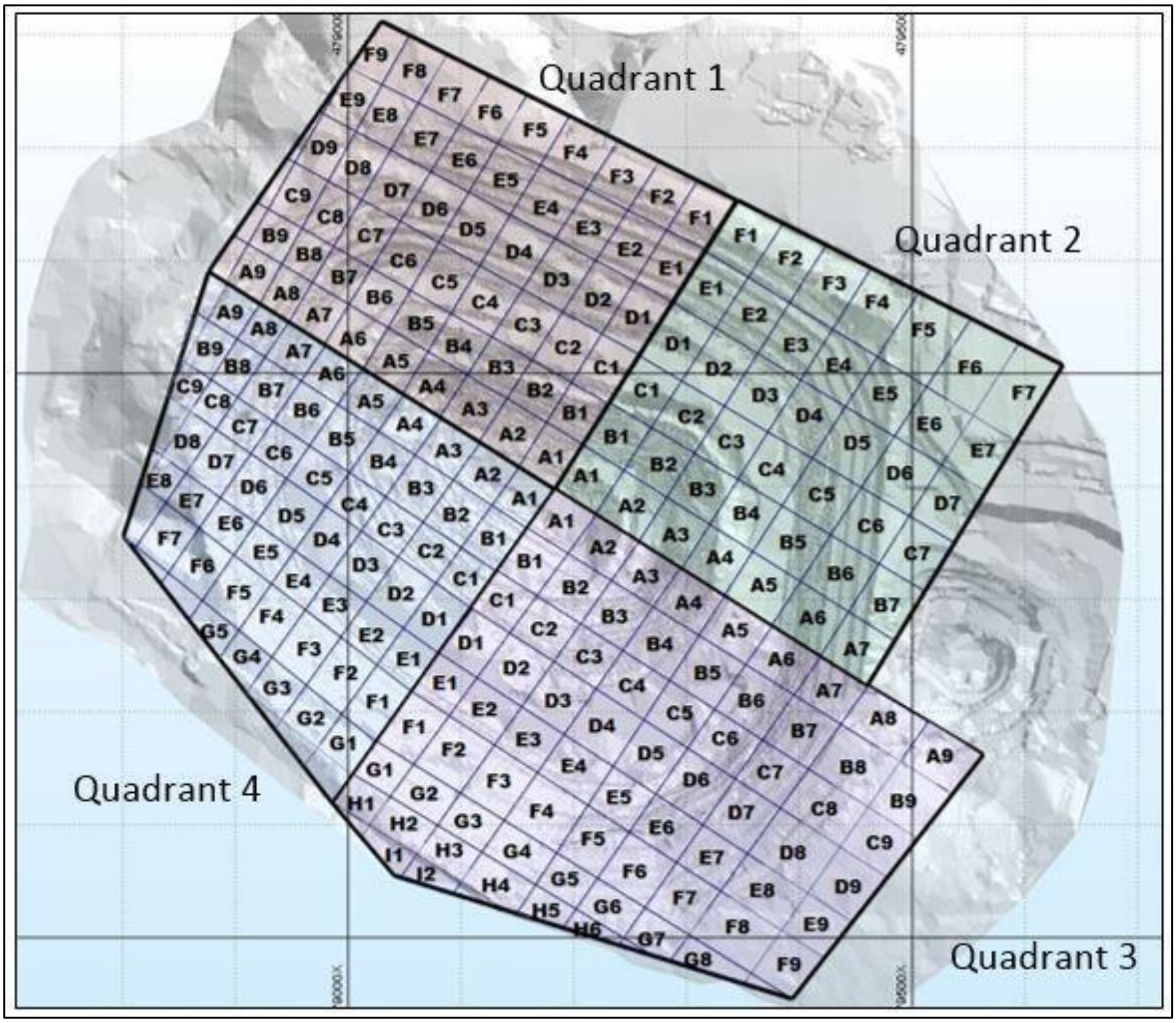

Figure 7-6 Quadrant and Sector nomenclature of the main pit

7.2.3.2 Photogrammetric Recording

The practice of photogrammetry post-window mapping of each geotechnical domain is recommended. The images are georeferenced in Micromine and allow for critical inspection of geological and geotechnical structures.

7.2.3.3 Piezometers

A dewatering program is imperative to the stability of the pit. Five piezometers are planned to be strategically positioned, to monitor the hydraulic pressure on the highwalls (Figure 7.7). Benefits of such piezometer installations include closing the current hydrogeological data gap, as well as allowing for an investigation into a strategy for pit dewatering. The effect of groundwater specifically on brittle failure mechanisms could be the difference between failure and stability. The same is true for mass or circular failure mechanisms. These effects are illustrated in the soil design charts by Hoek and Bray (1981) where 5 different charts have been inferred for the different levels of saturation. As the groundwater saturation level increases in these charts, so the allowable slope angle decreases (Hoek & Bray, 1981). The location of these monitoring wells will be distributed throughout the outer rim of the final pit so as to maximise on their lifespan as well as understand the overall character of the groundwater component. Points WP01 and WP02 are aimed at understanding the effect of the major shear zone in the South Eastern portion of the pit while WP03 and WP04 are aimed at identifying the influence of the North Western shear zone groundwater contribution. WP05 would be aimed at identifying the influence of the river to the North-West of the pit on the excavation.

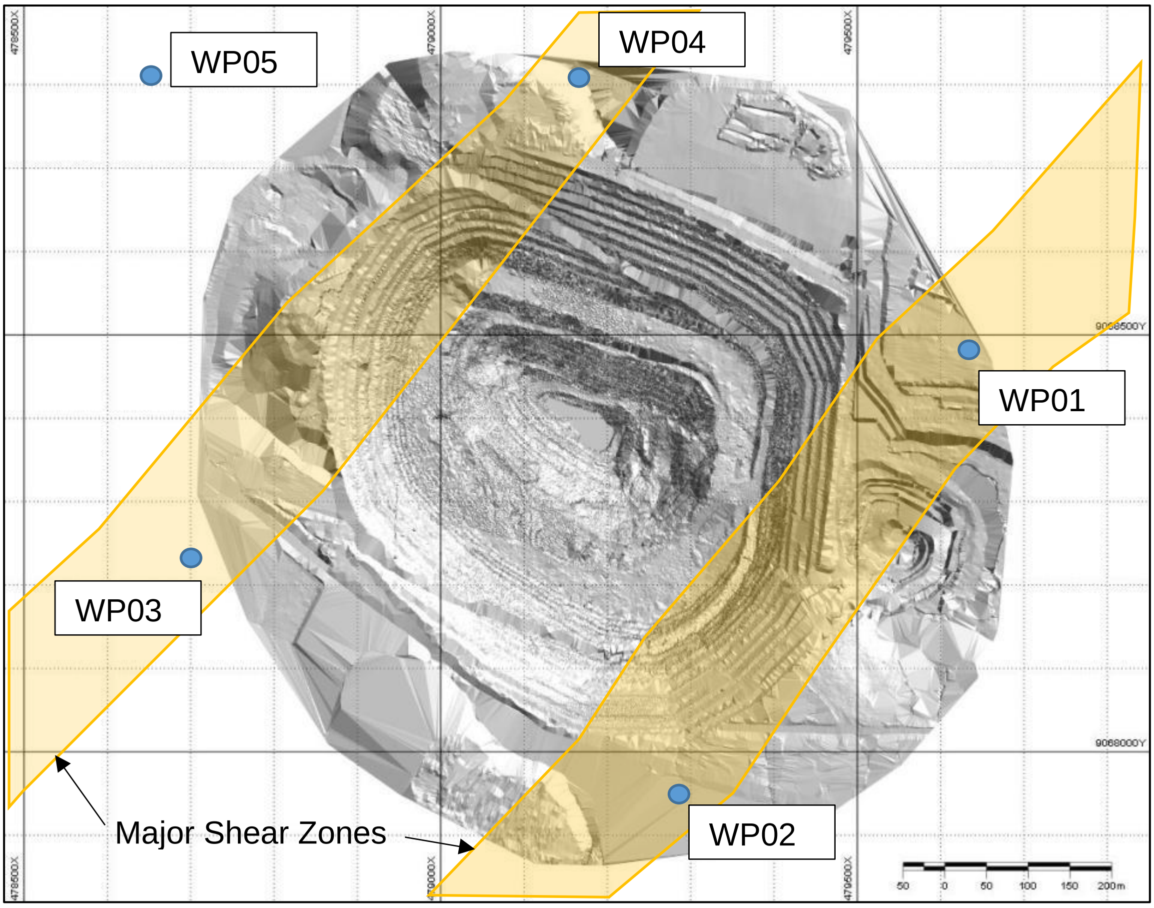

Figure 7-7 Proposed locations for installation of wireline piezometers for hydraulic pressure on highwalls investigation (shown by WP01 – WP05)

7.2.3.4 Precipitation Monitoring

A good record of rainfall data has been kept over the last 4 years through rain gauges and will continue to form part of the first pass hazard identification. The valuable databasing has allowed for the correlation between slope instability possibly caused by large rainfall events or prolonged periods of rainfall.

7.2.4 Strategic Monitoring Techniques

7.2.4.1 Prism Monitoring

Implementation of a strategic monitoring system is recommended to be gained through daily prism monitoring. Phase one of prism monitoring should involve the construction of monitoring infrastructures. These are namely the primary beacons, reference beacons and transfer station beacon. A design for the primary and reference beacons is seen below in Figure 7.8 and transfer station beacon in Figure 7.9. The steel rebar and reinforced concrete allow stability of mounted prisms and thus accuracy of readings from the totalstation.

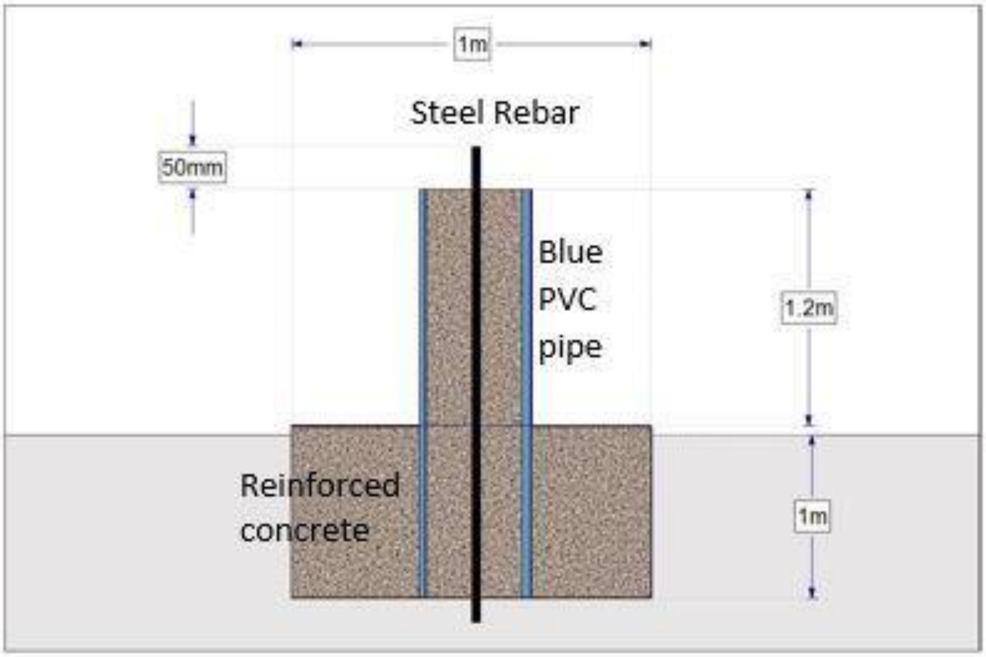

Figure 7-8 Primary and Reference Beacon Design

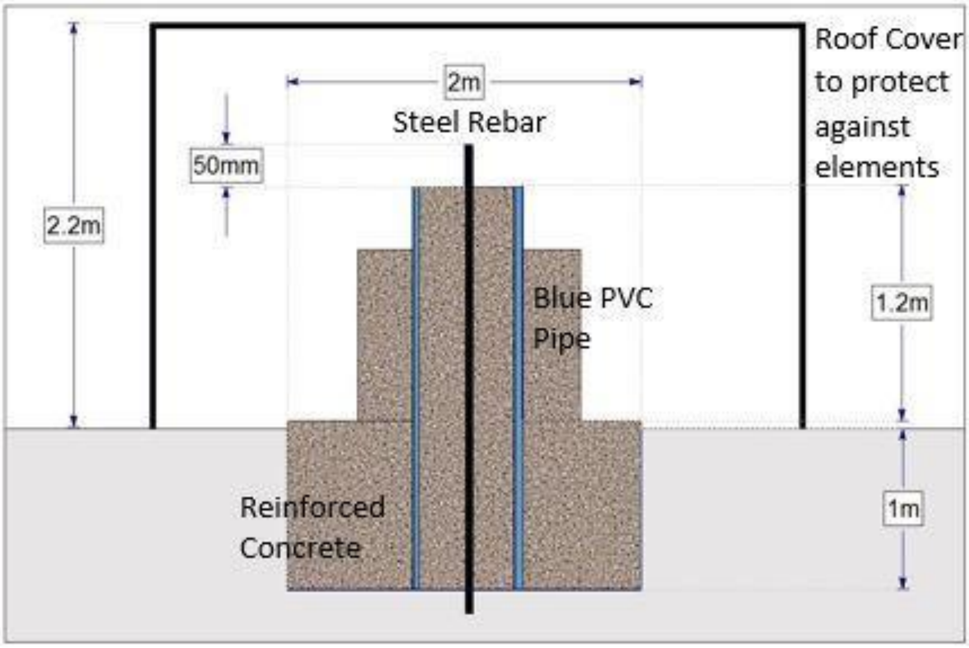

Figure 7-9 Transfer Beacon Design

The proposed positions of the beacons are shown in Figure 7.10. Reference beacons will be named PC-RB01 to PC-RB05 and transfer beacons will be named PC-TB01 and PC-TB02 as shown in Figure 7.10.

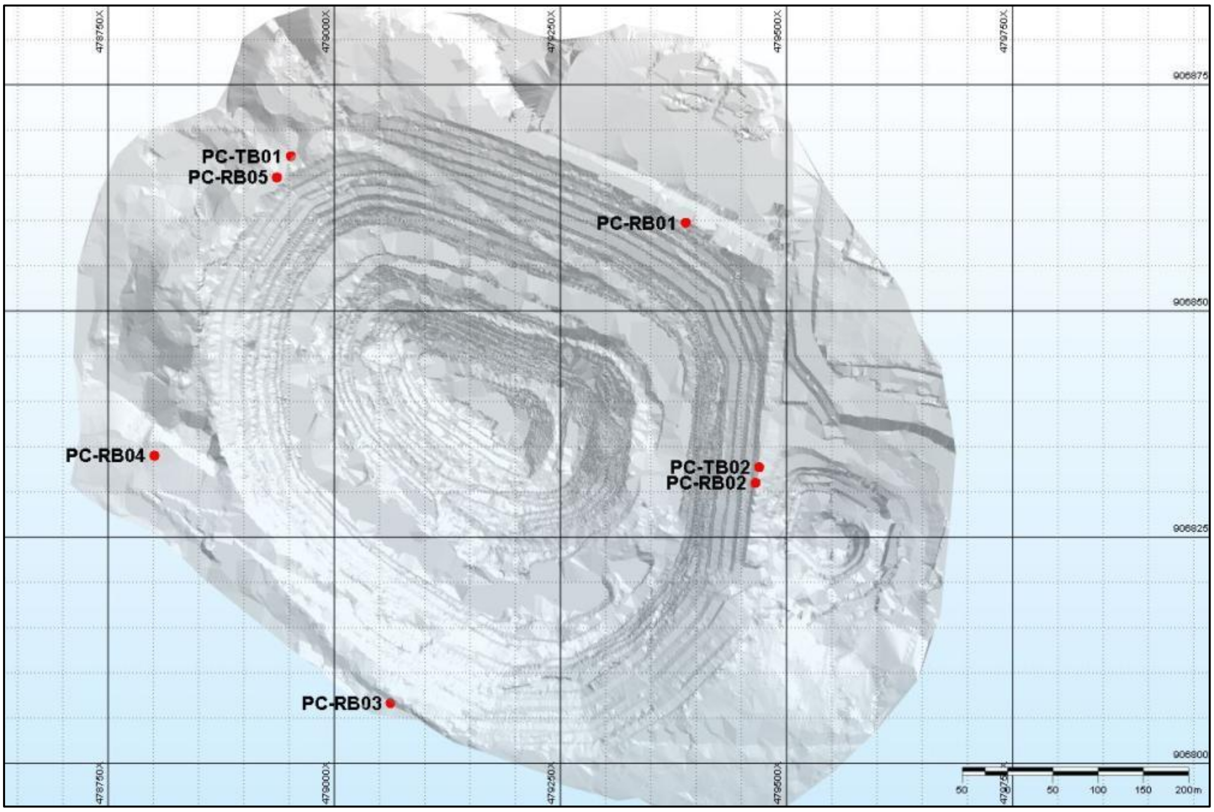

Figure 7-10 Location of reference and transfer beacons in the main pit

Initial daily measurements, using the prism monitoring program, will be made by use of a Leica TS02 total station from positions PC-TB01 and PC-TB02 in Figure 7.10. These vantage points will cover the total area of the pit. In addition, five reference and three primary beacons should be installed for georeferencing and check surveys. A temperature and pressure sensor is required for atmospheric correction of readings. These sensors should be placed within a Stevenson Screen housing. Initial prisms would need to be procured immediately and additional prisms added as mining advances.

7.2.4.2 Laser Scanning

The current Quarryman laser scanner should be used to do monthly pit surface scans, in addition to the daily prism monitoring strategic monitoring. These point cloud files can be converted into DTM surfaces within Micromine and compared to the previous month's scan to identify any deviations over a longer period. Additionally, these scans can be reconciled monthly to the pit design to consolidate planned against actual mining surfaces and in so doing identify under- or over-mined areas which would require remediation.

7.2.5 Safety Critical / Tactical Monitoring

7.2.5.1 Reutech MSR

The use of the currently operational MSR mobile trailer-mounted unit will continue. This allows for tactical monitoring of critical identified areas through prism monitoring, laser scanning and visual inspections. The radar is currently deployed in position PC-TB01 as shown in Figure 7.10, and is scanning the opposite critical volcanic kimberlite breccia faces which have been found unstable due to incorrect cut angle. As the next mining cut-back advances, however, the radar will be moved to scan areas identified as hazardous. The current configuration consists of the trailer-mounted radar unit as well as a receiver station which is trailer mounted. The data is thus transmitted from radar to the receiver unit and finally to the office block through a wifi connection. The system is illustrated in Figure 7.11.

MSR Trailer Mounted Unit	Trailer Mounted Receiver Unit	Office – Data receiving and Analysis
		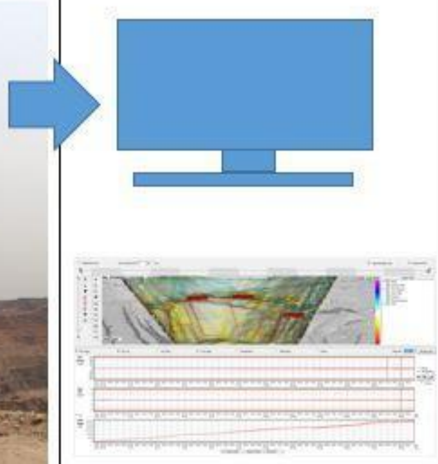

Figure 7-11 Radar data transfer process flow

Once strategic monitoring through prisms is available, this survey data can be integrated into the Reutech MSR software. This will allow for one viewing platform of all slope movement data and thus ease of data access.

7.2.6 Slope Management: Procedures, Planning and Databasing

7.2.6.1 Legal Framework

The document governing safe working practice and mining procedures is the Angolan Mining Code of 2015. Due to relative inexperience with open-pit mining, the code has not been adapted as yet to incorporate any requirements for slope stability monitoring. The framework is found in CHAPTER IV: "Responsibility of Holders of Mining Rights; Section I: Hygiene, Health and Safety and Training". It states that holders of mining rights are to take steps to ensure the hygiene, health and safety of the workplace, as well as prevent occupational risks and workplace accidents.

Although the Mine Health and Safety Act 29 of 1996 indicates that the monitoring of slopes is required only where ground movement has been identified (Chapter 17:7c), it does outline requirements for codes of practice and the need for evacuation procedures. In such instances, where legislation is found to be insufficient to provide guidelines, the standard should always be lifted to ensure the safety of such an operation. The accountability of the South African Mine Health and Safety Act 29 of 1996 will therefore be adopted. A description of the relevant requirements of the act are provided below:

7.2.6.2 Trigger Action Response Plans

The Trigger Action Response Plans (TARP) have been adapted from de Graaff (2019). The TARP has been adjusted to fit in with occupational levels in current use on the operations, as described in the following sections.

7.2.6.3 Evacuation Procedures

Evacuation procedures, as described in Tables 7.1 and 7.2, were developed by a team on the mine. The two critical levels of alarm (ORANGE and RED), would have two different evacuation procedures, with the only difference being that during ORANGE level alarms, enough time is available for evacuation of all equipment whereas for RED level alarms there is not. The time for evacuation is determined by an inverse velocity function where 1 is divided by the average velocity, which has been calculated from a change in relative position compared to time.

Table 7.1 Orange level alarm, by the instruction of the geotechnical engineer

Action	**Yes/No**
1. Stop work in the hazardous area upon the instruction of Shift Supervisor. Remove all equipment from the fall-out area.	
2. Restrict access to the hazardous area immediately (cordon off).	
3. Shift Supervisor to do role call at exploration parking and establish all personnel who were working in the hazardous area have been evacuated.	
4. Await outcome of RISK ASSESSMENT by Geotechnical Engineer, Health and Safety Superintendent, Mining Manager, Technical Services Manager and Mine Manager.	
5. Only upon de-escalation to level YELLOW or GREEN are Shift Supervisors permitted to re-enter area with the personnel.	

Table 7.2 Red level alarm, by the instruction of the geotechnical engineer

Action	**Yes/No**
1. Stop work in the hazardous area immediately and proceed to exploration parking.	
2. Restrict access to the hazardous area immediately (cordon off).	
3. Shift Supervisor to do role call at exploration parking and establish all personnel who were working in the hazardous area have been evacuated.	
4. Await outcome of RISK ASSESSMENT by Geotechnical Engineer, Health and Safety Superintendent, Mining Manager, Technical Services Manager and Mine Manager.	
5. Only upon de-escalation to level YELLOW or GREEN are Shift Supervisors permitted to re-enter area with the personnel.	

7.2.6.4 Risk Assessments

A risk assessment is recommended at intervals between yellow alarms going into orange level alarming, as well as orange level alarming into red level alarming. In addition to these evacuation risk assessments, re-entry risk assessments are suggested to be done before de-escalation is signed off by the relevant co-ordinating authority. These risk assessments need to be recorded and signed by all HOD's and conveyed to all affected personnel in the hazardous area. In both orange and red level risk assessments, the following competent people should participate and sign-off the final document.

Technical Services Manager; Geotechnical Engineer; Mining Manager; Health and Safety Superintendent; Production Manager; Mining Manager/Acting Mine Manager; Shift Superintendent

An example of a risk assessment checklist is provided in Table 7.3. The assessment should not be limited to the questions in the figure, but should be uniquely tailored to the situation and conditions being encountered.

Table 7.3 General template for a risk assessment questionnaire which could be completed between all levels of alarming

Question to be asked	**Yes/No/Answer**
Do the hazards affect necessary access?	
How can the hazards affect the job to be done?	
How can the hazards affect people doing the job?	
Can the work continue without direct supervision?	
Has the hazardous area been demarcated?	
Can the hazard be avoided?	

7.2.6.5 Geotechnical Bench Maintenance

An important aspect of risk management with regards to highwalls is to mine to the design. This includes cleaning all faces to final limit (pre-split barrels) and ensuring that benches are cleaned post-trim blasting. In conjunction with bench cleaning, to prevent pooling of rainwater and groundwater seepage, hazardous to highwall stability, drainage channels should be established on the highwall side of ramps all the way to pit bottom as a common practice.

7.2.6.6 Contingency planning – post-failure risk assessment and planning

In the event of major failure (failure volume above 5000 m^3), which will have a significant impact on the mine plan, a strategic meeting should be held with the CEO, Mine Planning, Production Manager, Mine Manager, Technical Services Manager and Geotechnical Engineer. The Geotechnical Engineer is responsible to convey the failure report, including the present risk assessment level. The team should then decide on the best remediation procedure to make the area safe.

7.2.6.7 Data Storage and Back-up

Due to the remoteness of the operation and limited connectivity, cloud storage of data has been deemed unfeasible. All geotechnical and slope monitoring data should thus be stored on an external hard drive, with back-up occurring weekly. This back-up should be sent quarterly to the head office and uploaded to cloud storage. This allows for back-analysis of all data, should such investigations be required.

7.3 Discussion and Summary

In the case of Mine A where geotechnical model information is limited and thus slopes have been designed on sub-standard levels of information, a robust slope stability monitoring strategy must be employed. Such a robust monitoring strategy should incorporate geotechnical hazard identification systems, strategic monitoring as well as critical monitoring systems. As indicated in this report, for initial strategic monitoring to be implemented will require minimal capital input costs. These include infrastructure for the beacon network as well as the initial prisms.

In addition to the first pass hazard identification, strategic monitoring and critical monitoring, the correct first response and emergency evacuation procedures will need to be implemented. These have been outlined as per Chapter 6 of this document. The five major sections of a slope stability monitoring strategy are thus fulfilled, with contingency planning to be implemented only upon failure.

When considering the national legal requirements for slope stability monitoring, it is suggested that the guidelines as indicated by the South African Mining Act be adopted as a high standard and all survey and monitoring systems be upgraded to comply with these high standards.

8 DISCUSSION OF RESULTS

The question which was investigated through the methodology followed by this research project was whether a reliable geotechnical model could be created from the limited geotechnical data on the mine and furthermore if the use of this low-level confidence geotechnical model could produce a dependable and safe slope design. A level of confidence was achieved by comparing the results of the collected data to published norms and standards, and comparing design charts to limit equilibrium and boundary element numerical models. There are uncertainties in the design, which must be mitigated by continuous monitoring.

8.1 Geotechnical Model creation

In addition to slope stability FOS comparisons, results from Chapter 4 indicate that a geotechnical model can be established and can be used in slope design through design charts. This can be done even when geotechnical model data is at pre-feasibility to feasibility study level geotechnical confidence as per Read and Stacey (2009).

Three of the cornerstones of the geotechnical model have been investigated thoroughly, with only the hydrogeological model remaining in pre-feasibility stage information. Each of the four parts of the geotechnical model will be discussed individually below.

The geotechnical model which comprises a combination of the four models can be assumed to be in the data confidence level in the region of 63%. This is determined through summing the lowest assumed data confidence percentages as per Read and

Stacey's (2009) project stage classification and described in Appendix A. A summary of the study areas specific level project stages per model is presented in Table 8.1. Much of the slope design was done assuming dry conditions, and significantly different results are possible if there is saturation and water pressure in the discontinuities.

Table 8.1 Project Stage and Level Classification of the four models of the geotechnical model adapted from Read and Stacey (2009)

Model	**Project Stage**	**Project Level**	**%**	**Description of Project Stage**
Geological Model	Design and Construction	4/5	90%	Target drilling and mapping; refinement of geological database and 3D model.
Structural Model	Design and Construction	4/5	75%	Refined interpretation of 3D structural model; refined interpretation of fabric data and structural domains
Rock Mass Model	Feasibility	3/5	70%	Targeted drilling and detailed sampling and laboratory testing; enhancement of database; detailed assessment and establishment of geotechnical units for 3D geotechnical model; Targeted sampling and laboratory testing; enhancement of database; detailed assessment and establishment of defect strengths within structural domains
Hydrogeological Model	Conceptual	1/5	<20%	Regional groundwater survey
Geotechnical Model	Feasibility	3/5	64%	Ongoing assessment and compilation of all new mine scale geotechnical data; enhancement of geotechnical database and 3D model.

8.1.1 Geology Model

Considering the classification of different study stages proposed by Read and Stacey (2009) as seen in Appendix A, the geological model of the study area has reached a level five confidence. This stage assumes that the model is robust enough for operations to continue. The pre-requisite for such a level of confidence in the geological information according to the classification assumes data confidence of more than 90%, as is the case in this study area. Ongoing mapping and drilling are suggested according to Read and Stacey (2009) with an increased refinement of the 3D geological database as mining advances.

8.1.2 Structural Model

Using the same classification system mentioned in the geological model (Read and Stacey (2009)), the structural model as presented in Section 4.2 indicates a project stage data level concurrent with the operations stage. According to Read and Stacey (2009), the data confidence is more than 75% when continued structural mapping on all pit benches is taking place to further refine the 3D structural model.

8.1.3 Rock Mass Model

When considering the Read and Stacey (2009) project stage data confidence table as presented in Appendix A, the current rock mass model is inferred to be one of design and construction stage. This level four confidence implies further work is required through infill drilling and laboratory testing to increase confidence in the intact rock mass strength database and 3D geotechnical model. At this project stage level, 70% to 80% data-confidence is inferred.

8.1.4 Hydrogeological Model

Although the previous three models have reached levels of data confidence above that required for a robust geotechnical model, the hydrogeological model is only at level one project stage (Read and Stacey, 2009). As can be seen from the data presented in Section 4.4, only regional groundwater studies have been conducted, and no groundwater testing or characterization has been done. The data confidence is thus assumed to be less than 20%, and thus in conceptual project stage.

8.1.5 Blasting Quality Effect

It should be noted regarding the suggested design that much of the success of the design is hinged on the implementation of good blasting practices as currently being experienced. Poor blasting practices will compromise the strength of the rock mass and result in slope instability.

8.1.6 Effect of Joint Orientation

The intersecting planes in the granitic gneiss rock of the main pit will definitely have a major effect on the stability of the slope. Wedge failure and toppling failure are expected in nearly all of the ten geotechnical discontinuity zones presented in Chapter 4. One positive is that the South Eastern and North Western shear zones are inclined away from the pit and are near vertical. These shear zones do not create massive wedge (North Western) or toppling failure (South Eastern) conditions, but rather smaller scale failure conditions which can be mitigated by excavation practices. These include bringing identified hazardous blocks down prior to failure, concurrent with excavation.

As a possible mitigation measure to the smaller wedge failure expected throughout the pit, the advantages of shallowing the bench face angles were investigated. A sensitivity analysis was conducted on geotechnical zone 6, as shown in Figure 8.1, using DIPS (2013) to investigate the possible advantages of reducing the bench face angle.

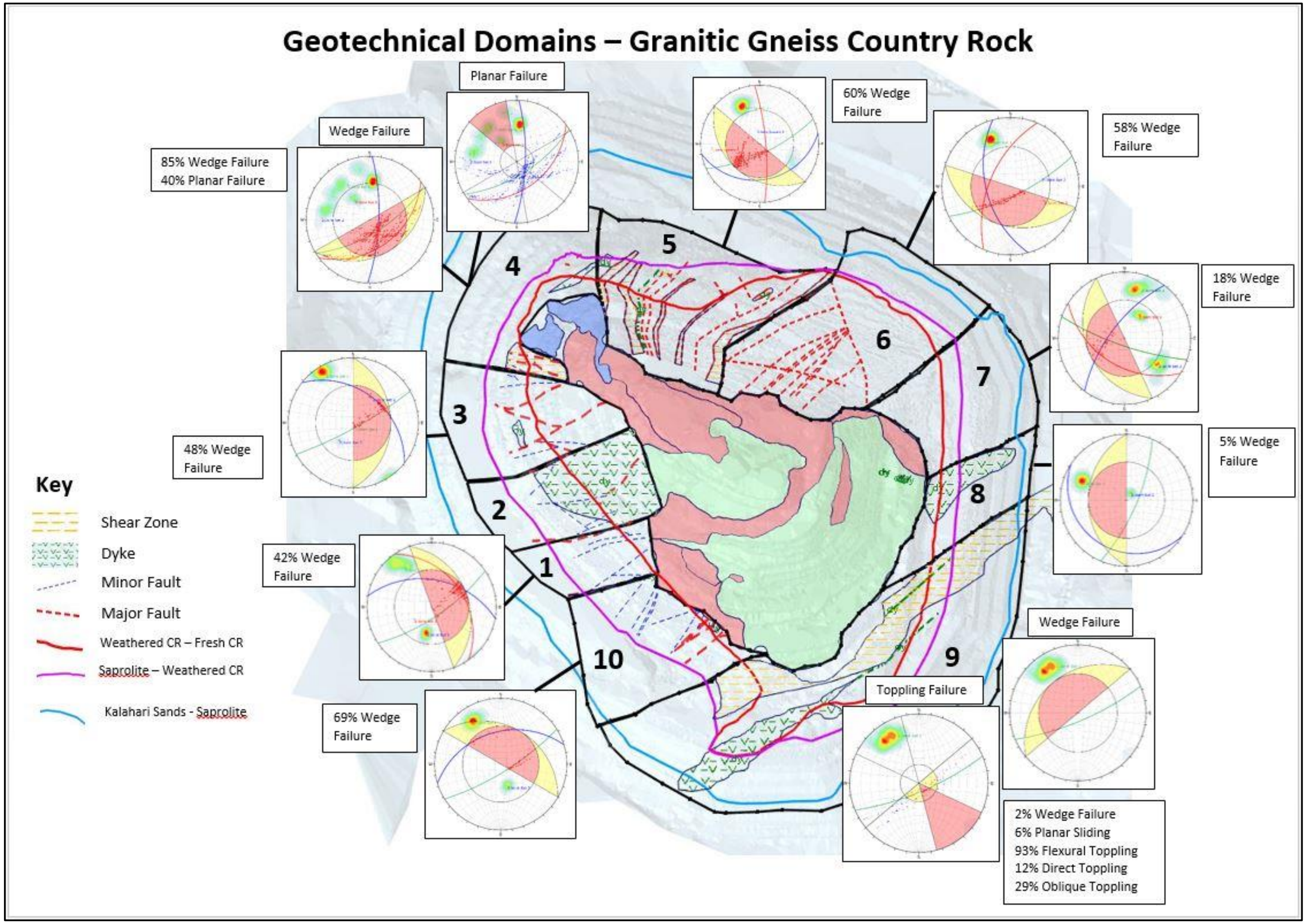

Figure 8-1 Geotechnical domains indicating various stereonet interpretations and failure risk probability

A bench face angle of 70˚ lowered the failure risk from 58% to 33% as shown in Figure 8.2. By decreasing the slope from 90° to 70°, there was a 25% decrease in overall failures predicted by DIPS (2013). This decrease equates to a significant reduction in risk. The bench configuration for this new face angle is presented in Figure 8.2.

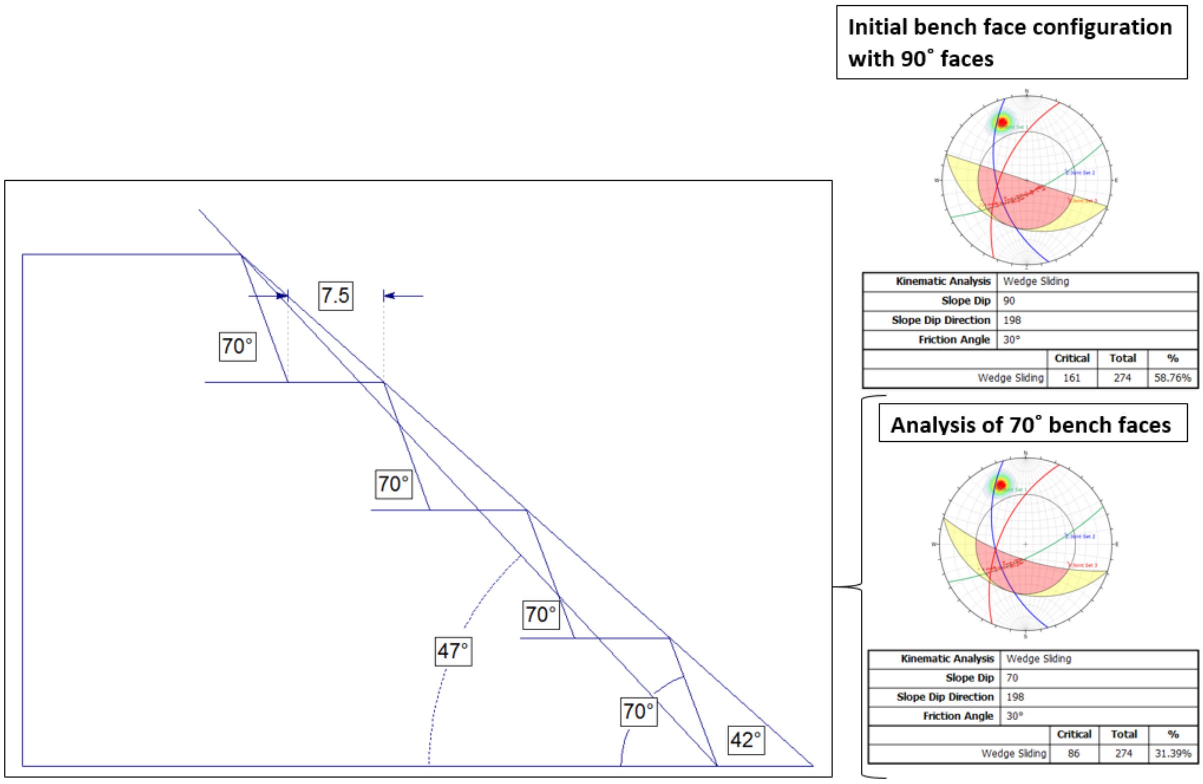

Figure 8-2 Bench configuration when face angle is changes to 70˚

To maintain the overall slope angle in the competent granitic gneiss, a bench height of 10 m is maintained and the berm width would be decreased to 7.5 m. It would thus theoretically be possible to make these changes and allow for a decreased failure risk.

The practicality of this design needs however to be weighed against the constraints on equipment and skills at Mine A. To achieve the 70˚ face angle, the drilling and blasting would need to be properly executed, specifically with regards to the pre-split, to ensure highwall stability and final wall results. Since the current skill complement is stretched already, and it has been made clear by management that funding for upskilling and equipment changes are not in the 5 year plan, the design will not be practicly implementable.

Since a decrease in risk of failure is not possible through bench face angle change, mitigation of wedge and toppling failure in the competent granitic gneiss rock will need to be considered. This is currently being implemented through identification of wedges in excavation faces and detachment of such blocks concurrent with mining. The blocks thus pose no threat since they are no longer present in the highwalls.

Geotechnical berms are also to be implemented in areas where higher risks of failure are presented. Since the entire competent granitic gneiss rock has a high risk of failure, these berms should be implemented throughout the pit design. These geotechnical berms would serve to lower the velocity of rockfall as well as serve as catchment for rockfall for operations below this. Windrows are to be installed at the crest of each of the geotechnical berms to further mitigate rockfall risks. According to Read and Stacey (2009) an internationally accepted standard for geotechnical safety berm installment is every 6 or 7 benches and catchment should be double the individual bench heights (10 m). In this study area, the geotechnical catch berms should thus be 20 m wide. Considering the maximum height of competent granitic gneiss rock to be expected in the fourth mining cut-back (180 m in the North Eastern pit faces), this would require the instalment of at least 3 geotechnical safety berms. The final layout of benches is shown in Figure 8.3.

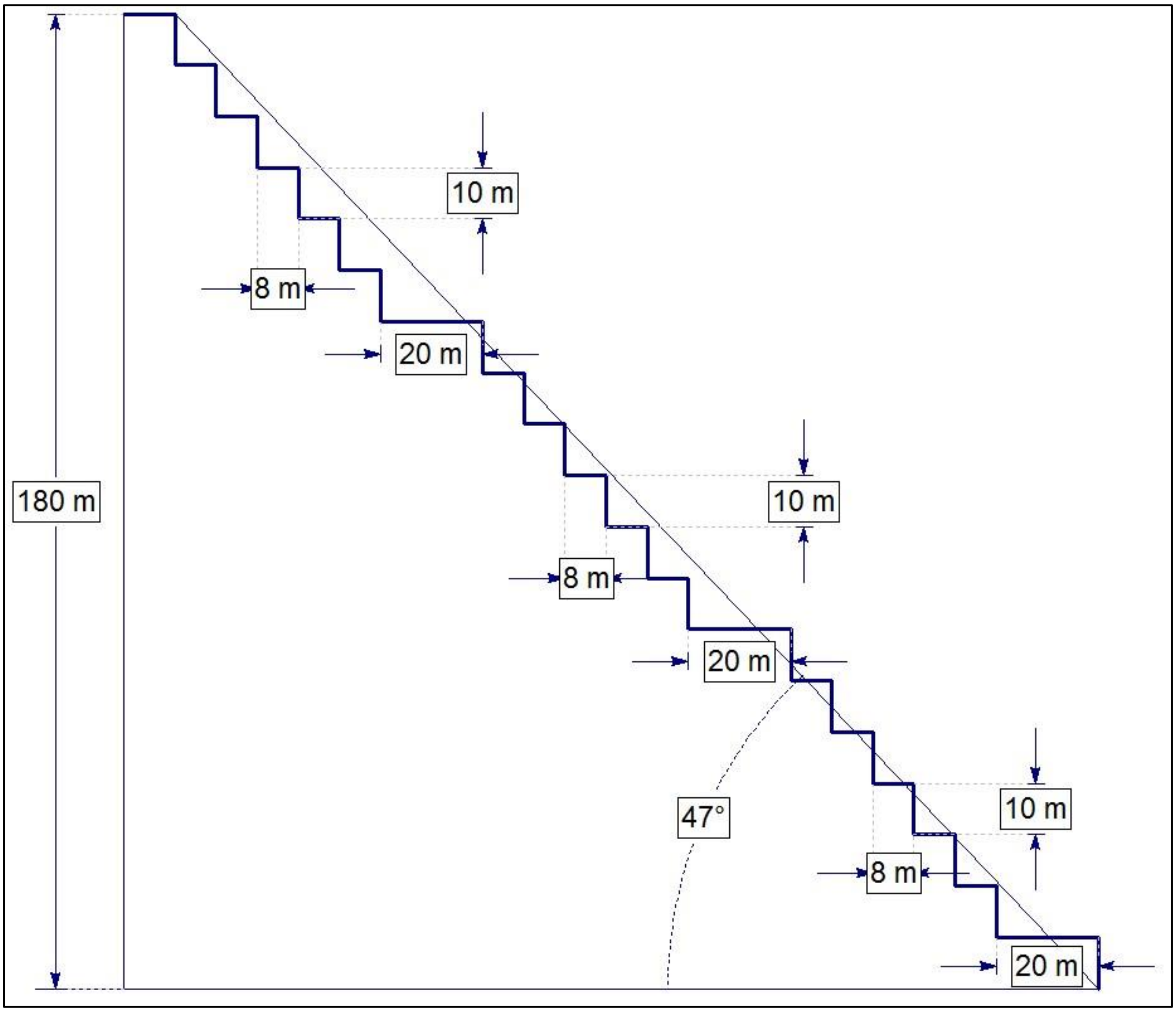

Figure 8-3 Bench configuration in NE competent granitic highwalls with geotechnical safety berms included

The new configuration shortens the benches in the granitic gneiss from 10.5 m to 8 m to allow for the 20 m geotechnical berms every 6 benches and to maintain the 47˚ crest-to-toe overall slope as suggested through the Haines and Terbrugge (1991) design charts.

The South Eastern shear zone running through geotechnical zone 9 has a signicantly lower rock mass rating than elsewhere in the pit. This zone is only 10 m high and must be treated differently to the rest of the pit. Special care should be taken to protect haulage roads below it, and no haulage road should be developed in it. In addition, particular attention should be given to instrumentation installation and monitoring of this zone. Geotechnical safety berms should be incorporated immediately below the shear zone (Figure 8.4). The berms are designed to arrest any wedge or toppling failures. Figure 8.4 shows a sectional view of the shear zone (shaded orange area) in relation to the geotechnical safety berm.

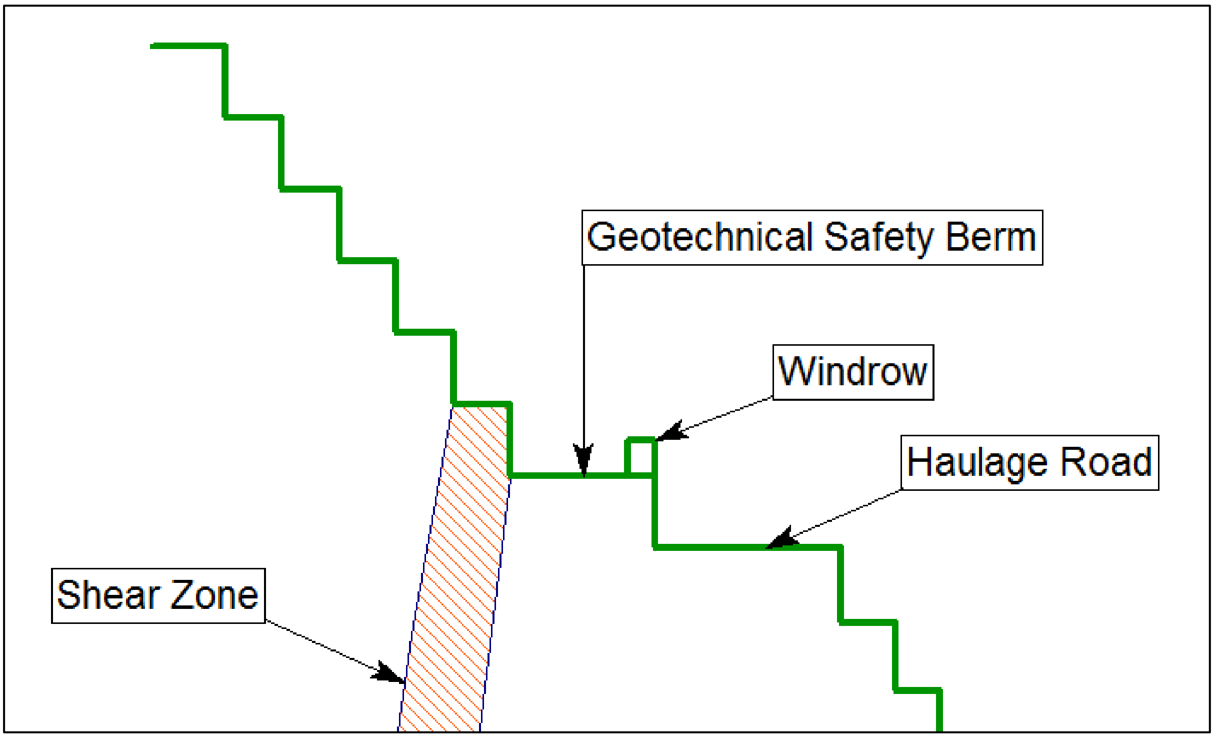

Figure 8-4 Cross-section view of the major South Eastern shear zone, geotechnical safety berm and haulage ramp

8.2 Numerical Modelling Analysis

8.2.1 Limit Equilibrium Analysis – SLIDE 2D (2018)

The purpose of the numerical modelling analysis was to establish whether the cross-sections and thus overall slope angle created from bench stack angles as per chart design would yield sufficient FOS to avoid circular failure. All FOS which were obtained for the sections indicated FOS's far above unity and thus failure is not expected in the proposed design. To further strengthen the results, saturated conditions were analysed by introducing a groundwater table at 10 m below surface. All lithological units were assigned a Hu value (saturation level) of unity indicating a saturated mass. Even when these conditions were present, the FOS's for each of the three overall slope angles proposed did not drop below unity, with overall slope angle FOS having its lowest value of 3.2 in saturated conditions in the South Eastern section.

The overall slope angles were initially determined from extrapolation of MRMR values for the different rock mass lithologies into the Haines and Terbrugge (1990) Chart and were then analysed through SLIDE 2D (2018) to confirm if the FOS was sufficient.

8.2.2 Boundary Element Analysis – Examine 2D (2006)

The main reason for boundary element analysis was to determine whether rock mass failure could occur in the pit slope due to the stress levels. The program required the average density of the rock and a k-ratio (virgin horizontal to vertical stress condition). The expected cross-sectional slope conditions were excavated from surface.

One of the observable differences between results from the two cross-sections is the difference in strength conditions, specifically at the toe of the slopes, as well as strength factor contours. This is explained by research done by Stacey (1973) where numerical modelling of slopes was used to establish a correlation between the width of the pit bottom and stress conditions in the toe of the slope. When considering specifically the two examples presented in this report, in slopes where a larger pit bottom is present less confinement on the toe exists and thus lower strength:stress conditions will be experienced, i.e. a lower strength factor or FOS. The inverse is also true, i.e. where confinement is greater, higher strength:stress conditions are present at the toe of the slope. The data is thus in good agreement with the previous literature presented by Stacey (1973).

Stacey (1973) showed that in section, stresses would be modelled higher than actual conditions experienced, due to the 2D nature of the software. The strength factors and thus the FOS results could thus be considered as extreme conditions where no confinement is present at the toe from the orthogonal slopes. A comparison of the FOS obtained from the different methods of analyses is presented in Table 8.2.

Table 8.2 FOS comparison between chart design and numerical modelling techniques

Lithological Unit	Factor of Safety through Design Charts	Factor of Safety through Examine 2D (2006)	Factor of Safety through SLIDE 2D (2018)
Kalahari Sands	1.25	N.A.	1 – 1.5
Saprolite	1.25	N.A.	1.5 – 1.8
Weathered Granitic Gneiss	1.5	N.A.	1.8
Competent Granitic Gneiss	1.5	1.2 – 1.4	1.8 – 2
Kimberlite 2	1.5	1.5 – 2	2
Kimberlite 4	1.5	1.6 - 2	2

The results obtained for the soil lithologies (Kalahari Sands and Saprolite) were determined from Chart 2 (Hoek and Bray, 1981) and shown in Figures 8.5 and 8.6. This chart was used because past experience suggested that the resulting slope angle of 24° was stable. However, there is a risk that these materials could become saturated in an abnormal rainy season. In such conditions Chart 5 should be used (Hoek and Bray, 1981) and the predicted stable angle drops to 18° (Figure 8.7). The groundwater saturation guide is provided in Figure 8.5.

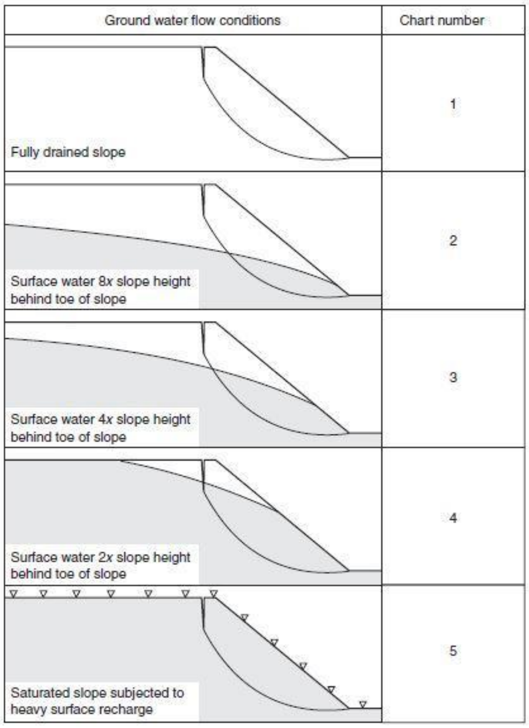

Figure 8-5 Groundwater Saturation level guide as designed by Hoek and Bray (1981)

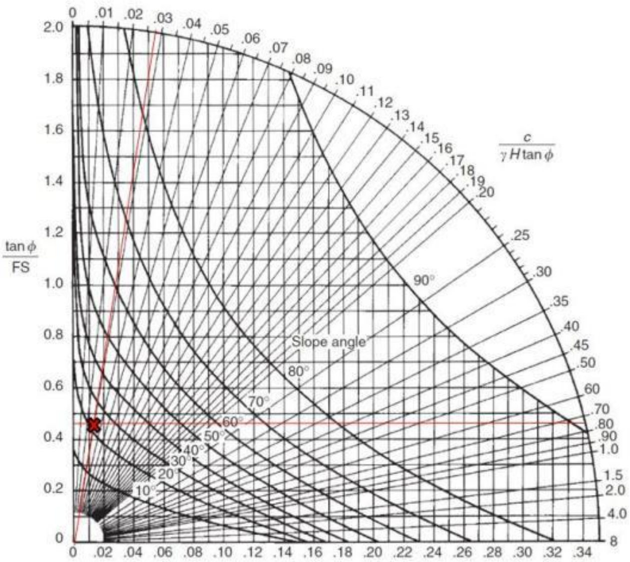

Figure 8-6 Saprolite soil strength parameters input into Hoek and Bray (1981) circular failure Chart 2 indicating a stable slope at 24˚

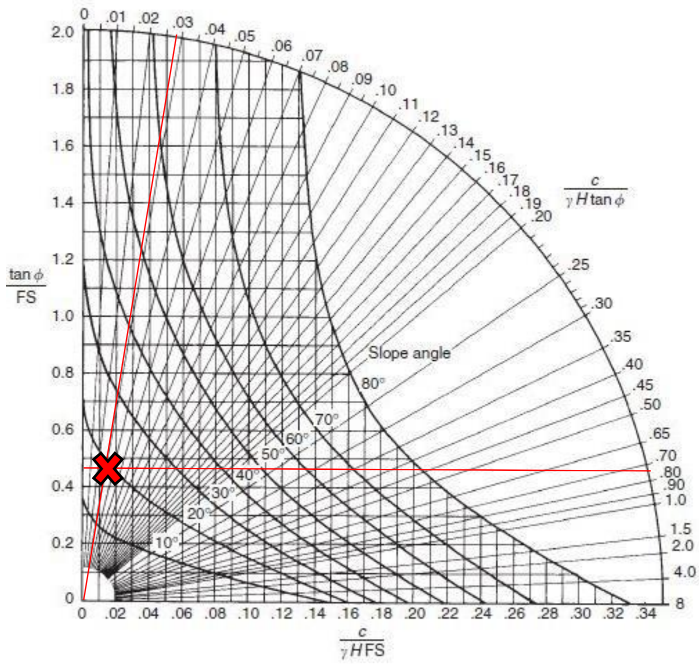

Figure 8-7 Saprolite soil parameters input into Hoek and Bray (1981) circular failure chart 5 indicating a stable slope at 18˚

A visible effect of groundwater seepage and circular failures in the upper saprolite was observed in the previous mining cut-back and resulted in an angle change from 47˚ crest-to-toe which was unstable to 27˚ crest-to-toe which remains stable.

9 CONCLUSIONS AND RECOMMENDATIONS

This chapter provides the conclusions to the investigation and makes some recommendations for further work. A slope stability strategy was determined for the fourth mining cut-back at Mine A using scan-line joint surveys in the existing pit, a limited number of UCS tests, PLTs and water inflows. The geotechnical model was verified using numerical analyses, and documented industry norms. The collected geotechnical data were found to be of a sufficient quality for stability analysis, however, due to the hydrogeological data gap there is a risk associated with the design, which needs to be conveyed to corporate management. Ultimately the risk allowable in the implementation of the design needs to be approved by corporate governance and responsibility for the associated possible failures weighed up against the cost of further hydrogeological studies.

9.1 Geotechnical Model

The geotechnical model, in its current form, is equivalent to a feasibility level study (Chapter 8). A confidence of 64% was calculated through the Read and Stacey (2009) project stage classification, as described in Chapter 2 (data in Appendix A). This confidence cannot be correlated with any factor of safety, but rather acts as an indicator to the level of confidence with which slope design has been completed and thus confidence in the design. The hydrogeological model needs to be better characterized to increase this confidence, according to the Read and Stacey (2009) guidelines. Although much work has been completed on determining seepage water inflows from the faces of the pit, these do not constitute elevation of the hydrogeological confidence from the current class. Only through groundwater characterization by piezometer and groundwater flow modelling will a greater confidence level be achieved as per Read and Stacey's (2009) guidelines. Since each different lithological layer has a different porosity and permeability, the groundwater will pass through each unit at a different rate of flow. A slower flowrate would thus allow for a longer period of saturation and thus increased pressure build up in planes of weakness. In addition, the added weight in clayey type lithologies would increase probability of failure.

Although the geotechnical model confidence level appears to be a high enough value for implementation to continue, the weighting of the data gaps has not been established. Specifically considering the impact of a poor hydrogeological understanding of the study area. This has the possibility of a change in slope angle from 24° to 18° for the same soil parameters under more saturated conditions (circular failure Charts 2 and 5 from Hoek and Bray (1981)). The more saturated groundmass conditions are less stable, and thus require a shallower slope angle than those of dry conditions. For hard rock conditions, this groundwater effect cannot be calculated using design charts. The risk of failure due to groundwater in discontinuities can be reduced if adequate dewatering of the pit bottom and sidewalls can be achieved.

9.2 Mitigation of Risk Imposed by Intersecting Planes in the Competent Granitic Gneiss

Initial investigation into shallowing the bench face angles from 90˚ to 70˚ showed a significant decrease the risk of failure and would in ideal open pit mining conditions be the best mitigation measure. Unfortunately, the limitations of the specific study area do not allow for the implementation of this method. An alternative method of risk mitigation is therefore recommended. To mitigate the risk imposed by possible failure, geotechnical safety berms and regular monitoring are suggested. These will allow for sufficient catchment of the smaller failures expected throughout the pit.

To allow for the 47˚ overall crest-to-toe slope angle and double bench height safety berms of 20 m, the intermediate berm widths will need to be 8 m. The design is based on incorporating the largest height of competent granitic gneiss, expected in the North Eastern walls of the fourth mining cut-back (180 m). In this area, three geotechnical safety berms are recommended to comply with the six-bench standard as suggested by Read and Stacey (2009). In addition to the catchment area provided, a windrow should be installed on the crest of each geotechnical safety berm to further slow any rockfall.

It is the prerogative of the mining department to determine the exact location of the haulage roads, and this report therefore provides guidence from a geotechnical perspective. Haulage roads developed below the major shear zone in geotechnical Domain 9, must be protected by a geotechnical safety berm. The cross-section provided in Figure 8.4, shows that the safety berm must be located immediately below the major shear zone. The catch benches will allow for containment of any rockfall that could result from toppling or wedge failure in this shear zone. No haulage road should be developed in the shear zone.

9.3 Slope Angle Design through Design Charts and subsequent Overall Slope Angle Analysis through Numerical Modelling

For the analysis of the upper soil lithologies, specifically the Kalahari Sands and Saprolite units, the Hoek and Bray (1981) Charts were used to analyse circular failure probability and thus factor of safety. These layers comprise the upper 20 m to 40 m of the main pit. It was determined that although it is possible to produce overall slope angles from the limited geotechnical model information, the confidence in these angles remains low. The groundwater conditions for the Kalahari Sands and Saprolite conditions for example have been estimated to be those of Chart 2 (24°). However, with quantitative hydrogeological data this angle could drop to 18°.

Two types of numerical modelling analysis were performed on the three proposed overall slope angles (Upper sediments, Competent Granitic Gneiss Rock and Kimberlite Domains) determined by design charts. Both models considered the rockmass as a single material type and the effects of individual discontinuities were excluded. The first model made use of a limit equilibrium approach using SLIDE 2D (2018). Four sections were individually analysed from the proposed pit layout. These included a North-West, North-East, South-West and North-East Section. The results from these analyses (Table 9.1) suggest that the FOS for the given lithologies are all above 1.5 and thus failure is not anticipated. Considering the uncertainty of the groundwater component, saturated conditions needed also to be modelled in SLIDE 2D (2018) to determine worst case scenarios in the proposed design. It was found that even with the mass saturated, the design remained stable with overall slope angles obtaining FOS's in the region of 1.6 to 4.0. The Examine2D (2006) elastic analysis considered the strength to stress ratios, and a Hoek-Brown (1980) failure criterion was used to cater for the effects of the discontinuities. This analysis suggests FOS's of between 1.2 and 2.0. It should be noted that the models did not consider individual discontinuities. Therefore, slope failure resulting from water pressure within these structures is a risk that needs to be monitored.

Table 9.1 Comparison of Factor of Safety results for lithologies in the study area making use of different slope instability analyses methods

Lithological Unit	Hoek and Bray (1981) Design Chart	Haines and Terbrugge (1991) Design Chart	SLIDE 2D (2018) DRY	SLIDE 2D (2018) WET	Examine 2D (2006)
Kalahari Sands	1.25*				N.A.
Saprolite	1.25*		8.6	1.6	N.A.
Weathered Granitic Gneiss		1.5			N.A.
Competent Granitic Gneiss		1.5	6.6	4.0	1.2 – 1.4
Kimberlite Domain 2		1.5	5.2	3.9	1.5 – 2
Kimberlite Domain 4 and 5		1.5	5.2	3.9	1.6 - 2

- Note that the angle to achieve the given FOS in dry and saturated conditions is 24° to 18°, respectively

All three methods have produced FOS which suggest stability. However, there is a hydrogeological data gap in knowledge, which introduces some risk to the quoted slope stability angles. Installation of the piezometers as suggested in Chapter 7.2.3.3 would allow for real groundwater pressures to be calculated and thus improve confidence. It is possible to reduce the hydrogeological data gap by installing suitable instrumentation, but the cost of such equipment needs to be offset against acceptable risk. This information would allow for pumping and dewatering systems to be calibrated and for effective dewatering of the pit and highwalls. The effective result is an increase in highwall stability. The effect of the 10 m thick major shear zone on overall slope stability was investigated by the use of anisotropic strength functions in SLIDE 2D (2018) numerical modelling analysis. Stability analysis on the major shear zone indicated FOS's above 2.5 and therefore no effect on the overall slope stability is suggested.

The proposed slope angles in the kimberlite Domain 2 and 6 lithologies have been reduced from the previous mining cut-back overall slope angle of 52˚ (crest-to-toe) to 39˚. This proposed slope angle was properly designed and is significantly less than the slope where failure took place. Since no failures have occurred on the slopes of the granitic gneiss, saprolite and Kalahari sands lithologies, the existing slope angles could be considered as an upper limit, with the three overall slope angles suggested in this report defining the lower boundaries. The existing slope angles are presented in Table 9.2 along with the new proposed angles for the fourth mining cut-back. Note that the minimum uncertainty principle was used to determine the provided angles. An improved knowledge on the hydrogeological conditions could be used to reduce the uncertainty and allow for an increase in the slope angles.

Table 9.2 Comparison of Third and Fourth Mining Cut-Back Overall Slope Angles

Lithological Unit	Third Mining Cut-back Overall Slope Angle (Crest-to-toe)	Fourth Mining Cut-back Overall Slope Angle (Crest-to-toe)	Change in Degrees
Kalahari Sands **Saprolite** **Weathered Granitic Gneiss**	37˚	24˚	13˚ shallower
Competent Granitic Gneiss	63˚	47˚	16˚ shallower
Kimberlite Domain 2 and 3 **Kimberlite Domain 4 and 5**	52˚	39˚	13˚ shallower

9.4 Recommendation for Further Studies

Of specific note for further study would be a correlation between Laubscher's (1990) blasting adjustment factor and pre-split barrel audits. Such a study should provide a quantitative measure that can be directly related to the adjustment factor.

10 REFERENCE LIST

Anon., 2018. *SRK Confidential Report: 455495 Camutue Failure Report 20181102.* s.l.:s.n.

Barton, N., Lien, R. & Lunde, J., 1974. Engineering Classification of Rock Masses for the Design of Tunnel Support. *Rock Mechanics,* 6(4), pp. 189-236.

Bieniawski, Z., 1973. Engineering classification of jointed rock masses. *The Civil Engineer in South Africa,* pp. 335-343.

Bieniawski, Z., 1991. In search of a design methodology for rock mechanics. *Rock Mechanics as a Multidisciplinary Science,* pp. 1027-1036.

Bieniawski, Z., 1992. *Invited Paper: Principles of Engineering Design for Rock Mechanics.* Rotterdam, Proc. 33rd US Symposium of Rock Mechanics; Balkema.

Bye, A., 2005. *The development and application of a 3D geotechnical model for mining optimisation, Sandsloot open pit platinum mine, South Africa: A thesis submitted in partial fulfilment for the degree Master of Science,* Durban: University of Natal.

Bye, A., Mossop, D. & Little, M. J., 2005. *The strategic and tactical value of slope stability risk management at Anglo Platinums's Sandsloot Open Pit.* Johannesburg, The South African Institute of Mining and Metallurgy: 1st International Seminar on Strategic vs Tactical Approaches in Mining.

Cruz, S. E. R., 2012. *Kimberlites Associated with the Lucapa Structure, Angola.* Barcelona: Facultat de Geologia, Universitat de Barcelona.

De Carvalho, H., Tassinari, C. & Alves, P. H., 2000. Geochronological review of the Precambrian in Western Angola: links with Brazil. *Journal of African Earth Sciences,* 31(2), pp. 383-402.

De Graaf, P., 2019. *Slope Stability Monitoring Course.* Johannesburg: University of Witwatersrand.

Haines, A. & Terbrugge, P., 1991. Preliminary estimation of rock slope stability using rock mass classification systems. *Proc. 7th Int. Cong. Int. Soc. Rock Mech.,* Volume 2, pp. 887-892.

Hoek, E. & Bray, J., 1981. Rock Slope Engineering. *Institute of Mining and Metallurgy,* Volume 3rd Edition, p. 357.

Hoek, E. & Brown, E., 1980. Underground Excavations in Rock. *London Institution of Mining and Metallurgy,* p. 527.

Hoek, E. & Karzulovic, A., 2000. Rock Mass Properties for Surface Mines,. *Society for Mining, Metallurgy and Exploration (SME),* pp. 59-70.

ISRM, 1985. Suggested methods for determining the point load strength; International Society for Rock Mechanics, Commission on standardization of Laboratory and Field Tests. *Int. J. Rock Mech. Min. Sci. Geomech.,* Volume 22, pp. 51-60.

Jager, A. & Ryder, J., 1999. *A Handbook on Rock Engineering Practice for Tabular Hard Rock Mines.* 1st ed. Johannesburg: The Safety in Mines Research Advisory Comittee (SIMRAC).

Laubscher, D., 1977. Geomechanics classification of jointed rock masses - mining applications. *Trans. Instn. Min. Metall.,* Volume 86, pp. A1-A8.

Laubscher, D., 1990. A geomechanics classification system for the rating of rock mass in mine design. *The Journal of the Southern African Institute of Mining and Metallurgy,* 90(10), pp. 257-273.

Little, M., 2006. The benefit to open pit rock slope design of geotechnical databases. *The South African Insitute of Mining and Metallurgy,* Volume 106, pp. 97-116.

Little, M., Bye, A. & Stacey, T., 2007. *Safety and financial value created by good slope management strategies and tactics.* Perth, The Australasian Institute of Mining and Metallurgy: 6th Large Open Pit Mining Conference Proceedings.

Marinos, P. & Hoek, E., 2001. Estimating the geotechnical properties of rock masses such as Flysch. *Bull. Engg. Geol. Env.,* Volume 60, pp. 85-92.

Marinos, V., Marinos, P. & Hoek, E., 2005. The geological strength index: applications and limitations. *Bull. Eng. Geol. Environ.,* Volume 64, pp. 55-65.

Mossop, D. & Terbrugge, P., 2019. *Slope Stability Monitoring Course.* Johannesburg: University of Witwatersrand.

Pereira, E., Rodrigues, J. & B, R., 2003. Synopsis of Lunda Geology, NE Angola: implications for diamond exploration. *Comun. Inst. Geol. Min.,* Volume 90, pp. 189-212.

Read, J. & Stacey, P., 2009. *Guidlines for Open Pit Slope Design.* Collingwood (Victoria): CSIRO Publishing.

Reis, B., 1972. *Preliminary note on the distribution and tectonic control of kimberlites in Angola.* Montreal, 24th Int. Geol. Congr., Rop. Sess. 4, pp. 276-281.

Russell, T. & Stacey, T., 2019. Using laser scanner face mapping to improve geotechnical data confidence at Sishen mine. *The Journal of the Southern African Institute of Mining and Metallurgy,* Volume 119, pp. 11-20.

Sayadi, A., Talebi, N., Monjezi, M. & Khandelwal, M., 2013. A comparative study on the application of various artificial neural networks to simultaneous prediction of rock fragmentation and backbreak. *Journal of Rock Mechanics and Geotechnical Engineering,* 5(4), pp. 318-324.

Stacey, T., 1973. Stability of Rock Slopes in Mining and Civil Engineering Situations. *National Mechanical Engineering Research Institute, Council for Scientific and Industrial Research,* Volume CSIR Report ME 1202, Pretoria, South Africa, p. 217.

Stacey, T., 2017. *Rock Engineering as a creator of value.* Cape Town, Southern African Institute of Mining and Metallurgy: ISRM International Symposium 'Rock Mechanics for Africa AfriRock Conference 2017.

Stacey, T. R. & Swart, A. H., 2001. *Booklet Practical Rock Engineering Practice for Shallow and Opencast Mines (SIMRAC).* Braamfontein South Africa: The Safety in Mines Research Advisory Committee.

Talobre, J., 1967. *La Mechanique des roches et ses applications.* Paris: Dunod.

Terbrugge, P., Contreras, L. & Steffen, O., 2009. *Value and Risk in Slope Design.* Santiago, Proceedings of the Slope Stability Conference.

van der Wijde, G., 2008. *Front-end loading in the oil and gas industry: towards a fit front-end development phase: A thesis submitted in partial fulfilment for the degree Master of Science,* s.l.: Delft University of Technology.

Appendix A: Read and Stacey (2009) Project Stage Classification

Project Stage Levels for each of the four geotechnical models as per Read & Stacey (2009)

Table A1: Suggested levels of geotechnical effort and target level of data confidence by project stage (Read & Stacey, 2009) *(Table 8.1 pg. 217)*

	Project Stage				
Project Level Status	Conceptual	Pre-feasibility	Feasibility	Design and Construction	Operations
Geotechnical level status	Level 1	Level 2	Level 3	Level 4	Level 5
Geological Model	Regional literature; advanced exploration mapping and core logging; database established; initial country rock model	Mine scale outcrop mapping and core logging, enhancement of geological database; initial 3D geological model	Infill drilling and mapping, further enhancement of geological database and 3D model	Target drilling and mapping; refinement of geological database and 3D model	Ongoing pit mapping and drilling; further refinement of geological database and 3D model
Structural Model (major features)	Aerial photos and initial ground proofing	Mine scale outcropping mapping; targeted oriented drilling; initial structural model	Trench mapping; infill oriented drilling; 3D structural model	Refined interpretation of 3D structural model	Structural mapping on all pit benches; further refinement of 3D model
Structural Model (fabric)	Regional outcrop mapping	Mine scale outcrop mapping; targeted oriented drilling; database established initial stereographic assessment of fabric data; initial structural domains established	Infill trench mapping and oriented drilling; enhancement of database; advanced stereographic assessment of fabric data; confirmation of structural domains	Refined interpretation of fabric data and structural domains	Structural mapping on all pit benches; further refinement of fabric data and structural domains
Hydrogeological Model	Regional groundwater survey	Mine scale airlift, pumping and packer testing to establish initial hydrogeological parameters; initial hydrogeological database and model establishment	Targeted pumping and airlift testing; piezometer installation; enhancement of hydrogeological database and 3D model; initial assessment of depressurisation	Installation of piezometers and dewatering wells; refinement of hydrogeological database, 3D model, depressurization and dewatering requirements	Ongoing management of piezometer and dewatering well network; continued refinement of hydrogeological database and 3D model
Intact Rock Strength	Literature values supplemented by index tests on core from geological drilling	Index and laboratory testing on samples selected from targeted mine scale drilling; database establishment; initial assessment of lithological domains	Targeted drilling and detailed sampling and laboratory testing; enhancement of database; detailed assessment and establishment of geotechnical units for 3D geotechnical model	Infill drilling, sampling and laboratory testing; refinement of database and 3D geotechnical model	Ongoing maintenance of database and 3D geotechnical model
Strength of Structural defects	Literature values supplemented by index tests on core from geological drilling	Laboratory direct shear tests of saw cut and defect samples selected from targeted mine scale drill holes and outcrops; database establishment; assessment of defect strength within initial structural domains	Targeted sampling and laboratory testing; enhancement of database; detailed assessment and establishment of defect strengths within structural domains	Selected sampling and laboratory testing and refinement of database	Ongoing maintenance of database
Geotechnical Characterization	Pertinent regional information; geotechnical assessment of advanced exploration data	Assessment and compilation of initial mine scale geotechnical data; preparation of initial geotechnical database and 3D model	Ongoing assessment and compilation of all new mine scale geotechnical data; enhancement of geotechnical database and 3D model	Refinement of geotechnical database and 3D model	Ongoing maintenance of geotechnical database and 3D model

Target Levels of Data Confidence

Geology	>50%	50-70%	65-85%	80-90%	>90%
Structural	>20%	40-50%	45-70%	60-75%	>75%
Hydrogeological	>20%	30-50%	40-65%	60-75%	>75%
Rock Mass	>30%	40-65%	60-75%	70-80%	>80%
Geotechnical	>30%	40-60%	50-75%	65-85%	>80%

Appendix B: Diamond Core Holes

Diamond Core Holes for Mine A Main Pit Kimberlite Pipe

Hole	East	North	Elev	Tdepth	Azimuth	Dip	Status	Date_S	Date_F	Rig
CW001i	479263.20	9068189.50	795.10	61.9	158.71	-54.33	completed	7/31/2009	8/10/2009	ED01
CW002i	479263.20	9068189.50	795.10	72	158.71	-70	completed	8/10/2009	8/19/2009	ED01
CW003i	479260.90	9068188.60	795.20	72.2	244.31	-53.24	completed	8/20/2009	8/27/2009	ED01
CW004i	479260.95	9068188.58	795.20	76.7	244.31	-69.45	completed	8/28/2009	9/5/2009	ED01
CW005	479206.66	9068264.08	788.32	114	0	-90	stopped	3/18/2010	5/13/2010	ED01
CW006i	479206.52	9068263.59	788.05	84	203	-65	stopped	5/13/2010	5/20/2010	ED01
CW007i	479208.27	9068266.19	788.06	105	113	-65	stopped	5/21/2010	6/7/2010	ED01
CW008	479234.25	9068329.24	779.95	110	0	-90	stopped	6/14/2010	7/13/2010	ED01
CW009i	479234.47	9068329.73	779.95	198	23	-65	stopped	7/13/2010	8/4/2010	ED01
CW010i	479235.31	9068330.17	779.88	138	115	-65.16	stopped	8/13/2010	8/23/2010	ED01
CW011i	479257.28	9068383.98	770.80	114	27	-58.5	completed	8/25/2010	9/1/2010	ED01
CW012	479262.46	9068395.78	770.45	213	0	-90	completed	9/3/2010	10/1/2010	ED01
CW013i	479262.46	9068395.78	770.45	90	22.83	-49.5	completed	10/4/2010	10/7/2010	ED01
CW014	479141.57	9068292.09	788.42	207	0	-90	stopped	10/12/2010	10/25/2010	ED01
CW015i	479141.46	9068291.77	788.58	128	205.8	-67	completed	10/29/2010	11/3/2010	ED01
CW016i	479141.34	9068291.46	788.57	78	205.8	-50	completed	11/5/2010	11/9/2010	ED01
CW017	479123.68	9068338.52	783.91	141	0	-90	completed	11/15/2010	11/25/2010	ED01
CW018i	479122.91	9068337.59	783.73	105	206.8	-53	completed	11/29/2010	12/2/2010	ED01
CW019i	479122.91	9068337.59	783.73	102	206.8	-70	stopped	12/3/2010	12/8/2010	ED01
CW020	479169.16	9068356.71	778.48	144	0	-90	stopped	12/14/2010	12/20/2010	ED01
CW021i	479169.33	9068357.50	778.43	141	26.25	-61.2	stopped	12/22/2010	12/31/2010	ED01
CW022i	479168.73	9068356.45	778.43	141	295.6	-61.6	stopped	1/5/2011	1/14/2011	ED01
CW023	479014.21	9068499.20	780.59	100	0	-90	completed	1/25/2011	1/28/2011	ED01
CW024i	479014.21	9068499.20	780.59	120	113	-70	stopped no rods	1/31/2011	2/15/2011	ED01
CW025	479290.35	9068189.31	784.21	138	0	-90	completed	8/11/2011	8/24/2011	ED02
CW026i	479290.14	9068188.80	784.17	66	203	-60	completed	8/29/2011	9/7/2011	ED02
CW027i	479255.57	9068198.11	783.65	93	23	-50	stopped	9/19/2011	9/26/2011	ED02
CW028	479326.83	9068366.73	766.75	102	0	-90	stopped	9/29/2011	10/7/2011	ED02
CW029i	479103.87	9068383.63	759.78	78	202.44	-65.68	completed	10/5/2011	10/7/2011	ED03
CW030i	479326.34	9068365.77	766.59	66	203.15	-54.97	stopped stuck	10/10/2011	10/20/2011	ED02
CW031	479103.95	9068384.12	759.99	90	0	-90	stopped	10/10/2011	10/17/2011	ED03
CW032i	479104.17	9068384.70	759.96	102	22.95	-68.77	stopped	10/18/2011	10/24/2011	ED03
CW033i	479104.46	9068385.42	759.87	144	23	-49.64	completed	10/25/2011	11/7/2011	ED03

CW034i	479327.17	9068366.44	766.66	81	113.17	-66.14	completed	10/27/2011	11/10/2011	ED02
CW035i	479328.41	9068369.24	766.65	72	23.86	-66.52	completed	11/15/2011	11/21/2011	ED02
CW036	479196.95	9068421.68	754.24	159	0	-90	completed	11/22/2011	12/5/2011	ED03
CW037i	479326.35	9068366.74	766.60	210	292.64	-59.84	completed	11/28/2011	12/17/2011	ED02
CW038i	479197.18	9068422.46	756.00	84	24.06	-60.51	completed	12/7/2011	12/12/2011	ED03
CW039i	479195.75	9068421.68	756.02	153	293.46	-54.28	completed	12/16/2011	1/5/2012	ED03
CW040	479229.40	9068408.00	757.85	186	0	-90	completed	12/26/2011	1/5/2012	ED02
CW041	479218.73	9068369.53	759.64	117	0	-90	stopped A1	1/19/2012	2/3/2012	ED02
CW042i	479218.85	9068368.79	758.35	99	171.06	-59.66	stopped stuck	2/7/2012	2/16/2012	ED02
CW043	479210.97	9068303.22	761.12	181	0	-90	stopped A1	2/10/2012	2/20/2012	ED03
CW044	479298.90	9068300.53	759.82	222	0	-90	stopped deep	2/24/2012	3/16/2012	ED03
CW045	479149.97	9068403.14	754.03	222	0	-90	stopped deep	3/20/2012	4/6/2012	ED03
CW046	479125.18	9068444.38	753.05	195.7	0	-90	stopped deep	4/4/2012	4/20/2012	ED01
CW047	479061.17	9068436.55	754.05	216	0	-90	stopped deep	4/11/2012	4/21/2012	ED03
CW048i	479125.52	9068445.04	753.12	93	24.44	-60.85	completed	4/23/2012	5/2/2012	ED01
CW049	479084.82	9068476.15	753.95	177	0	-90	completed	4/25/2012	5/14/2012	ED02
CW050	479296.09	9068379.05	756.64	180	0	-90	completed	5/3/2012	5/18/2012	ED01
CW051i	479085.59	9068475.96	754.08	123	293.4	-57.25	completed	5/17/2012	5/23/2012	ED03
CW052i	479061.51	9068435.87	753.99	102	290.12	-64.67	completed	5/23/2012	5/30/2012	ED01
CW053	479176.11	9068322.23	753.69	108	0	-90	stopped water	5/25/2012	5/30/2012	ED03
CW054i	479175.74	9068321.43	753.95	63	204.74	-50.57	stopped	5/31/2012	6/1/2012	ED03
CW055	479177.40	9068330.48	753.77	150	0	-90	stopped hole colapse	6/7/2012	6/18/2012	ED03
CW056i	479106.57	9068474.06	752.70	60	22.97	63.72	completed	7/27/2012	8/1/2012	ED03
CW057i	479088.94	9068429.93	750.93	72	224.45	50.33	completed	6/2/2012	8/6/2012	ED03
Total				7060.5						

Appendix C: Rock Laboratory Testing Results

Direct Shear Tests; Triaxial Compressive Strength Tests; Uniaxial Compressive Strength Tests

DIRECT SHEAR TESTS ON SAW-CUT ROCK SURFACE

Tel: 0027 12 813 4910
E-mail: Chenj@rocklab.co.za

Client: SRK Consulting SA

Sampling Site: Camutue

28-11-2016

ROCKLAB Specimen No	Borehole ID	Sample ID	Depth From.. To..	Rock Type	Shear Area	Shear Cycle	Hor. Force	Vert. Force	Dil. Angle	Normal Stress	Shear Stress	Angle or App. Angle	Base Friction Angle	Note
6827-			m		(mm^2)	No	(kN)	(kN)	(°)	(MPa)	(MPa)	(°)	(°)	
BFA-237	CWGT01	SRK-16-237		GNS	1477	1	1.02	1.00	-1.4	0.66	0.71	47.0		
					1476	2	1.72	2.00	-0.5	1.34	1.18	41.3	37.0	
					1474	3	2.46	3.00	-1.5	1.99	1.72	40.9		
BFA-239	CWGT02	SRK-16-239		GNS	1406	1	1.00	1.00	-2.4	0.68	0.74	47.5		
					1404	2	1.68	2.00	-1.5	1.39	1.23	41.5	32.0	
					1405	3	2.43	3.00	1.1	2.17	1.69	37.9		

Note: The tests were conducted using ROCKLAB servo-controlled direct rock shear testing equipment.

The test was conducted according to the ISRM standard - 2014.

TABLE 3 RESULTS OF TRIAXIAL COMPRESSIVE STRENGTH TESTS

ROCKLAB
Tel: 0027 12 813 4910
E-mail: Chenj@rocklab.co.za

Client: SRK Consulting

Sampling Site: Camutue

25-11-2016

SPECIMEN PARTICULARS						SPECIMEN DIMENSIONS					SPECIMEN TEST RESULTS				
Rocklab Specimen No 6827-	BH ID	Sample ID	Depth From m	Depth To m	Rock Type	Diameter mm	Height mm	Ratio of Height to Diameter	Mass g	Density g/cm³	Confining Pressure δ_3 MPa	Failure Load P kN	Strength (TCS) δ_1 MPa	Failure Mode	Note
TCS-04A	CW052i	SRK-16-4-A	87.28	87.43	GNS	47.74	93.9	2.0	454.3	2.70	5.0	370.2	206.8	XA	
TCS-04B		SRK-16-4-B				47.74	94.6	2.0	458.6	2.71	10.0	541.9	302.7	XA	
TCS-04C		SRK-16-4-C	87.43	87.55		47.74	97.2	2.0	472.7	2.72	20.0	406.7	227.2	3B	
TCS-19A	CWGT01	SRK-16-19-A	74.65	74.80	GNS	47.60	92.5	1.9	433.9	2.64	5.0	475.8	267.4	2B	
TCS-19B		SRK-16-19-B				47.63	89.7	1.9	420.2	2.63	10.0	488.4	274.1	2B	
TCS-19C		SRK-16-19-C				47.63	98.4	2.1	461.7	2.63	20.0	728.6	408.9	2B	

Note: All tests were conducted according to the ISRM's Specification.
1 -- No suitable specimen could be prepared for the test.
Failure code refers to Appendix 3

TABLE 1 RESULTS OF UNIAXIAL COMPRESSIVE STRENGTH TESTS

ROCKLAB
Tel: 0027 12 813 4910
E-mail: Chenj@rocklab.co.za

Client: SRK Consulting SA

Project: Camutue

04-11-2016

SPECIMEN PARTICULARS						SPECIMEN DIMENSIONS					SPECIMEN TEST RESULTS			
Rocklab Specimen No. 6827-	Borehole No	Sample ID	Depth From.. m	Depth To.. m	Rock Type	Diameter mm	Height mm	Ratio of Height to Diameter	Mass g	Density g/cm³	Failure Load kN	Strength (UCS) MPa	Failure Code	Note
UCS-02	CW052i	SRK-16-2	78.00	78.15	GNS (W)	47.52	117.5	2.5	527.75	2.53	124.6	70.2	3B	
UCS-07	CW052i	SRK-16-7	90.55	90.69	GNS (F)	47.75	119.1	2.5	583.31	2.73	253.2	141.4	4B	
UCS-200	CW052i	SRK-16-200	28.35	28.50	KIMB 2	47.12	111.7	2.4	393.15	2.02	13.4	7.7	XA	
UCS-201	CW052i	SRK-16-201	28.50	28.60	KIMB 2	47.05	124.3	2.6	429.38	1.99	15.0	8.6	XA	
UCS-204	CW052i	SRK-16-204	30.69	30.87	KIMB 3	46.90	122.5	2.6	430.49	2.03	18.6	10.7	XA	
UCS-206	CW052i	SRK-16-206	48.73	48.88	KIMB 3	47.14	113.0	2.4	425.49	2.16	12.2	7.0	XA	
UCS-207	CW052i	SRK-16-207	48.88	49.03	KIMB 3	47.13	122.3	2.6	461.66	2.16	17.2	9.9	XA	
UCS-209	CW052i	SRK-16-209	61.61	61.81	KIMB 3	47.08	127.1	2.7	469.26	2.12	22.1	12.7	XA	
UCS-211	CW052i	SRK-16-211	63.06	63.21	KIMB 3	47.34	121.3	2.6	442.80	2.07	19.1	10.8	XA	
UCS-212	CW052i	SRK-16-212	63.21	63.37	KIMB 3	47.38	120.4	2.5	439.15	2.07	16.6	9.4	XA	
UCS-15	CWGT01	SRK-16-15	36.42	36.57	GNS (F)	47.71	117.3	2.5	562.14	2.68	222.4	124.4	2B	
UCS-24	CWGT01	SRK-16-24	123.00	123.15	GNS (SZ)	47.32	116.3	2.5	537.50	2.63	20.9	11.9	2B	
UCS-27	CWGT01	SRK-16-27	135.77	135.92	GNS (F)	47.45	119.2	2.5	691.41	3.28	337.9	191.1	3B	
UCS-28	CWGT02	SRK-16-28	30.25	30.44	GNS (F)	47.16	118.7	2.5	626.96	3.02	275.4	157.7	5B	
UCS-30	CWGT02	SRK-16-30	30.58	30.76	GNS (F)	47.00	122.6	2.6	618.56	2.91	451.3	260.1	YA	
UCS-42	CWGT02	SRK-16-42	68.85	69.09	GNS (F)	47.44	120.6	2.5	569.32	2.67	361.3	204.4	0B	
UCS-43	CWGT02	SRK-16-43	81.00	81.15	GNS (F)	47.38	113.9	2.4	526.39	2.62	438.7	248.8	YA	
UCS-44	CWGT02	SRK-16-44	81.15	81.25	GNS (F)	47.37	115.6	2.4	533.91	2.62	423.0	240.0	YA	
UCS-47	CWGT02	SRK-16-47	142.22	142.39	GNS (F)	47.41	119.7	2.5	561.32	2.66	302.5	171.3	2B	
UCS-113	CWGT02	SRK-16-113	114.00	114.22	GNS (W)	47.33	115.1	2.4	544.74	2.69	68.5	38.9	2B	
UCS-48	CW056i	SRK-16-48	41.49	41.74	GNS (W)	47.24	114.4	2.4	540.82	2.70	360.8	205.8	YA	
UCS-108	CW056i	SRK-16-108	41.22	41.36	GNS (F)	47.65	118.3	2.5	569.32	2.70	69.1	38.7	4B	
UCS-109	CW056i	SRK-16-109	57.72	57.98	GNS (W)	47.64	98.4	2.1	471.48	2.69	57.9	32.5	4B	
UCS-216	CW056i	SRK-16-216	24.04	24.17	KIMB 2	46.69	111.8	2.4	384.17	2.01	5.6	3.3	XA	
UCS-221	CW056i	SRK-16-221	31.62	31.80	KIMB 2	46.92	112.8	2.4	383.42	1.97	15.8	9.1	XA	
UCS-111	CW025	SRK-16-111	126.65	126.85	GNS (F)	47.64	124.3	2.6	594.27	2.68	298.4	167.4	2B	
UCS-112	CW025	SRK-16-112	126.22	126.38	GNS (W)	47.33	122.7	2.6	579.84	2.69	128.3	72.9	0B	
UCS-116	CW025	SRK-16-116	137.55	137.71	GNS (W)	47.36	116.8	2.5	549.15	2.67	127.9	72.6	2B	

Note: All tests were conducted according to the ISRM's (International Society for Rock Mechanics) specification.
Failure code refers to Appendix 3

Appendix D: Point-Load Test Results

Point-Load Testing Results for core which was grab sampled, machine cored and cut to 50mm standard testing size

Test ID	Date	Kimberlite Type	D (in mm)	L	W	Test Type	P (in Newton)	Pass/Fail	De2	Is	F	Is(50)	C	UCS
Diametral Testing														
PC-PLT-D-01	31-Oct-19	Kim 2	53	22		Diametral	418	Not long enough	2809	0.148807405	1.026567804	0.152760891	24	3.67
PC-PLT-D-02	31-Oct-19	Kim 2	53	27		Diametral	330	pass	2809	0.11747953	1.026567804	0.120600703	24	2.89
PC-PLT-D-03	31-Oct-19	Kim 2	53	27		Diametral	300	fail	2809	0.106799573	1.026567804	0.109637003	24	2.63
PC-PLT-D-04	31-Oct-19	Kim 2	53	27		Diametral	514	pass	2809	0.182983268	1.026567804	0.187844732	24	4.51
PC-PLT-D-05	31-Oct-19	Kim 2	53	27		Diametral	738	pass	2809	0.262726949	1.026567804	0.269707027	24	6.47
PC-PLT-D-06	31-Oct-19	Kim 2	53	27		Diametral	744	fail	2809	0.264862941	1.026567804	0.271899767	24	6.53
PC-PLT-D-07	31-Oct-19	Kim 2	53	27		Diametral	686	pass	2809	0.244215023	1.026567804	0.25070328	24	6.02
PC-PLT-D-08	31-Oct-19	Kim 2	53	27		Diametral	418	pass	2809	0.148807405	1.026567804	0.152760891	24	3.67
PC-PLT-D-09	11-Nov-19	Kim 2	53	59		Diametral	474	pass	2809	0.168743325	1.026567804	0.173226465	24	4.16
PC-PLT-D-10	11-Nov-19	Kim 2	53	28.5		Diametral	518	pass	2809	0.184407262	1.026567804	0.189306558	24	4.54
PC-PLT-D-11	11-Nov-19	Kim 2	53	47		Diametral	388	pass	2809	0.138127447	1.026567804	0.14179719	24	3.40
PC-PLT-D-12	11-Nov-19	Kim 2	53	47		Diametral	466	pass	2809	0.165895336	1.026567804	0.170302811	24	4.09
PC-PLT-D-13	11-Nov-19	Kim 2	53	48		Diametral	466	pass	2809	0.165895336	1.026567804	0.170302811	24	4.09
PC-PLT-D-14	11-Nov-19	Kim 2	53	40		Diametral	474	pass	2809	0.168743325	1.026567804	0.173226465	24	4.16
PC-PLT-D-15	11-Nov-19	Kim 2	53	57		Diametral	532	pass	2809	0.189391242	1.026567804	0.194422952	24	4.67
PC-PLT-D-16	11-Nov-19	Kim 2	53	38		Diametral	626	pass	2809	0.222855109	1.026567804	0.228775879	24	5.49
PC-PLT-D-17	11-Nov-19	Kim 2	53	57		Diametral	370	pass	2809	0.131719473	1.026567804	0.13521897	24	3.25
PC-PLT-D-18	11-Nov-19	Kim 2	53	50.5		Diametral	602	pass	2809	0.214311143	1.026567804	0.220004919	24	5.28
PC-PLT-D-19	11-Nov-19	Kim 2	53	45		Diametral	518	pass	2809	0.184407262	1.026567804	0.189306558	24	4.54
PC-PLT-D-20	11-Nov-19	Kim 2	53	54		Diametral	442	pass	2809	0.157351371	1.026567804	0.161531851	24	3.88
PC-PLT-D-21	11-Nov-19	Kim 2	53	34.5		Diametral	380	pass	2809	0.135279459	1.026567804	0.138873537	24	3.33
PC-PLT-D-22	11-Nov-19	Kim 8	53	41		Diametral	6552	pass	2809	2.33250267	1.026567804	2.394472143	24	57.47
PC-PLT-D-23	11-Nov-19	Kim 8	53	41		Diametral	3934	pass	2809	1.400498398	1.026567804	1.437706565	24	34.50
PC-PLT-D-24	11-Nov-19	Kim 8	53	42		Diametral	6490	pass	2809	2.310430758	1.026567804	2.371813829	24	56.92
PC-PLT-D-25	11-Nov-19	Kim 8	53	42		Diametral	6908	pass	2809	2.459238163	1.026567804	2.52457472	24	60.59
PC-PLT-D-26	11-Nov-19	Kim 3	53	39		Diametral	818	pass	2809	0.291206835	1.026567804	0.298943561	24	7.17
PC-PLT-D-27	11-Nov-19	Kim 3	53	59		Diametral	760	pass	2809	0.270558918	1.026567804	0.277747074	24	6.67
PC-PLT-D-28	11-Nov-19	Kim 3	53	61		Diametral	566	pass	2809	0.201495194	1.026567804	0.206848479	24	4.96
PC-PLT-D-29	11-Nov-19	Kim 3	53	45		Diametral	484	pass	2809	0.172303311	1.026567804	0.176881031	24	4.25
PC-PLT-D-30	11-Nov-19	Kim 3	53	41		Diametral	634	pass	2809	0.225703097	1.026567804	0.231699533	24	5.56
PC-PLT-D-31	11-Nov-19	Kim 4	53	35		Diametral	766	pass	2809	0.272694909	1.026567804	0.279939814	24	6.72
PC-PLT-D-32	11-Nov-19	Kim 4	53	55		Diametral	962	pass	2809	0.34247063	1.026567804	0.351569323	24	8.44
PC-PLT-D-33	11-Nov-19	Kim 4	53	55		Diametral	972	pass	2809	0.346030616	1.026567804	0.355223889	24	8.53
PC-PLT-D-34	11-Nov-19	Kim 4	53	39.5		Diametral	1178	pass	2809	0.419366323	1.026567804	0.430507965	24	10.33
PC-PLT-D-35	11-Nov-19	Kim 4	53	51		Diametral	1382	pass	2809	0.491990032	1.026567804	0.505061127	24	12.12
PC-PLT-D-36	21-Nov-19	Granitic Gneiss	47	55		Diametral	11090	pass	2209	5.020371209	0.972540138	4.882512506	22.4	109.37
PC-PLT-D37	21-Nov-19	Granitic Gneiss	47	48		Diametral	11818	pass	2209	5.349932096	0.972540138	5.203023697	22.4	116.55
PC-PLT-D38	21-Nov-19	Granitic Gneiss	47	80		Diametral	4042	pass	2209	1.829787234	0.972540138	1.779541529	22.4	39.86
PC-PLT-D39	21-Nov-19	Granitic Gneiss	47	51		Diametral	26340	pass	2209	11.92394749	0.972540138	11.59651753	22.4	259.76
PC-PLT-D40	21-Nov-19	Granitic Gneiss	47	53		Diametral	34304	pass	2209	15.52919873	0.972540138	15.10276907	22.4	338.30

Figure D1: Diametric Testing Results

Test ID	Date	Kimberlite Type	D (in mm)	L	W	Test Type	P (in Newton)	Pass/Fail	De2	Is	F	Is(50)	C	UCS
Axial Testing														
PC-PLT-A-01	6-Nov-19	Kim 2	55	55	53	Axial	640	pass	3711.493273	0.172437333	1.092979334	0.188470441	24	4.523290584
PC-PLT-A-02	13-Nov-19	Kim 2	50	50	53	Axial	506	pass	3374.084794	0.149966593	1.069790154	0.160432784	24	3.850386823
PC-PLT-A-03	16-Nov-19	Kim 2	35	35	53	Axial	346	pass	2361.859355	0.146494752	0.987292085	0.144633109	24	3.471194614
PC-PLT-A-04	16-Nov-19	Kim 2	35	35	53	Axial	378	pass	2361.859355	0.308571429	0.987292085	0.304650129	24	7.311603099
PC-PLT-A-05	16-Nov-19	Kim 2	39	39	53	Axial	618	pass	2631.786139	0.406311637	1.011625765	0.411035321	24	9.8648477
PC-PLT-A-06	16-Nov-19	Kim 2	34	34	53	Axial	454	pass	2294.37766	0.392733564	0.980873726	0.385222034	24	9.245328826
PC-PLT-A-07	16-Nov-19	Kim 2	32	32	53	Axial	338	pass	2159.414268	0.330078125	0.967584919	0.319378616	24	7.665086777
PC-PLT-A-08	16-Nov-19	Kim 2	34	34	53	Axial	428	pass	2294.37766	0.370242215	0.980873726	0.363160861	24	8.715860656
PC-PLT-A-09	16-Nov-19	Kim 2	34	34	53	Axial	262	pass	2294.37766	0.226643599	0.980873726	0.222308751	24	5.335410028
PC-PLT-A-10	16-Nov-19	Kim 2	49	49	53	Axial	540	pass	3306.603098	0.224906289	1.064938341	0.23951133	24	5.74827193
PC-PLT-A-11	16-Nov-19	Kim 2	40	40	53	Axial	304	pass	2699.267835	0.19	1.017404943	0.193306939	24	4.639366542
PC-PLT-A-12	16-Nov-19	Kim 2	41	41	53	Axial	482	pass	2766.749531	0.286734087	1.023073212	0.293349963	24	7.040399115
PC-PLT-A-13	16-Nov-19	Kim 2	48	48	53	Axial	448	pass	3239.121402	0.194444444	1.060009174	0.206112895	24	4.946709477
PC-PLT-A-14	16-Nov-19	Kim 2	44	44	53	Axial	534	pass	2969.194618	0.275826446	1.039458602	0.286710172	24	6.881044134
PC-PLT-A-15	16-Nov-19	Kim 2	43	43	53	Axial	424	pass	2901.712922	0.229313142	1.034095737	0.237131743	24	5.69116183
PC-PLT-A-16	16-Nov-19	Kim 2	42	42	53	Axial	412	pass	2834.231227	0.233560091	1.028635328	0.24024816	24	5.76595585
PC-PLT-A-17	16-Nov-19	Kim 2	42	42	53	Axial	368	pass	2834.231227	0.20861678	1.028635328	0.21459059	24	5.150174158
PC-PLT-A-18	16-Nov-19	Kim 3	34	34	53	Axial	508	pass	2294.37766	0.439446367	0.980873726	0.431041395	24	10.34499349
PC-PLT-A-19	16-Nov-19	Kim 3	47	47	53	Axial	234	pass	3171.639706	0.105930285	1.054999766	0.111756426	24	2.682154227
PC-PLT-A-20	16-Nov-19	Kim 3	47	47	53	Axial	330	pass	3171.639706	0.149388864	1.054999766	0.157605216	24	3.782525192
PC-PLT-A-21	16-Nov-19	Kim 3	38	38	53	Axial	326	pass	2564.304443	0.225761773	1.005730578	0.227055518	24	5.449332441
PC-PLT-A-22	16-Nov-19	Kim 3	42	42	53	Axial	250	pass	2834.231227	0.141723356	1.028635328	0.145781651	24	3.498759618
PC-PLT-A-23	16-Nov-19	Kim 3	43	43	53	Axial	578	pass	2901.712922	0.312601406	1.034095737	0.323259782	24	7.758234758
PC-PLT-A-24	16-Nov-19	Kim 3	38	38	53	Axial	664	pass	2564.304443	0.459833795	1.005730578	0.462468909	24	11.09925381
PC-PLT-A-25	16-Nov-19	Kim 4	22	22	53	Axial	438	pass	1484.597309	0.904958678	0.889355609	0.804830076	24	19.31592183
PC-PLT-A-26	16-Nov-19	Kim 4	42	42	53	Axial	544	pass	2834.231227	0.308390023	1.028635328	0.317220872	24	7.613300929
PC-PLT-A-27	16-Nov-19	Kim 4	25	25	53	Axial	706	pass	1687.042397	1.1296	0.915307134	1.033930939	24	24.81434253
PC-PLT-A-28	16-Nov-19	Kim 4	36	36	53	Axial	806	pass	2429.341051	0.62191358	0.993569859	0.617914588	24	14.82995011
PC-PLT-A-29	16-Nov-19	Kim 4	41	41	53	Axial	1650	pass	2766.749531	0.981558596	1.023073212	1.004206305	24	24.10095133
PC-PLT-A-30	16-Nov-19	Kim 4	38	38	53	Axial	1322	pass	2564.304443	0.915512465	1.005730578	0.920758881	24	22.09821315
PC-PLT-A-31	16-Nov-19	Kim 4	41	41	53	Axial	1352	pass	2766.749531	0.804283165	1.023073212	0.82284056	24	19.74817345
PC-PLT-A-32	16-Nov-19	Kim 4	21	21	53	Axial	1622	pass	1417.115613	3.678004535	0.88009527	3.236994393	24	77.68786543
PC-PLT-A-33	16-Nov-19	Kim 8	40	40	53	Axial	5980	pass	2699.267835	3.7375	1.017404943	3.802550976	24	91.26122342
PC-PLT-A-34	16-Nov-19	Kim 8	36	36	53	Axial	4928	pass	2429.341051	3.802469136	0.993569859	3.778018722	24	90.67244932
PC-PLT-A-35	16-Nov-19	Kim 8	46	46	53	Axial	7304	pass	3104.15801	3.451795841	1.049907063	3.624064835	24	86.97755605
PC-PLT-A-36	21-Nov-19	Granitic Gneiss	49	49	47	Axial	11026	pass	2932.270672	4.592253228	1.036536049	4.760036017	22.4	106.6248068
PC-PLT-A-37	21-Nov-19	Granitic Gneiss	49	49	47	Axial	19796	pass	2932.270672	8.244897959	1.036536049	8.546133956	22.4	191.4334006
PC-PLT-A-38	21-Nov-19	Granitic Gneiss	46	46	47	Axial	21984	pass	2752.743896	10.38941399	1.021905661	10.61700097	22.4	237.8208217
PC-PLT-A-39	21-Nov-19	Granitic Gneiss	47	47	47	Axial	23360	pass	2812.586154	10.57492078	1.026862539	10.85899	22.4	243.2413761
PC-PLT-A-40	21-Nov-19	Granitic Gneiss	62	62	47	Axial	13986	pass	3710.220033	3.638397503	1.092894959	3.976386291	22.4	89.07105291

Figure D2: Axial Testing Results

	RMR = 1+2+3+4+5						MRMR=RMR*1*2*3			
Test ID	1. Point Load Index	2. RQD	3. Js	4. Jcon	5. Ground Water	RMR	1. Blasting	2. Weathering	3. J orientation	MRMR
Diametral Testing										
PC-PLT-D-01	1	8	20	10	4	**43**	0.85	0.70	1.00	**26**
PC-PLT-D-02	1	8	20	10	4	**43**	0.85	0.70	1.00	**26**
PC-PLT-D-03	1	8	20	10	4	**43**	0.85	0.70	1.00	**26**
PC-PLT-D-04	1	8	20	10	4	**43**	0.85	0.70	1.00	**26**
PC-PLT-D-05	2	8	20	10	4	**44**	0.85	0.70	1.00	**26**
PC-PLT-D-06	2	8	20	10	4	**44**	0.85	0.70	1.00	**26**
PC-PLT-D-07	2	8	20	10	4	**44**	0.85	0.70	1.00	**26**
PC-PLT-D-08	1	8	20	10	4	**43**	0.85	0.70	1.00	**26**
PC-PLT-D-09	1	8	20	10	4	**43**	0.85	0.70	1.00	**26**
PC-PLT-D-10	1	8	20	10	4	**43**	0.85	0.70	1.00	**26**
PC-PLT-D-11	1	8	20	10	4	**43**	0.85	0.70	1.00	**26**
PC-PLT-D-12	1	8	20	10	4	**43**	0.85	0.70	1.00	**26**
PC-PLT-D-13	1	8	20	10	4	**43**	0.85	0.70	1.00	**26**
PC-PLT-D-14	1	8	20	10	4	**43**	0.85	0.70	1.00	**26**
PC-PLT-D-15	1	8	20	10	4	**43**	0.85	0.70	1.00	**26**
PC-PLT-D-16	2	8	20	10	4	**44**	0.85	0.70	1.00	**26**
PC-PLT-D-17	1	8	20	10	4	**43**	0.85	0.70	1.00	**26**
PC-PLT-D-18	2	8	20	10	4	**44**	0.85	0.70	1.00	**26**
PC-PLT-D-19	1	8	20	10	4	**43**	0.85	0.70	1.00	**26**
PC-PLT-D-20	1	8	20	10	4	**43**	0.85	0.70	1.00	**26**
PC-PLT-D-21	1	8	20	10	4	**43**	0.85	0.70	1.00	**26**
PC-PLT-D-22	7	8	20	10	4	**49**	0.95	0.98	1.00	**46**
PC-PLT-D-23	4	8	20	10	4	**46**	0.95	0.98	1.00	**43**
PC-PLT-D-24	7	8	20	10	4	**49**	0.95	0.98	1.00	**46**
PC-PLT-D-25	7	8	20	10	4	**49**	0.95	0.98	1.00	**46**
PC-PLT-D-26	2	8	20	10	4	**44**	0.92	0.70	1.00	**28**
PC-PLT-D-27	2	8	20	10	4	**44**	0.92	0.70	1.00	**28**
PC-PLT-D-28	1	8	20	10	4	**43**	0.92	0.70	1.00	**28**
PC-PLT-D-29	1	8	20	10	4	**43**	0.92	0.70	1.00	**28**
PC-PLT-D-30	2	8	20	10	4	**44**	0.92	0.70	1.00	**28**
PC-PLT-D-31	2	8	20	10	4	**44**	0.92	0.88	1.00	**36**
PC-PLT-D-32	2	8	20	10	4	**44**	0.92	0.88	1.00	**36**
PC-PLT-D-33	2	8	20	10	4	**44**	0.92	0.88	1.00	**36**
PC-PLT-D-34	2	8	20	10	4	**44**	0.92	0.88	1.00	**36**
PC-PLT-D-35	2	8	20	10	4	**44**	0.92	0.88	1.00	**36**
PC-PLT-D-36	12	13	8	25	10	**68**	0.90	1.00	1.00	**61**
PC-PLT-D37	12	13	8	25	10	**68**	0.90	1.00	1.00	**61**
PC-PLT-D38	4	13	8	25	10	**60**	0.90	1.00	1.00	**54**
PC-PLT-D39	15	13	8	25	10	**71**	0.90	1.00	1.00	**64**
PC-PLT-D40	15	13	8	25	10	**71**	0.90	1.00	1.00	**64**

Figure D3: RMR and MRMR determination from Point-Load Results (Diametric Testing)

	RMR = 1+2+3+4+5						MRMR=RMR*1*2*3			
Test ID	**1. Point Load Index**	**2. RQD**	**3. Js**	**4. Jcon**	**5. Ground Water**	**RMR**	**1. Blasting**	**2. Weathering**	**3. J orientation**	**MRMR**
Axial Testing										
PC-PLT-A-01	1	8	20	10	4	**43**	0.85	0.70	1.00	**26**
PC-PLT-A-02	1	8	20	10	4	**43**	0.85	0.70	1.00	**26**
PC-PLT-A-03	1	8	20	10	4	**43**	0.85	0.70	1.00	**26**
PC-PLT-A-04	2	8	20	10	4	**44**	0.85	0.70	1.00	**26**
PC-PLT-A-05	2	8	20	10	4	**44**	0.85	0.70	1.00	**26**
PC-PLT-A-06	2	8	20	10	4	**44**	0.85	0.70	1.00	**26**
PC-PLT-A-07	2	8	20	10	4	**44**	0.85	0.70	1.00	**26**
PC-PLT-A-08	2	8	20	10	4	**44**	0.85	0.70	1.00	**26**
PC-PLT-A-09	2	8	20	10	4	**44**	0.85	0.70	1.00	**26**
PC-PLT-A-10	2	8	20	10	4	**44**	0.85	0.70	1.00	**26**
PC-PLT-A-11	1	8	20	10	4	**43**	0.85	0.70	1.00	**26**
PC-PLT-A-12	2	8	20	10	4	**44**	0.85	0.70	1.00	**26**
PC-PLT-A-13	1	8	20	10	4	**43**	0.85	0.70	1.00	**26**
PC-PLT-A-14	2	8	20	10	4	**44**	0.85	0.70	1.00	**26**
PC-PLT-A-15	2	8	20	10	4	**44**	0.85	0.70	1.00	**26**
PC-PLT-A-16	2	8	20	10	4	**44**	0.85	0.70	1.00	**26**
PC-PLT-A-17	2	8	20	10	4	**44**	0.85	0.70	1.00	**26**
PC-PLT-A-18	2	8	20	10	4	**44**	0.92	0.70	1.00	**28**
PC-PLT-A-19	1	8	20	10	4	**43**	0.92	0.70	1.00	**28**
PC-PLT-A-20	1	8	20	10	4	**43**	0.92	0.70	1.00	**28**
PC-PLT-A-21	2	8	20	10	4	**44**	0.92	0.70	1.00	**28**
PC-PLT-A-22	1	8	20	10	4	**43**	0.92	0.70	1.00	**28**
PC-PLT-A-23	2	8	20	10	4	**44**	0.92	0.70	1.00	**28**
PC-PLT-A-24	2	8	20	10	4	**44**	0.92	0.70	1.00	**28**
PC-PLT-A-25	2	8	20	10	4	**44**	0.92	0.88	1.00	**36**
PC-PLT-A-26	2	8	20	10	4	**44**	0.92	0.88	1.00	**36**
PC-PLT-A-27	2	8	20	10	4	**44**	0.92	0.88	1.00	**36**
PC-PLT-A-28	2	8	20	10	4	**44**	0.92	0.88	1.00	**36**
PC-PLT-A-29	2	8	20	10	4	**44**	0.92	0.88	1.00	**36**
PC-PLT-A-30	2	8	20	10	4	**44**	0.92	0.88	1.00	**36**
PC-PLT-A-31	2	8	20	10	4	**44**	0.92	0.88	1.00	**36**
PC-PLT-A-32	7	8	20	10	4	**49**	0.92	0.88	1.00	**40**
PC-PLT-A-33	7	8	20	10	4	**49**	0.95	0.98	1.00	**46**
PC-PLT-A-34	7	8	20	10	4	**49**	0.95	0.98	1.00	**46**
PC-PLT-A-35	7	8	20	10	4	**49**	0.95	0.98	1.00	**46**
PC-PLT-A-36	12	13	8	25	10	**68**	0.90	1.00	1.00	**61**
PC-PLT-A-37	12	13	8	25	10	**68**	0.90	1.00	1.00	**61**
PC-PLT-A-38	12	13	8	25	10	**68**	0.90	1.00	1.00	**61**
PC-PLT-A-39	12	13	8	25	10	**68**	0.90	1.00	1.00	**61**
PC-PLT-A-40	7	13	8	25	10	**63**	0.90	1.00	1.00	**57**

Figure D4: RMR and MRMR determination from Point-Load Results (Axial Testing)

Appendix E: SLIDE 2D (2018) Results

Numerical Modelling Results of each of the four section of the Mine A Main Pit by SLIDE 2D (2018), including NW, SE, SW and NE cross-sections

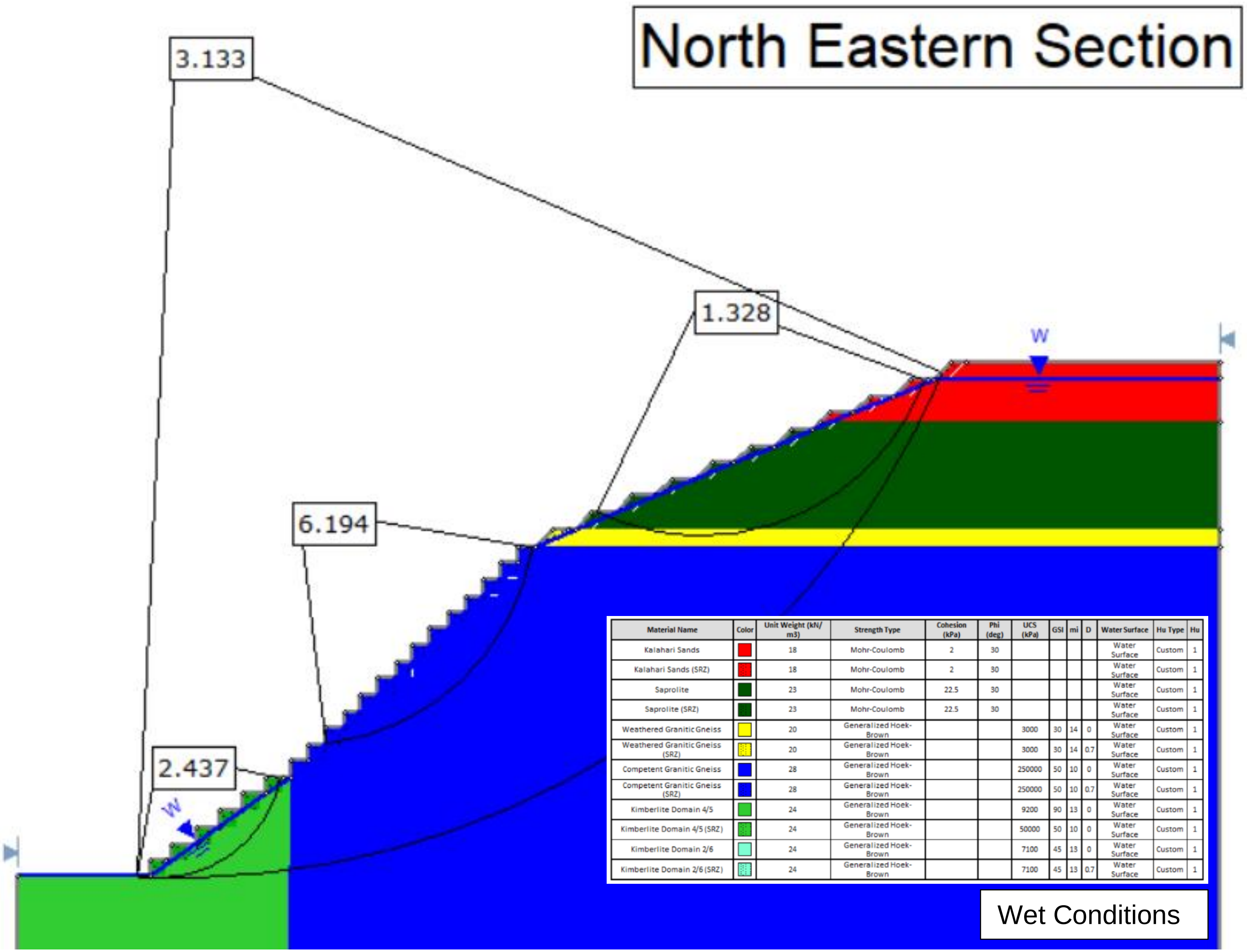

Figure E1: North Eastern Section SLIDE 2D(2018) analysis of the main pit under wet conditions

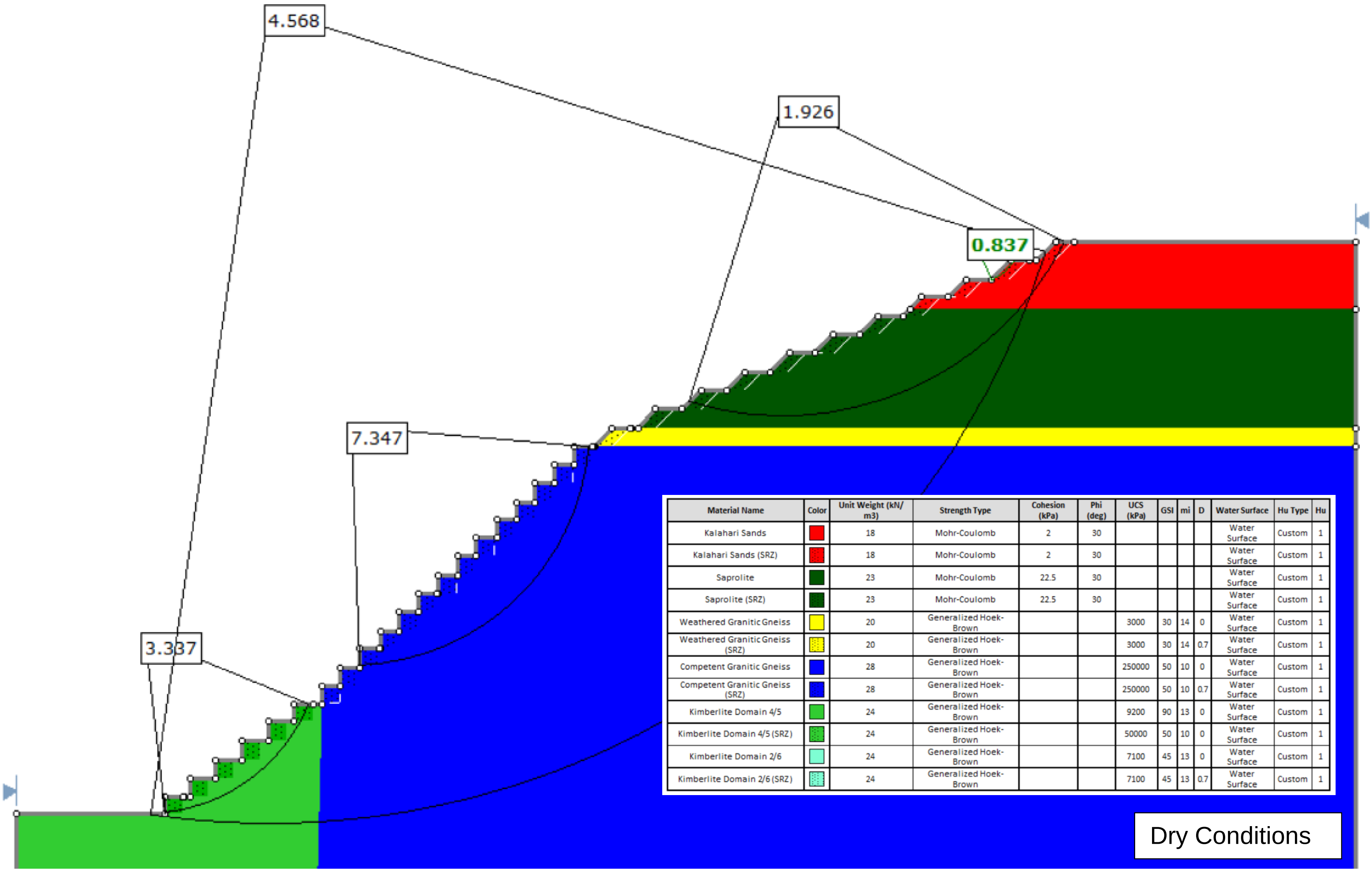

Material Name	Color	Unit Weight (kN/m3)	Strength Type	Cohesion (kPa)	Phi (deg)	UCS (kPa)	GSI	mi	D	Water Surface	Hu Type	Hu
Kalahari Sands		18	Mohr-Coulomb	2	30					Water Surface	Custom	1
Kalahari Sands (SRZ)		18	Mohr-Coulomb	2	30					Water Surface	Custom	1
Saprolite		23	Mohr-Coulomb	22.5	30					Water Surface	Custom	1
Saprolite (SRZ)		23	Mohr-Coulomb	22.5	30					Water Surface	Custom	1
Weathered Granitic Gneiss		20	Generalized Hoek-Brown			3000	30	14	0	Water Surface	Custom	1
Weathered Granitic Gneiss (SRZ)		20	Generalized Hoek-Brown			3000	30	14	0.7	Water Surface	Custom	1
Competent Granitic Gneiss		28	Generalized Hoek-Brown			250000	50	10	0	Water Surface	Custom	1
Competent Granitic Gneiss (SRZ)		28	Generalized Hoek-Brown			250000	50	10	0.7	Water Surface	Custom	1
Kimberlite Domain 4/5		24	Generalized Hoek-Brown			9200	90	13	0	Water Surface	Custom	1
Kimberlite Domain 4/5 (SRZ)		24	Generalized Hoek-Brown			50000	50	10	0	Water Surface	Custom	1
Kimberlite Domain 2/6		24	Generalized Hoek-Brown			7100	45	13	0	Water Surface	Custom	1
Kimberlite Domain 2/6 (SRZ)		24	Generalized Hoek-Brown			7100	45	13	0.7	Water Surface	Custom	1

Figure E2: North Eastern Section SLIDE 2D(2018) analysis of the main pit under dry conditions

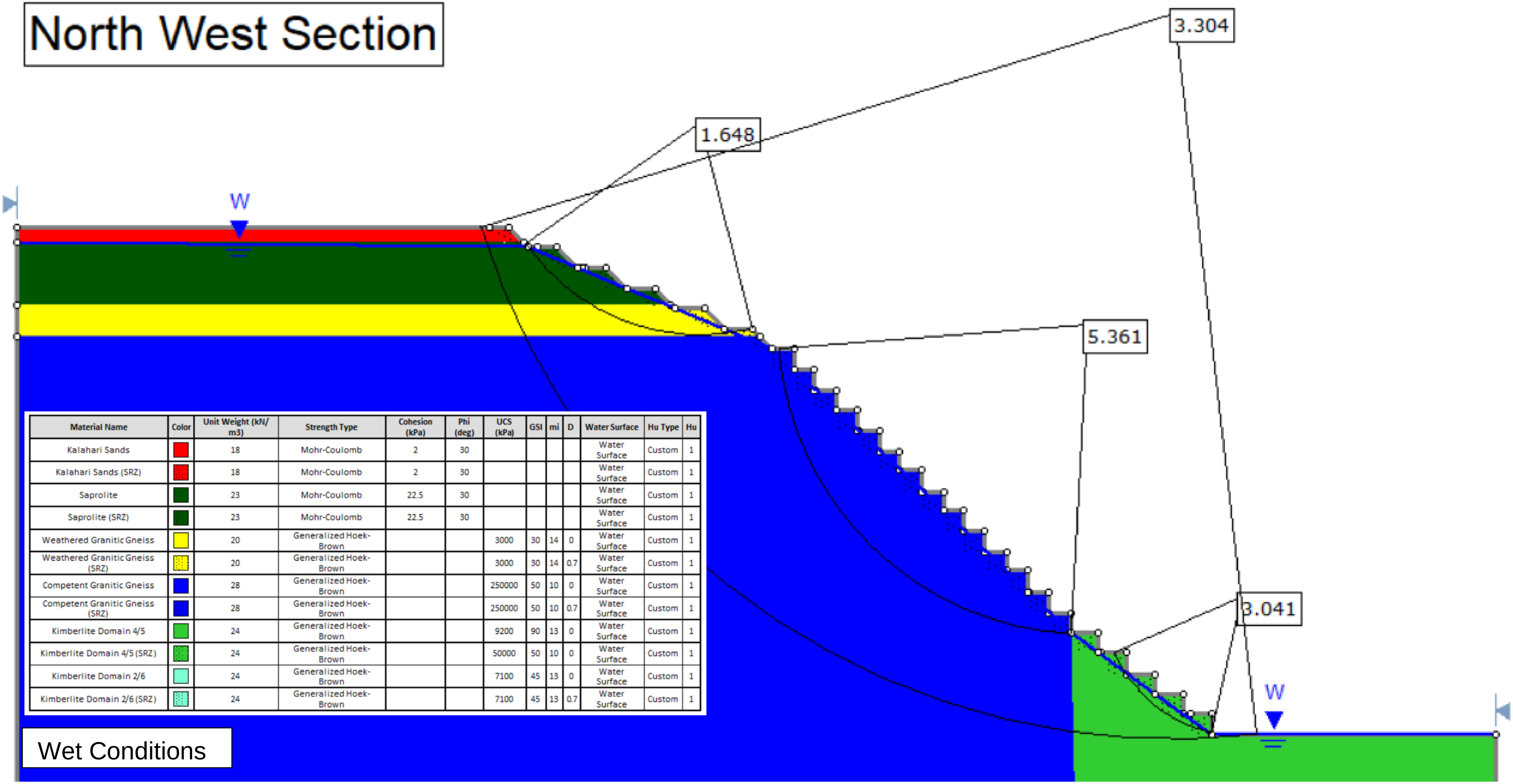

Material Name	Color	Unit Weight (kN/m3)	Strength Type	Cohesion (kPa)	Phi (deg)	UCS (kPa)	GSI	mi	D	Water Surface	Hu Type	Hu
Kalahari Sands		18	Mohr-Coulomb	2	30					Water Surface	Custom	1
Kalahari Sands (SRZ)		18	Mohr-Coulomb	2	30					Water Surface	Custom	1
Saprolite		23	Mohr-Coulomb	22.5	30					Water Surface	Custom	1
Saprolite (SRZ)		23	Mohr-Coulomb	22.5	30					Water Surface	Custom	1
Weathered Granitic Gneiss		20	Generalized Hoek-Brown			3000	30	14	0	Water Surface	Custom	1
Weathered Granitic Gneiss (SRZ)		20	Generalized Hoek-Brown			3000	30	14	0.7	Water Surface	Custom	1
Competent Granitic Gneiss		28	Generalized Hoek-Brown			250000	50	10	0	Water Surface	Custom	1
Competent Granitic Gneiss (SRZ)		28	Generalized Hoek-Brown			250000	50	10	0.7	Water Surface	Custom	1
Kimberlite Domain 4/5		24	Generalized Hoek-Brown			9200	90	13	0	Water Surface	Custom	1
Kimberlite Domain 4/5 (SRZ)		24	Generalized Hoek-Brown			50000	50	10	0	Water Surface	Custom	1
Kimberlite Domain 2/6		24	Generalized Hoek-Brown			7100	45	13	0	Water Surface	Custom	1
Kimberlite Domain 2/6 (SRZ)		24	Generalized Hoek-Brown			7100	45	13	0.7	Water Surface	Custom	1

Figure E3: North Western Section SLIDE 2D(2018) analysis of the main pit under wet conditions

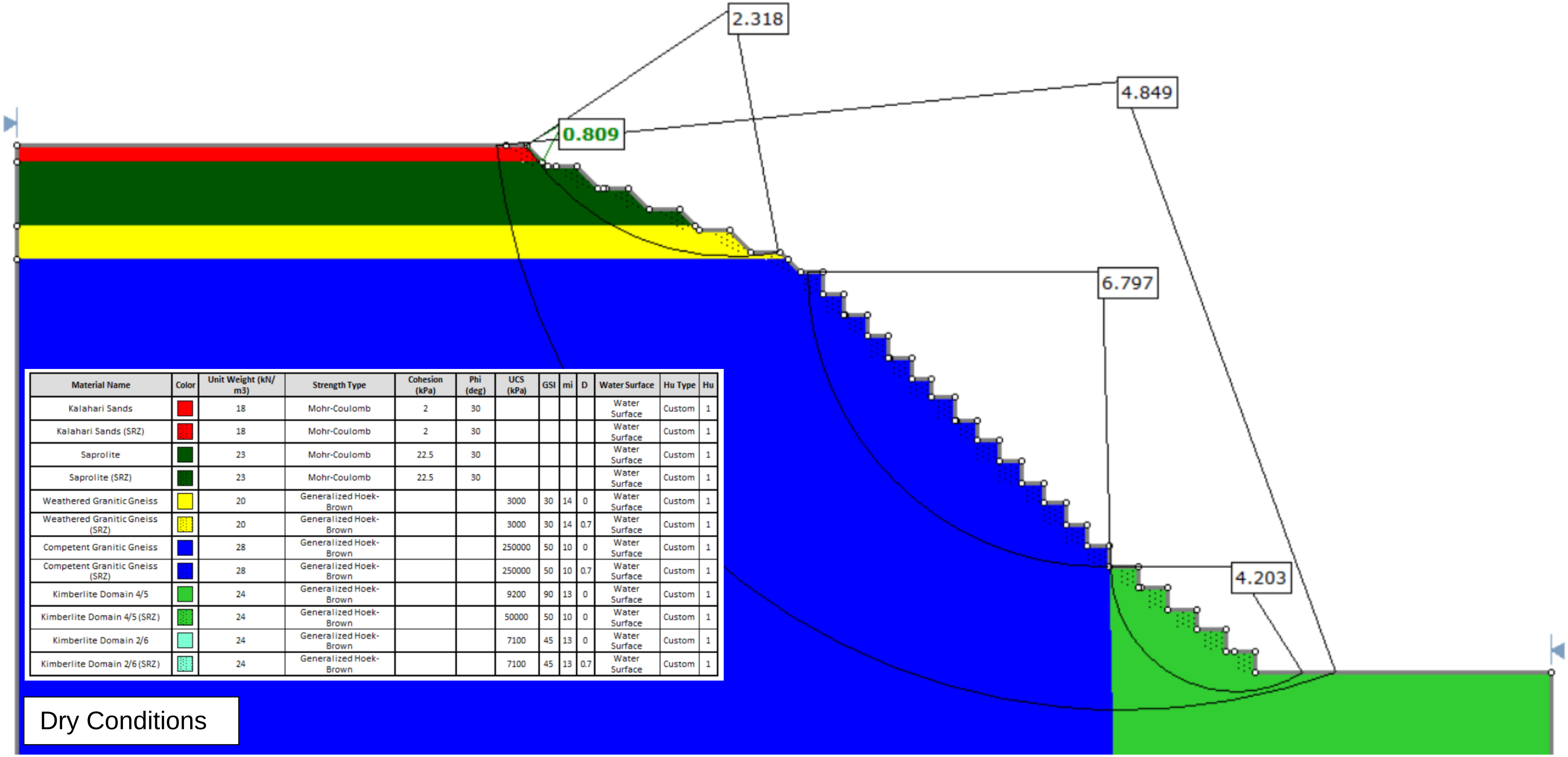

Material Name	Color	Unit Weight (kN/ m3)	Strength Type	Cohesion (kPa)	Phi (deg)	UCS (kPa)	GSI	mi	D	Water Surface	Hu Type	Hu
Kalahari Sands		18	Mohr-Coulomb	2	30					Water Surface	Custom	1
Kalahari Sands (SRZ)		18	Mohr-Coulomb	2	30					Water Surface	Custom	1
Saprolite		23	Mohr-Coulomb	22.5	30					Water Surface	Custom	1
Saprolite (SRZ)		23	Mohr-Coulomb	22.5	30					Water Surface	Custom	1
Weathered Granitic Gneiss		20	Generalized Hoek-Brown			3000	30	14	0	Water Surface	Custom	1
Weathered Granitic Gneiss (SRZ)		20	Generalized Hoek-Brown			3000	30	14	0.7	Water Surface	Custom	1
Competent Granitic Gneiss		28	Generalized Hoek-Brown			250000	50	10	0	Water Surface	Custom	1
Competent Granitic Gneiss (SRZ)		28	Generalized Hoek-Brown			250000	50	10	0.7	Water Surface	Custom	1
Kimberlite Domain 4/5		24	Generalized Hoek-Brown			9200	90	13	0	Water Surface	Custom	1
Kimberlite Domain 4/5 (SRZ)		24	Generalized Hoek-Brown			50000	50	10	0	Water Surface	Custom	1
Kimberlite Domain 2/6		24	Generalized Hoek-Brown			7100	45	13	0	Water Surface	Custom	1
Kimberlite Domain 2/6 (SRZ)		24	Generalized Hoek-Brown			7100	45	13	0.7	Water Surface	Custom	1

Figure E4: North Western Section SLIDE 2D(2018) analysis of the main pit under dry conditions

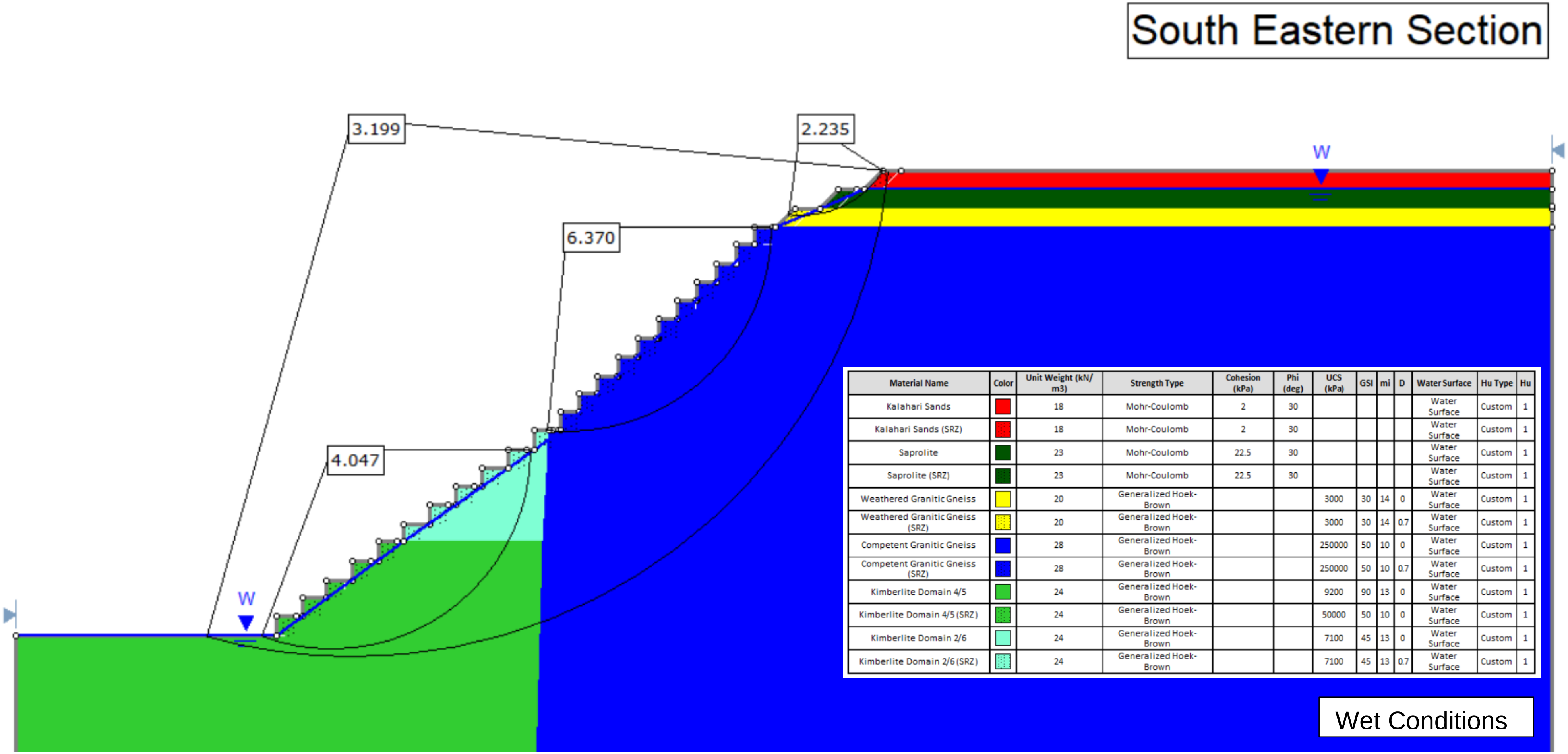

Material Name	Color	Unit Weight (kN/m3)	Strength Type	Cohesion (kPa)	Phi (deg)	UCS (kPa)	GSI	mi	D	Water Surface	Hu Type	Hu
Kalahari Sands		18	Mohr-Coulomb	2	30					Water Surface	Custom	1
Kalahari Sands (SRZ)		18	Mohr-Coulomb	2	30					Water Surface	Custom	1
Saprolite		23	Mohr-Coulomb	22.5	30					Water Surface	Custom	1
Saprolite (SRZ)		23	Mohr-Coulomb	22.5	30					Water Surface	Custom	1
Weathered Granitic Gneiss		20	Generalized Hoek-Brown			3000	30	14	0	Water Surface	Custom	1
Weathered Granitic Gneiss (SRZ)		20	Generalized Hoek-Brown			3000	30	14	0.7	Water Surface	Custom	1
Competent Granitic Gneiss		28	Generalized Hoek-Brown			250000	50	10	0	Water Surface	Custom	1
Competent Granitic Gneiss (SRZ)		28	Generalized Hoek-Brown			250000	50	10	0.7	Water Surface	Custom	1
Kimberlite Domain 4/5		24	Generalized Hoek-Brown			9200	90	13	0	Water Surface	Custom	1
Kimberlite Domain 4/5 (SRZ)		24	Generalized Hoek-Brown			50000	50	10	0	Water Surface	Custom	1
Kimberlite Domain 2/6		24	Generalized Hoek-Brown			7100	45	13	0	Water Surface	Custom	1
Kimberlite Domain 2/6 (SRZ)		24	Generalized Hoek-Brown			7100	45	13	0.7	Water Surface	Custom	1

Figure E5: South Eastern Section SLIDE 2D(2018) analysis of the main pit under wet conditions

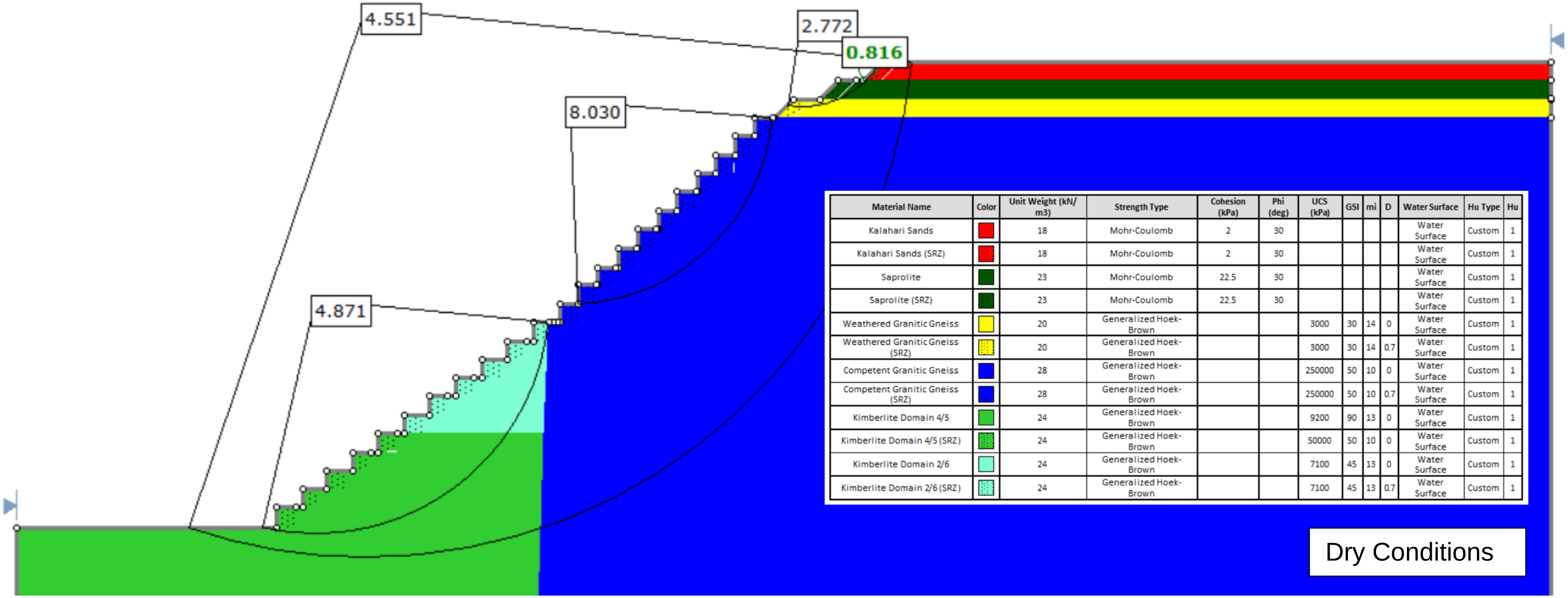

Figure E6: South Eastern Section SLIDE 2D(2018) analysis of the main pit under dry conditions

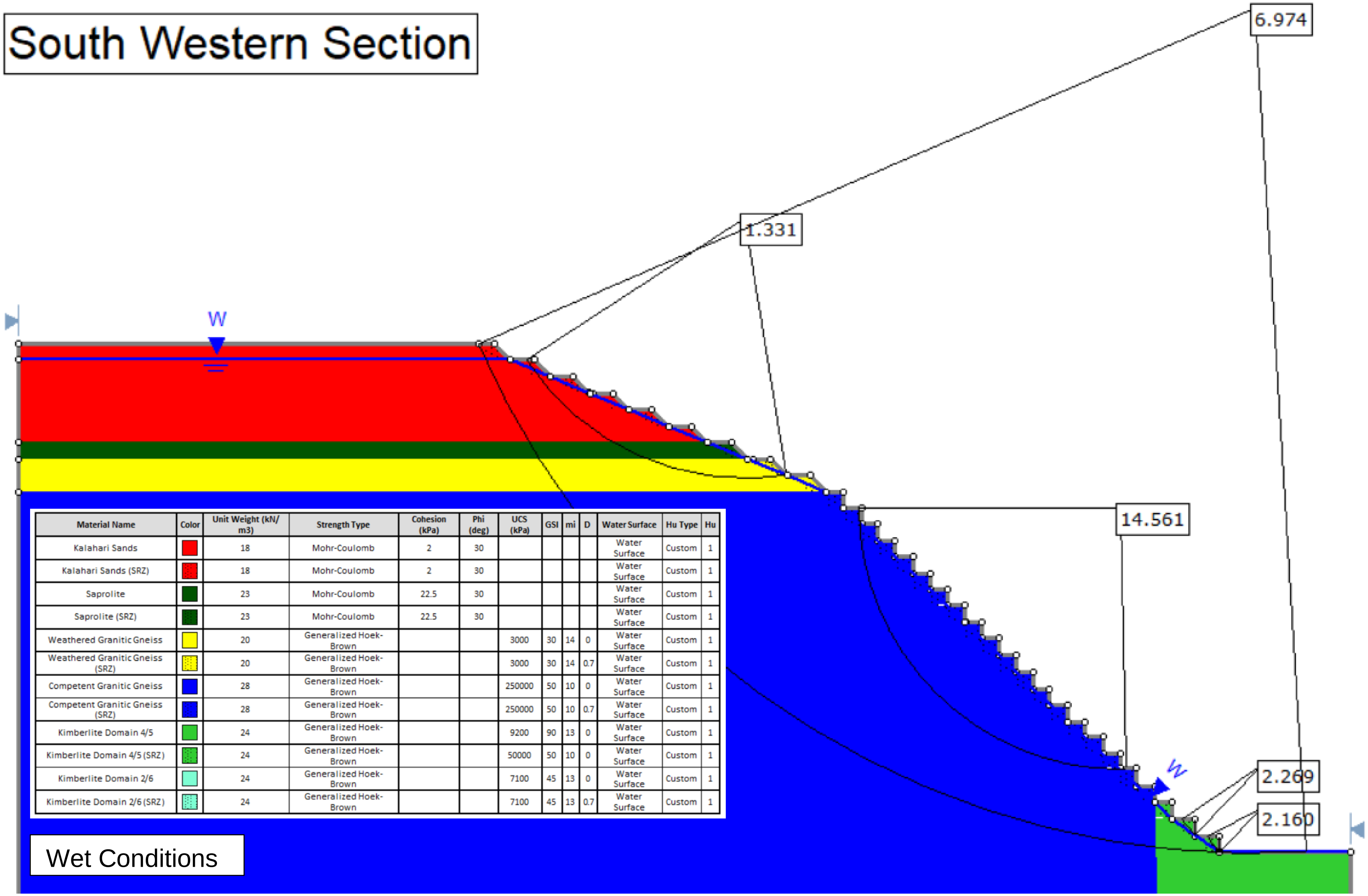

Material Name	Color	Unit Weight (kN/m3)	Strength Type	Cohesion (kPa)	Phi (deg)	UCS (kPa)	GSI	mi	D	Water Surface	Hu Type	Hu
Kalahari Sands		18	Mohr-Coulomb	2	30					Water Surface	Custom	1
Kalahari Sands (SRZ)		18	Mohr-Coulomb	2	30					Water Surface	Custom	1
Saprolite		23	Mohr-Coulomb	22.5	30					Water Surface	Custom	1
Saprolite (SRZ)		23	Mohr-Coulomb	22.5	30					Water Surface	Custom	1
Weathered Granitic Gneiss		20	Generalized Hoek-Brown			3000	30	14	0	Water Surface	Custom	1
Weathered Granitic Gneiss (SRZ)		20	Generalized Hoek-Brown			3000	30	14	0.7	Water Surface	Custom	1
Competent Granitic Gneiss		28	Generalized Hoek-Brown			250000	50	10	0	Water Surface	Custom	1
Competent Granitic Gneiss (SRZ)		28	Generalized Hoek-Brown			250000	50	10	0.7	Water Surface	Custom	1
Kimberlite Domain 4/5		24	Generalized Hoek-Brown			9200	90	13	0	Water Surface	Custom	1
Kimberlite Domain 4/5 (SRZ)		24	Generalized Hoek-Brown			50000	50	10	0	Water Surface	Custom	1
Kimberlite Domain 2/6		24	Generalized Hoek-Brown			7100	45	13	0	Water Surface	Custom	1
Kimberlite Domain 2/6 (SRZ)		24	Generalized Hoek-Brown			7100	45	13	0.7	Water Surface	Custom	1

Figure E7: South Western Section SLIDE 2D(2018) analysis of the main pit under wet conditions

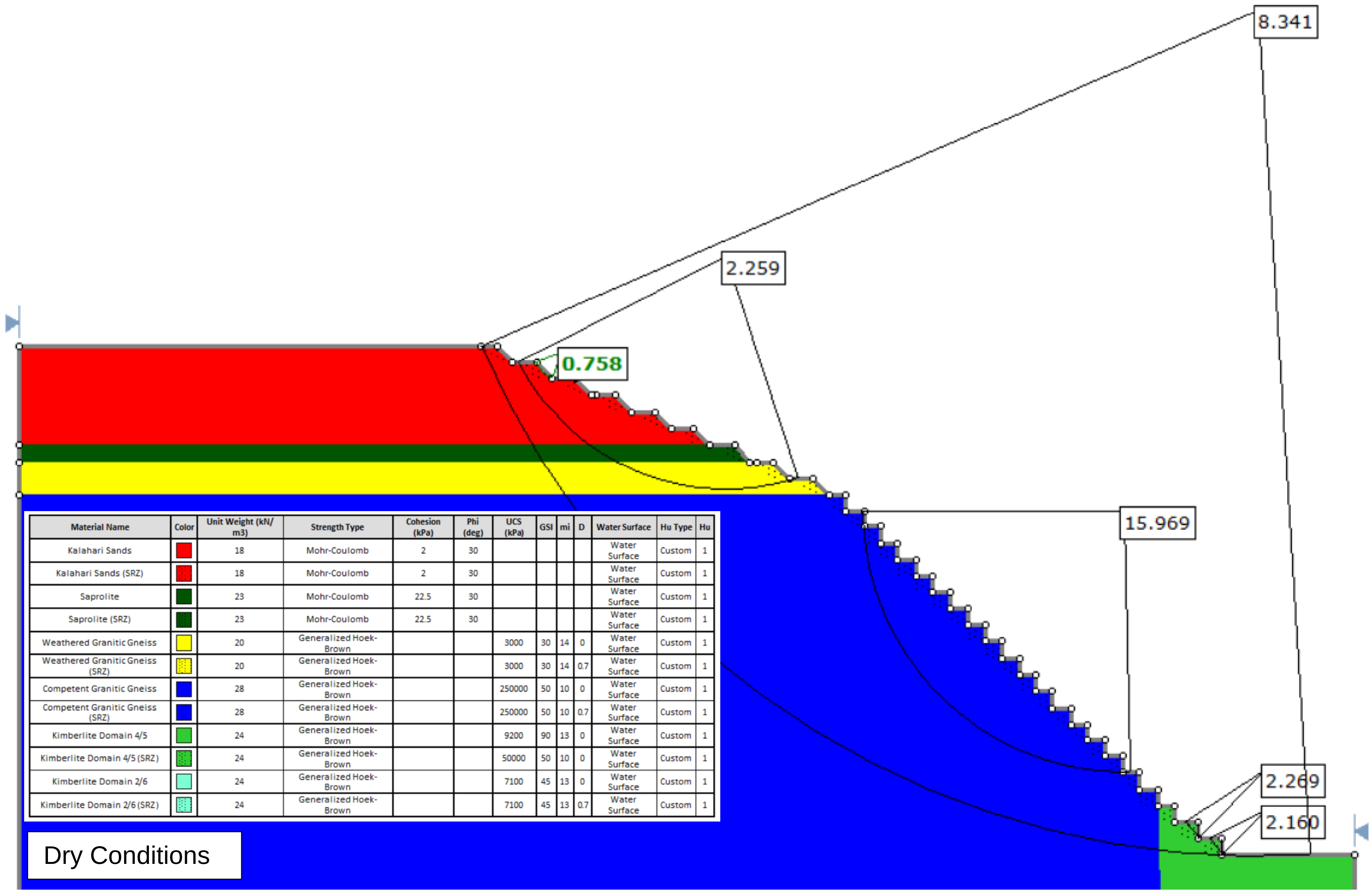

Figure E8: South Western Section SLIDE 2D(2018) analysis of the main pit under dry conditions

Appendix F: Stereonet Projections

Stereonet projections of each geotechnical domain as presented in the following table

Geotechnical Domain	Bieniawski (1973) RMR	Laubscher (1990) MRMR	Fracture Frequency (Jn/m)	Major Joint Systems (Dip/Dip Direction)
Geotechnical Domain 1	55	42	5	1. 72/146 2. 44/010 3. 36/055

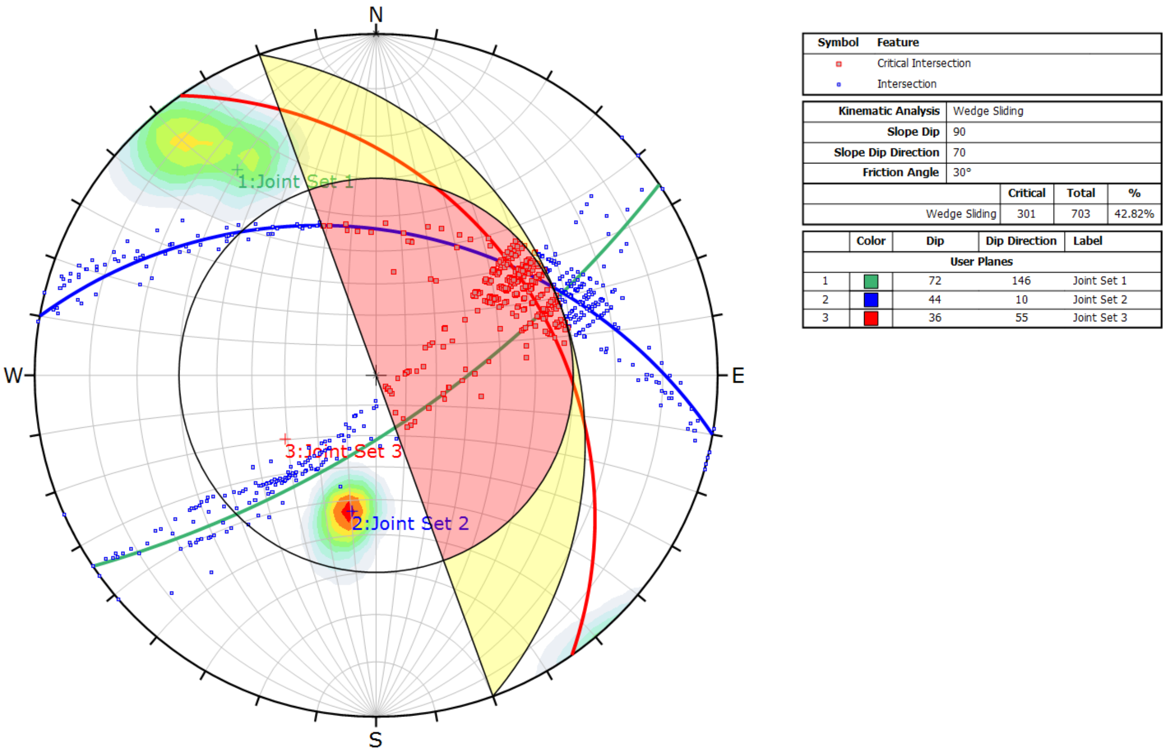

Figure F1: Geotechnical Domain 1 Stereonet projections

Geotechnical Domain 3	56	47	5	1. 81/151 2. 38/038

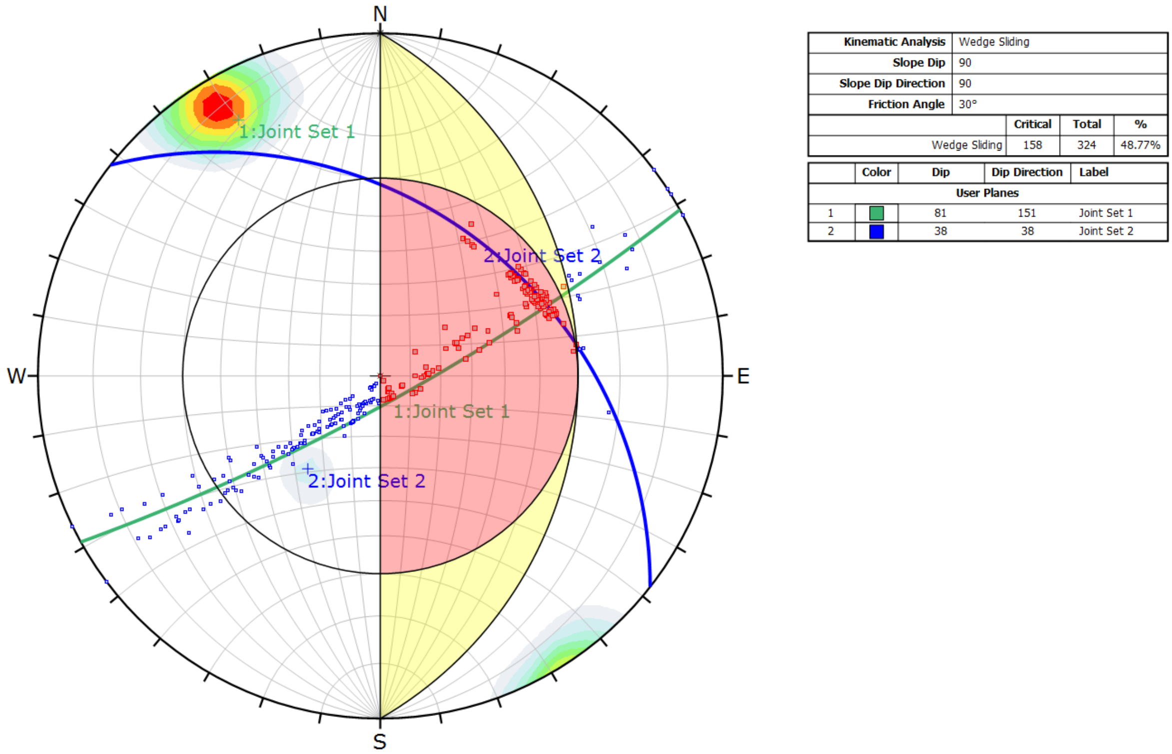

Figure F2: Geotechnical Domain 3 Stereonet projections

Geotechnical Domain 4	49	31	15	1. 66/148 2. 42/143 3. 74/092

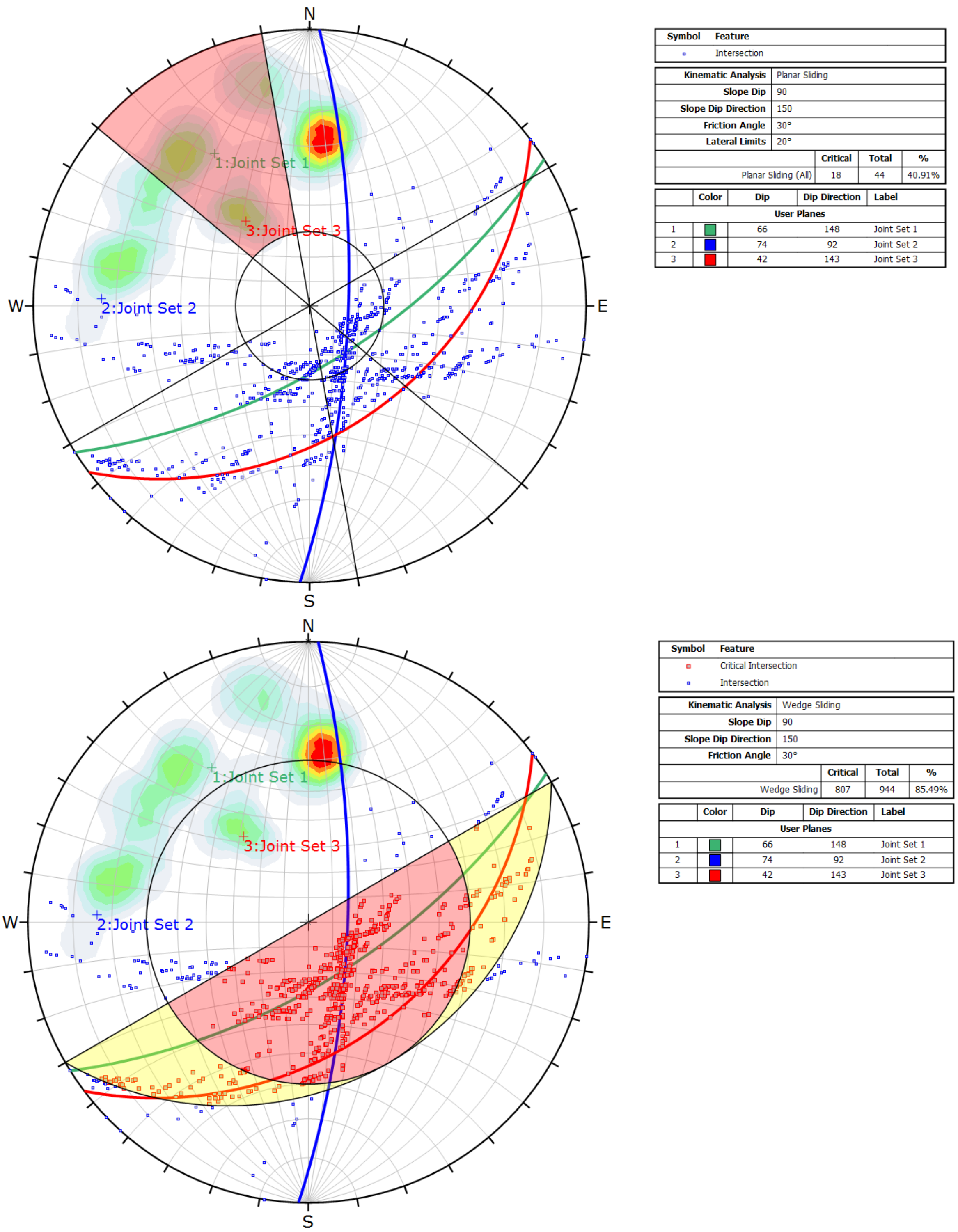

Figure F3: Geotechnical Domain 4 Stereonet projections

Geotechnical Domain 5	50	48	5	1. 71/155 2. 27/170 3. 78/085

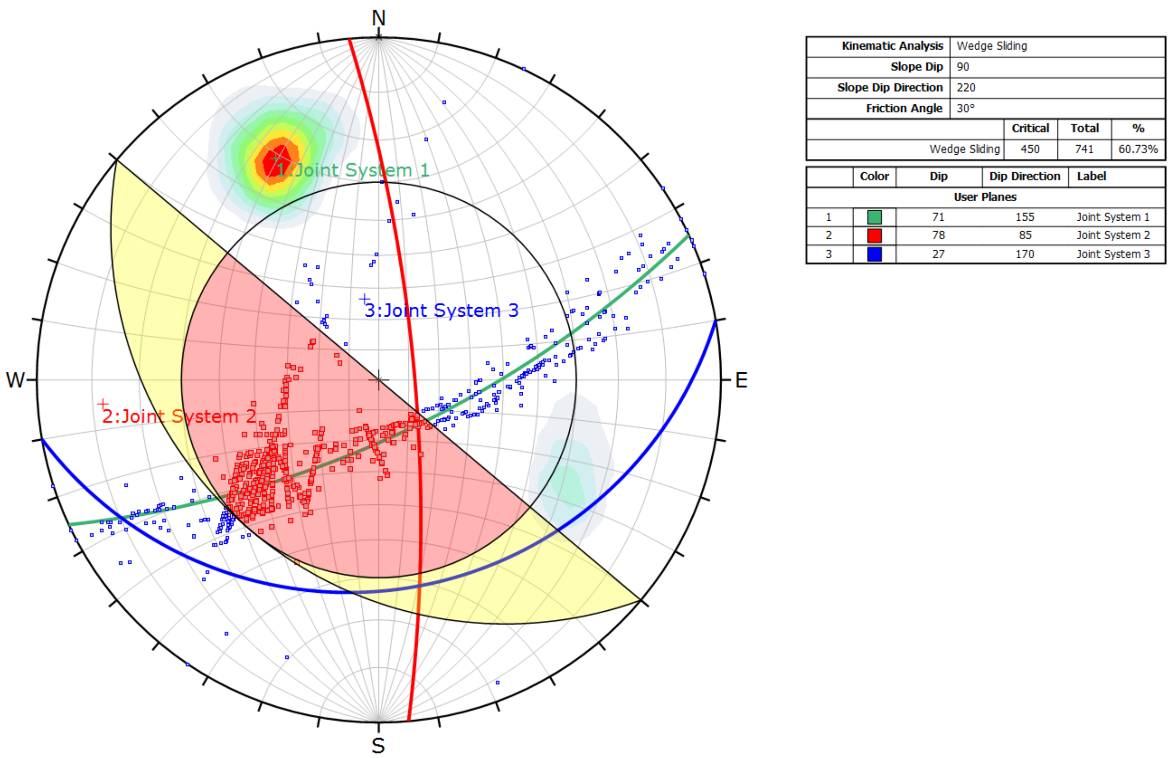

Figure F4: Geotechnical Domain 5 Stereonet projections

Geotechnical Domain 6	53	51	7	1. 73/154 2. 51/255 3. 56/293

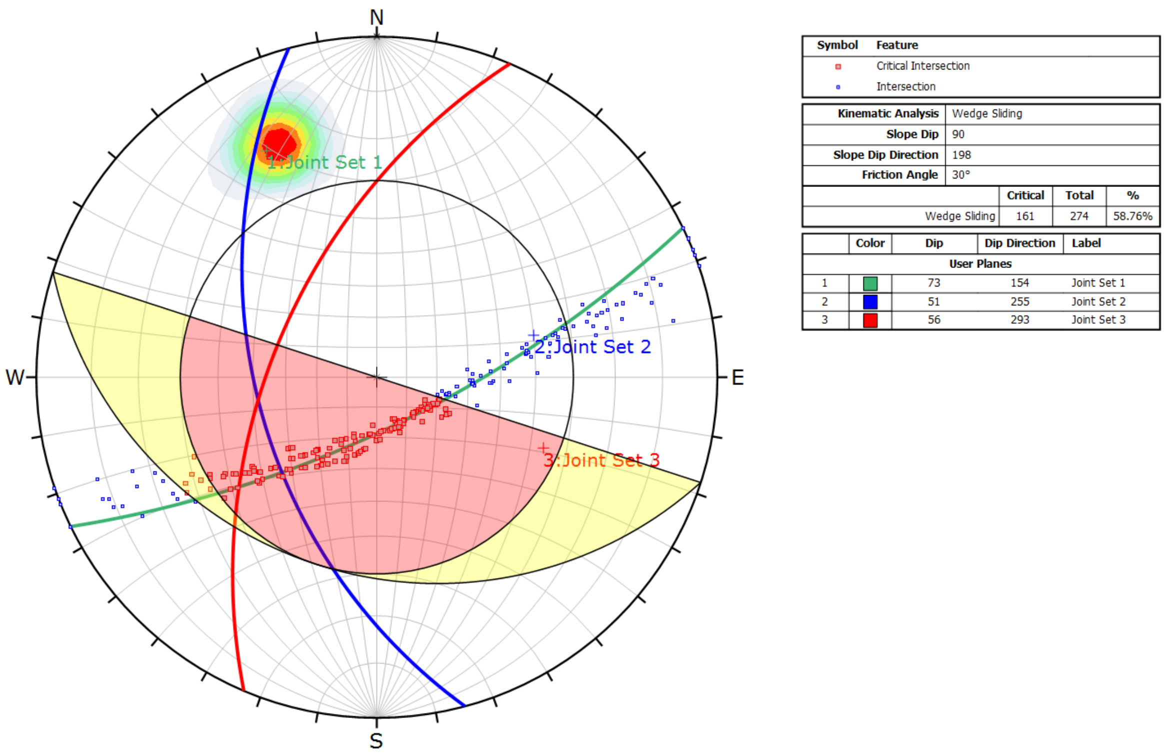

Figure F5: Geotechnical Domain 6 Stereonet projections

Geotechnical Domain 7	55	52	5	1. 77/199 2. 66/307 3. 45/212

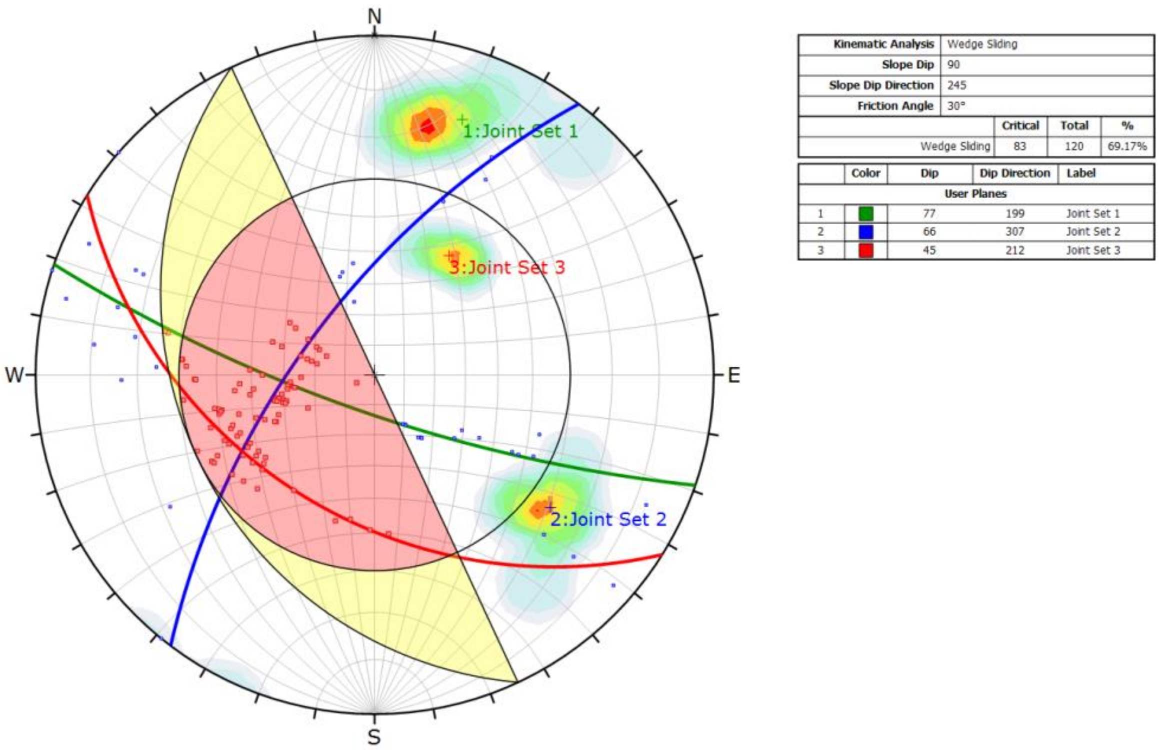

Figure F6: Geotechnical Domain 7 Stereonet projections

Geotechnical Domain 8	55	52	5	1. 72/113 2. 15/213

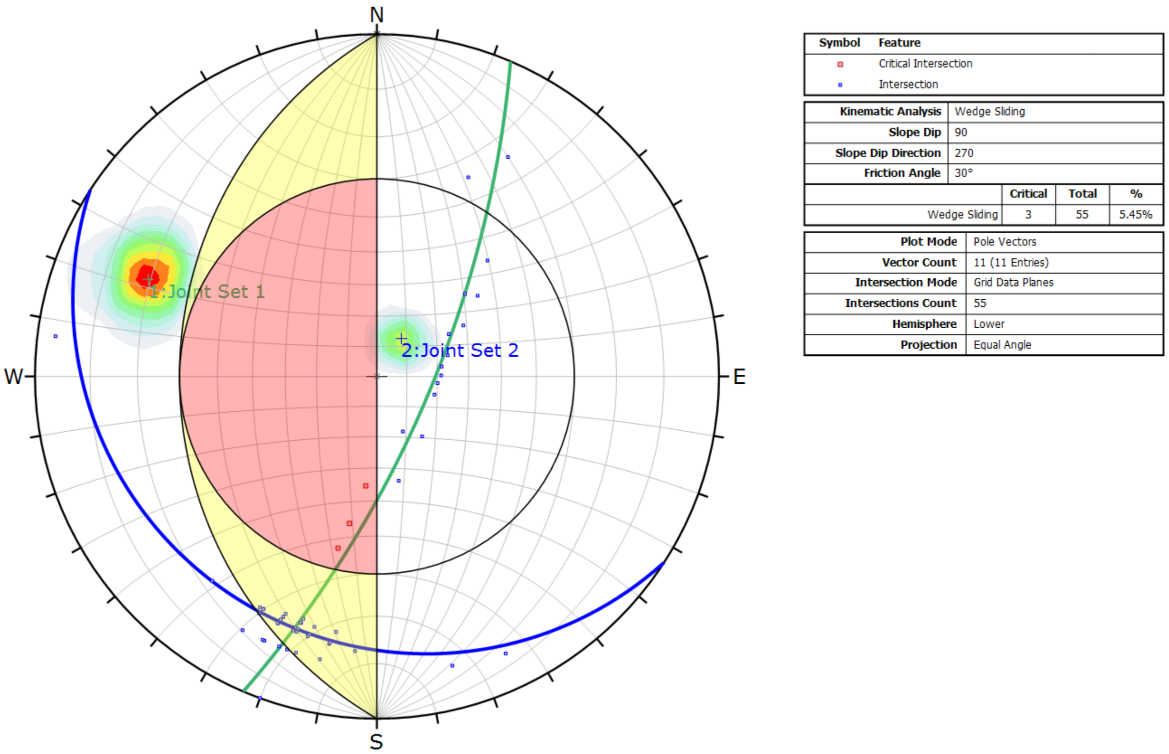

Figure F7: Geotechnical Domain 8 Stereonet projections

Geotechnical Domain 9	56	52	5	1. 76/157

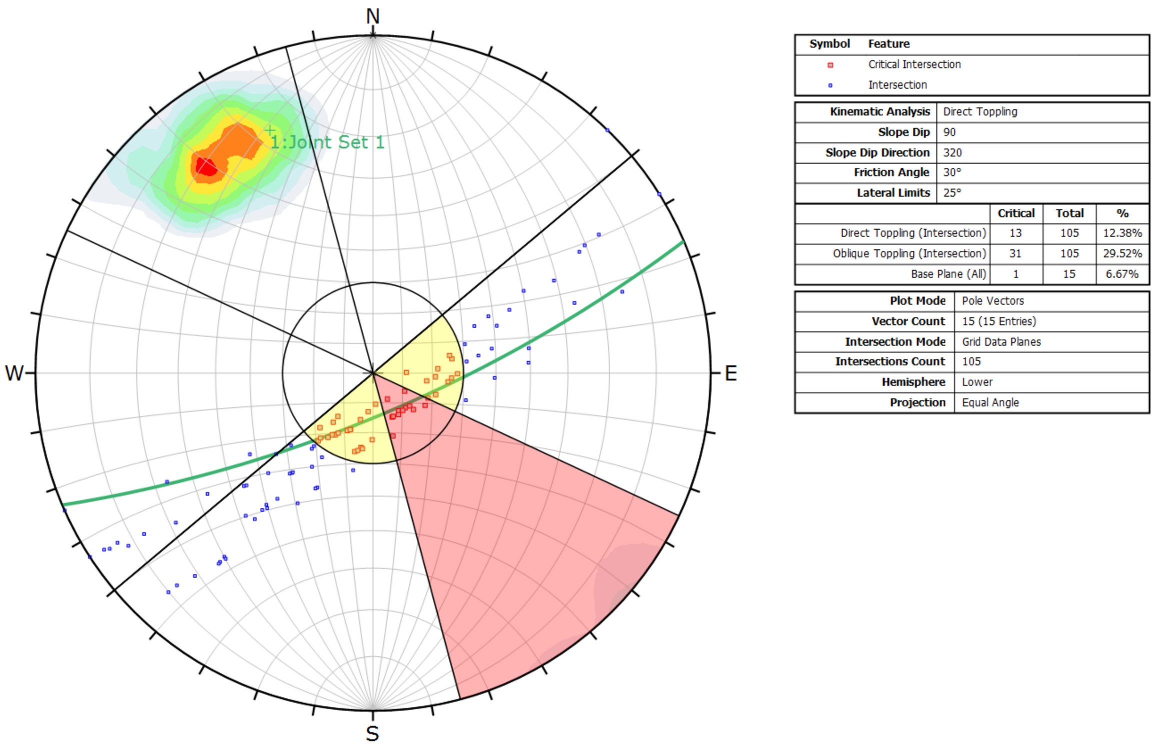

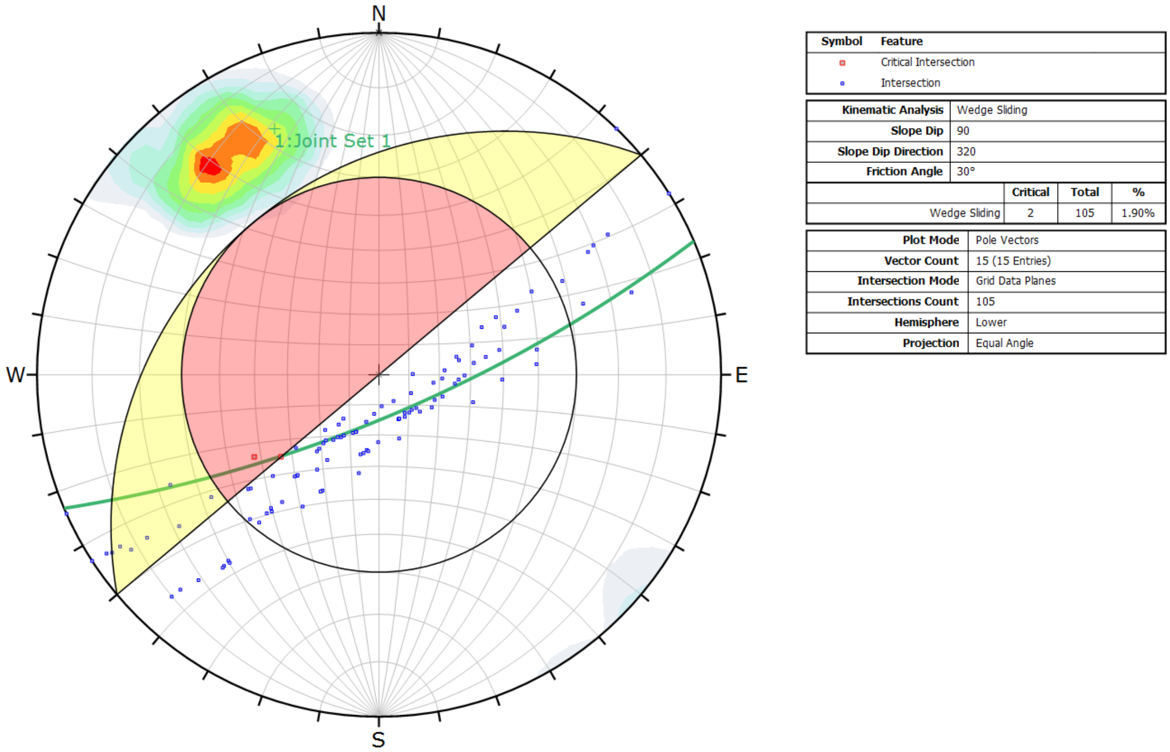

Figure F8: Geotechnical Domain 9 Stereonet projections

Geotechnical Domain 10	52	49	7	1. 76/148 2. 38/343

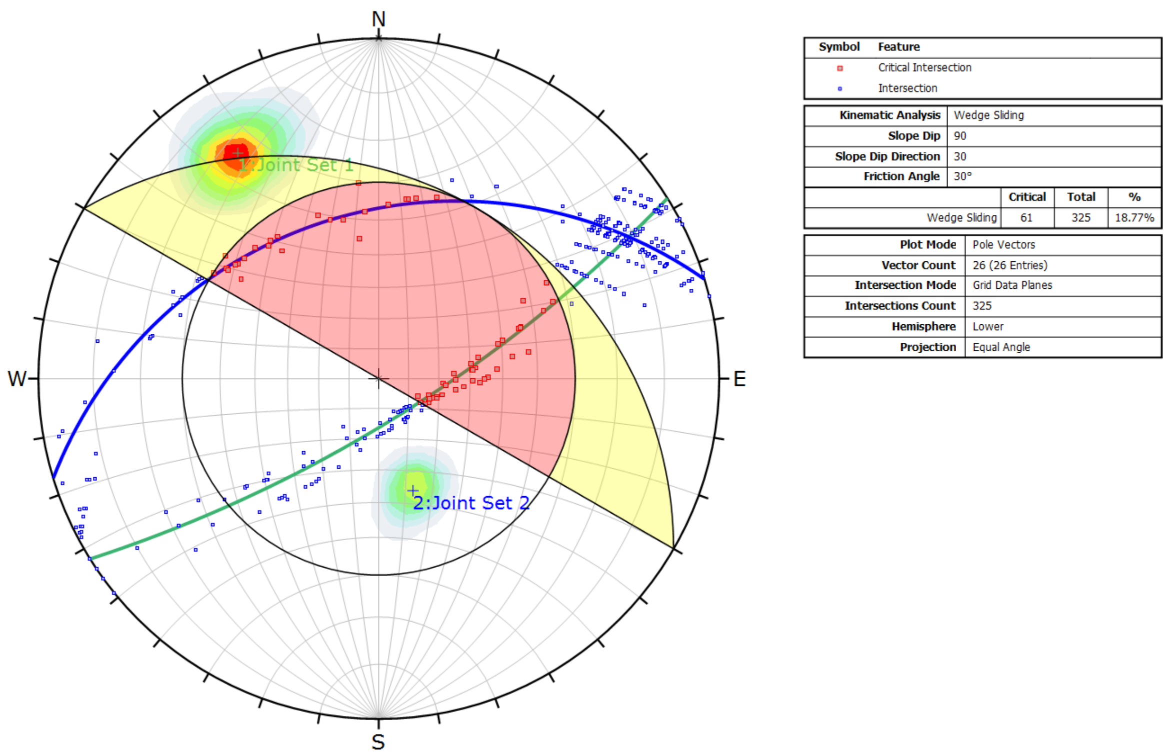

Figure F9: Geotechnical Domain 10 Stereonet projections

Appendix G: Examine 2D (2006) Results

Examine 2D (2006) analysis of additional rock masses encountered in Mine A main pit

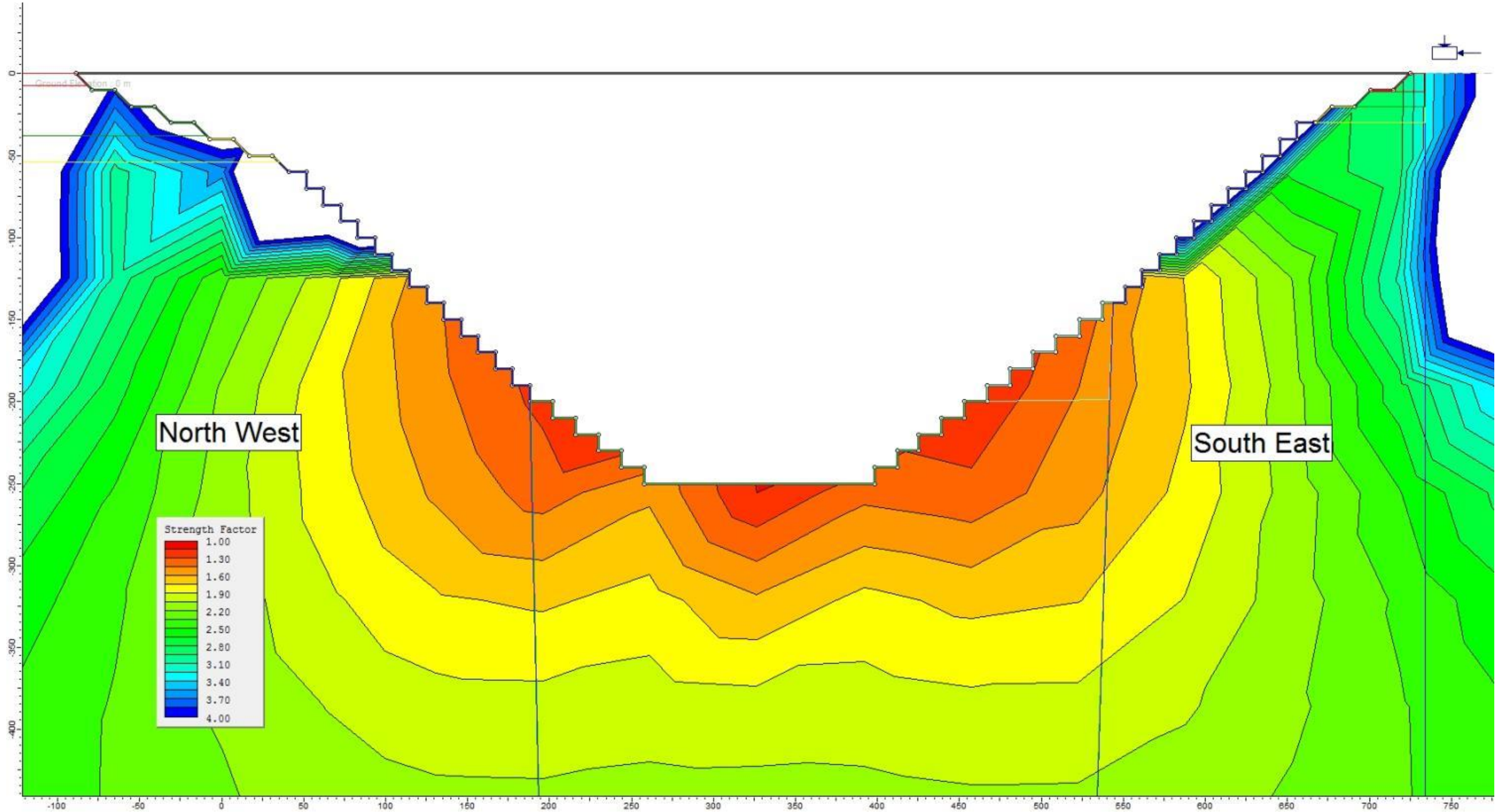

Figure G1: North West – South East Section: Granitic Gneiss Country Rock with down-rated rock mass parameters modelled

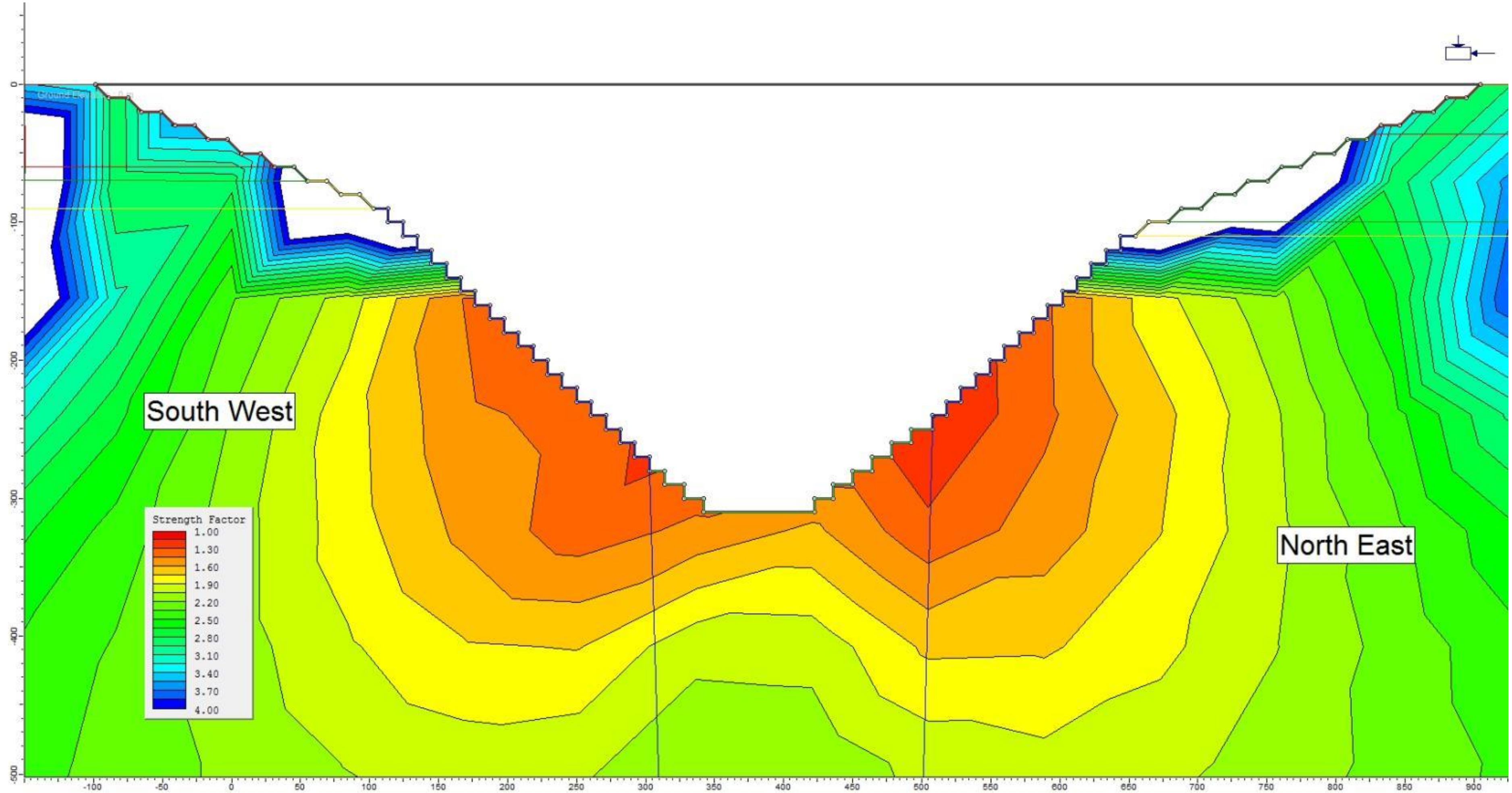

Figure G2: South West – North East Section: Granitic Gneiss Country Rock with down-rated rock mass parameters modelled

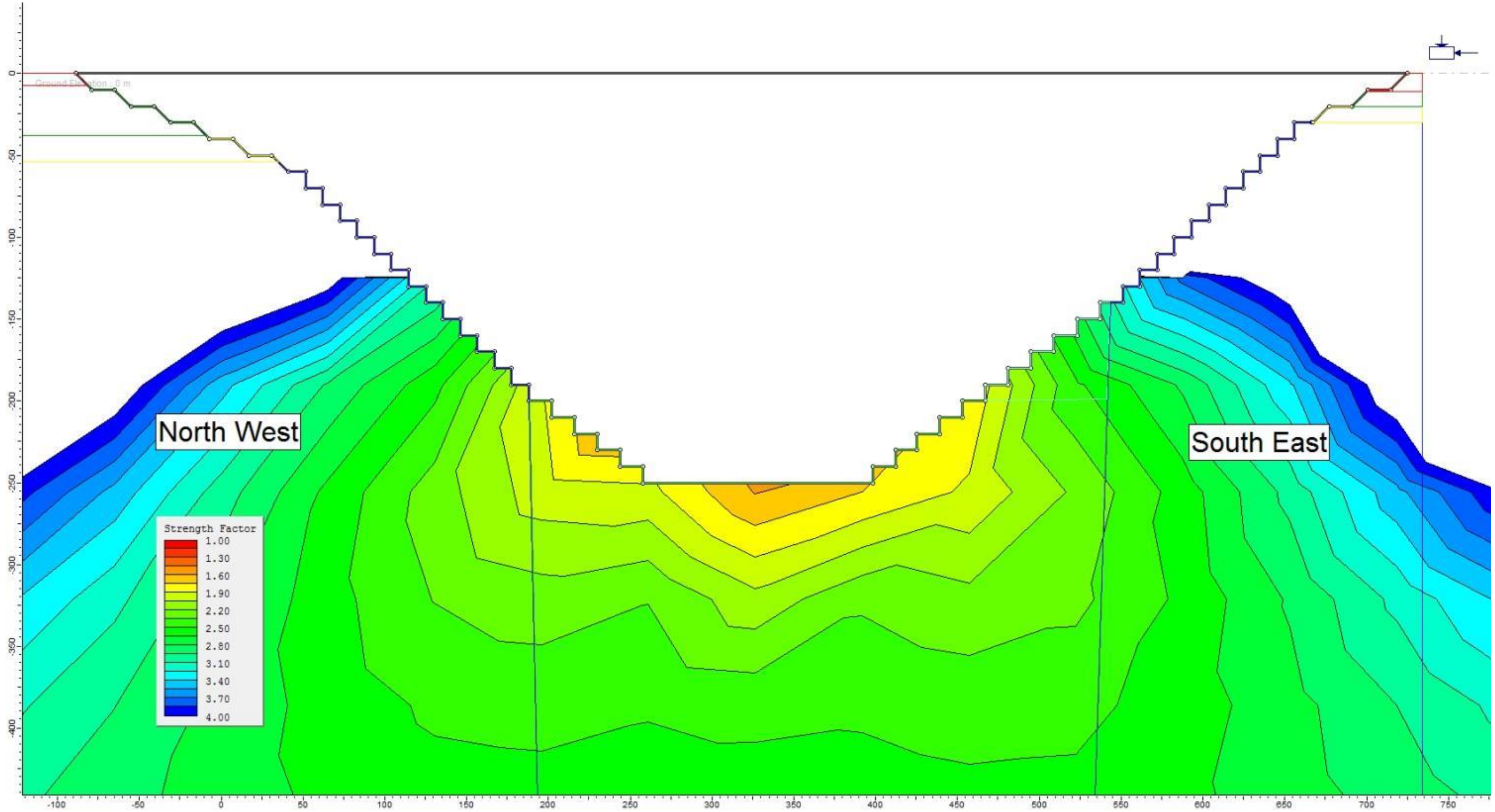

Figure G3: North West – South East Section: Kimberlite 2 with down-rated rock mass parameters modelled

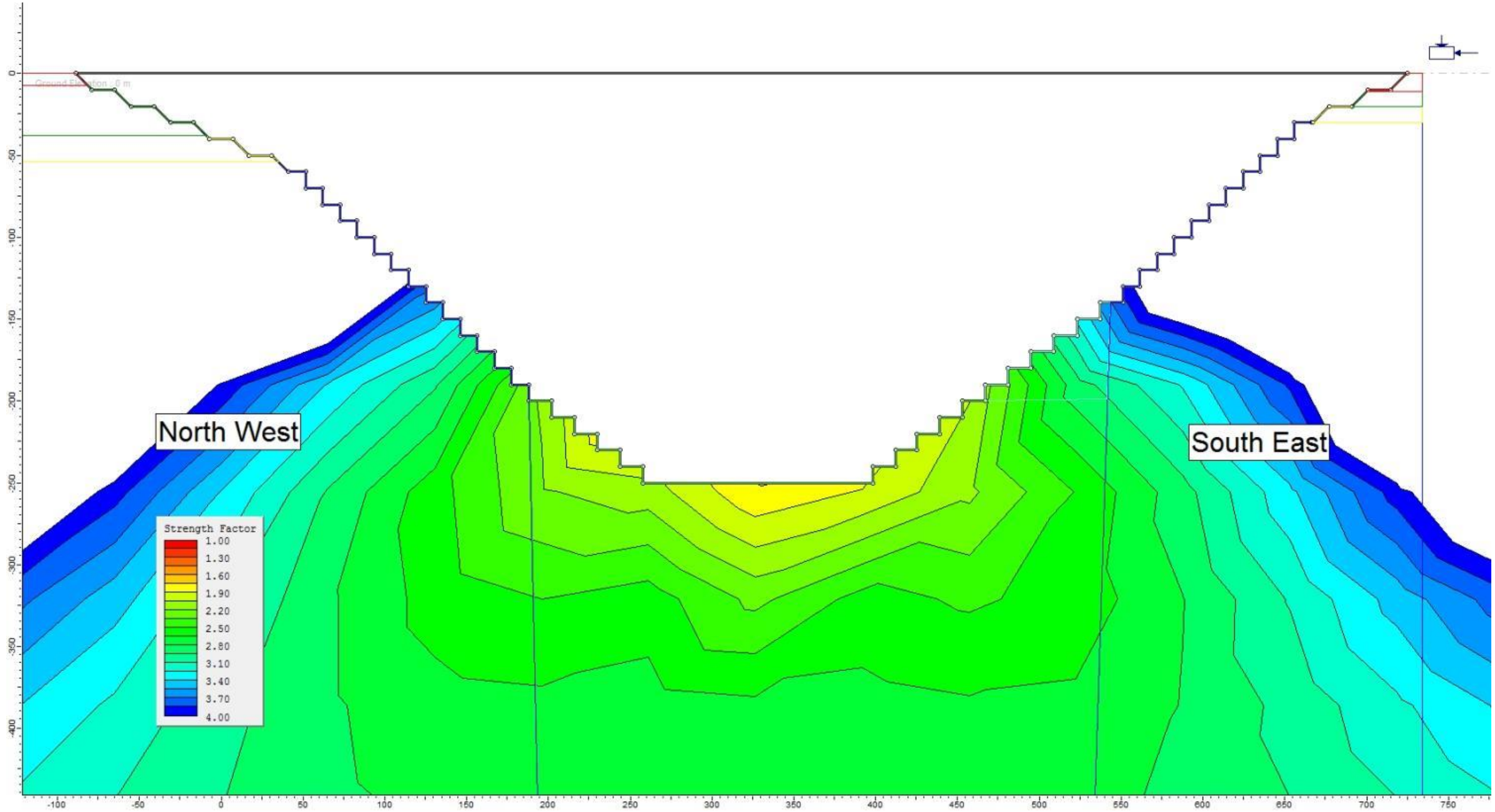

Figure G4: North West – South East Section: Kimberlite 4 with down-rated rock mass parameters modelled

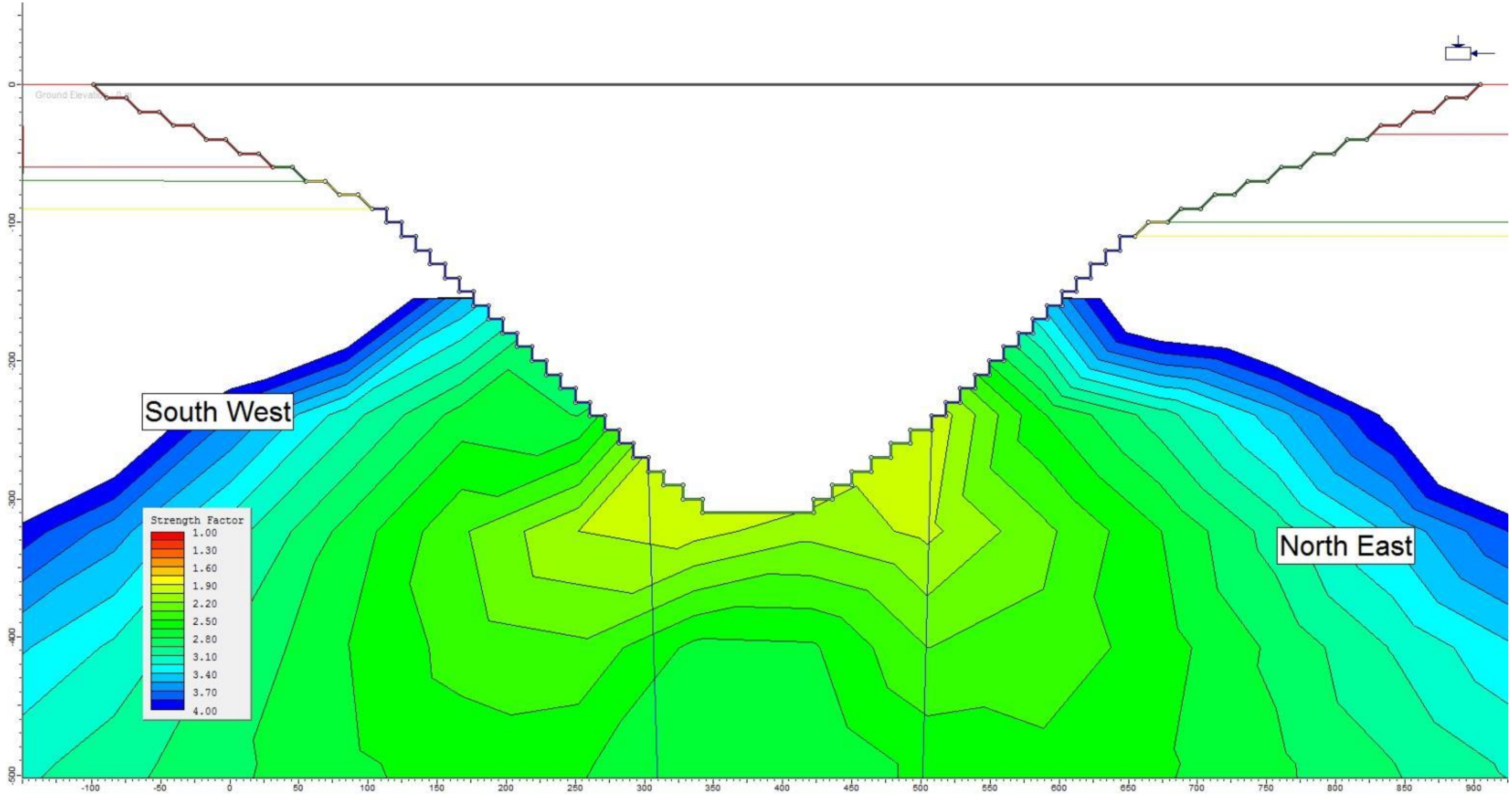

Figure G5: South West – North East Section: Kimberlite 4 with down-rated rock mass parameters modelled